Spring 5-15-2020

Development of an in vitro Culture System for Cryptosporidium parvum

Georgia Wilke
Washington University in St. Louis

WASHINGTON UNIVERSITY IN ST. LOUIS

Division of Biology and Biomedical Sciences
Molecular Microbiology and Microbial Pathogenesis

Dissertation Examination Committee:
L. David Sibley, Chair
Megan Baldridge
Daniel Goldberg
Audrey Odom John
Thaddeus Stappenbeck
Phillip Tarr

Development of an *in vitro* Culture System for *Cryptosporidium parvum*

by
Georgia Wilke

A dissertation presented to
The Graduate School
of Washington University in
partial fulfillment of the
requirements for the degree
of Doctor of Philosophy

May 2020
St. Louis, Missouri

TABLE OF CONTENTS

LIST OF FIGURES

Chapter 1: Introduction

LIST OF TABLES

ACKNOWLEDGMENTS

This thesis would not have been possible without the support and guidance of many individuals. I would like to thank the MSTP and Infectious Disease training grants for monetary support, as well as the Bill & Melinda Gates Foundation. I am grateful for my thesis committee for seeing the potential in this project and providing advice that helped me navigate the past five years. My mentor, David Sibley, has demonstrated incredible resourcefulness, inspiring me to continually move forward. I believe the greatest gift a mentor can give their student is their time, and David has devoted considerable time and effort to my training. I am especially indebted to Thad Stappenbeck, along with Kelli VanDussen and Yi Wang, for lending their expertise to this project. The Sibley lab has been a wonderful environment to grow as a scientist; I would especially like to thank Soumya Ravindran and Lisa Funkhouser-Jones. The Medical Scientist Training Program at Washington University has been an amazing resource and community and I am privileged to be surrounded by peers with such devotion to research. Finally, I would like to thank my friends and family for their love and support. My parents have always been excellent role models when it comes to hard work and dedication; they have encouraged my interest in science since the very beginning. I would not be here without their support and sacrifice and I am incredibly indebted to them. Most importantly, I would like to thank my wonderful husband, Ishan, whose kindness, thoughtfulness, and generosity amazes me every day. He is a devoted father to our beautiful daughter Theeya, who has brought much happiness into our lives. I appreciate everyone's support and I am truly grateful for you all.

Georgia Wilke

Washington University in St. Louis

May 2020

Dedicated to my husband.

ABSTRACT OF THE DISSERTATION

Development of an *in vitro* Culture System for *Cryptosporidium parvum*

by

Georgia Wilke

Doctor of Philosophy in Biology and Biomedical Sciences

Molecular Microbiology and Microbial Pathogenesis

Washington University in St. Louis, 2020

Professor L. David Sibley, Chair

Cryptosporidium is a genus of protozoan parasites that causes diarrheal disease in humans and other animals. There are two major species that cause disease in humans: *C. parvum*, which infects both humans and animals, and *C. hominis*, which primarily infects humans. A recent study investigating the etiologies of pediatric diarrheal illness in Africa and South Asia found that *Cryptosporidium* is the 2nd most prevalent cause of diarrhea in infants and may be a contributing factor to chronic malnutrition. This discovery has led to renewed interest in studying this parasite and a reexamination of the barriers to studying *Cryptosporidium*. The main obstacle hindering research on this parasite is that it cannot be propagated *in vitro* and instead must be passaged through large animals such as calves to generate infectious oocysts. The cell culture models that are available rely on adenocarcinoma cells and only support a few days of growth and do not enable complete life cycle development *in vitro*. These limitations have stalled the development of research tools for investigating *Cryptosporidium* biology and have also slowed developmental progress of new therapies.

Recent developments in stem cell culture have allowed for the isolation of human and mouse intestinal stem cells, which can be propagated indefinitely and differentiated into primary intestinal epithelial cells (IECs). We found that mouse IEC monolayers supported robust *C. parvum* growth. We utilized this system to create a hybridoma bank of novel antibodies targeting the intracellular stages of *C. parvum*, something that had not been attempted previously due to the lack of a mouse cell line that supported *Cryptosporidium* growth. These antibodies have unique staining patterns for many life cycle stages, enabling unambiguous identification of different stages and facilitating life cycle description in diverse culture platforms.

The mouse IEC monolayers supported superior parasite growth to adenocarcinoma cell lines, but they had a short lifespan and did not support complete life cycle development *in vitro*. In order to improve the longevity of the IEC monolayers, we introduced several components to the system: the use of stem cell culture medium to grow the monolayers, the inclusion of a feeder cell layer to create a robust extracellular matrix, and an air-liquid interface at the surface of the monolayer. These modifications led to long-lasting monolayers with improved differentiation status; the monolayers contained proliferating cells and all of the differentiated lineages of the intestinal epithelium. These monolayers supported long-term *C. parvum* growth as well as the development of infectious oocysts, indicating complete life cycle development *in vitro*. This improved IEC system will be a valuable tool for selecting transgenic parasites *in vitro*, as well as investigating drug mechanism and target identification. Since the monolayers are great models of the intestinal epithelium, this system will be vital to studying host-pathogen interactions in a platform that resembles the parasite's natural niche.

Chapter 1

Introduction

The first draft of this work was written by GW. Comments from LDS were incorporated into the final chapter here.

Cryptosporidium and cryptosporidiosis

Cryptosporidium is an obligate intracellular parasite that belongs to the phylum Apicomplexa, which includes other disease-causing parasites such as *Toxoplasma*, *Plasmodium*, and *Eimeria*. Over 20 different species of *Cryptosporidium* are recognized, many of which are specific to a single vertebrate host (1). The majority of human infections are caused by *C. hominis*, which is limited to humans, and *C. parvum*, which can be spread from ruminants (2-4). Cryptosporidiosis is characterized by profuse watery diarrhea and abdominal pain that is self-limiting in healthy individuals (5).

Cryptosporidium was first identified as a gastrointestinal parasite in mice by Edward Tyzzer early in the 20th century (6-8). It was named *Cryptosporidium* due to the lack of sporocysts within the oocyst, a characteristic of other coccidia (a subclass of the Apicomplexans that includes *Toxoplasma* and *Cyclospora*). It was not recognized as a human pathogen until the late 1970s when it was found in a rectal biopsy from a 3-year-old child suffering from enterocolitis (9). In the 1980s, *Cryptosporidium* was identified as an opportunistic pathogen in patients immunocompromised from HIV/AIDS (10). During this time, the parasite became strongly associated with the disease and cryptosporidiosis was one of the first recognized AIDS-defining illnesses. Cryptosporidiosis in immunocompromised patients is a protracted, deadly illness (11), with potential for extra-gastrointestinal infection by the parasite in either the hepatobiliary (12) or respiratory tracts (13). Fortunately, with the introduction of anti-retroviral therapy, morbidity and mortality from *Cryptosporidium* in HIV/AIDS patients has declined significantly over the ensuing years.

At the same time cryptosporidiosis became recognized as a severe illness in immunocompromised patients, it was also identified as a cause of short-term diarrhea in

immunocompetent individuals (14). This latter scenario became well-appreciated with two major waterborne outbreaks of cryptosporidiosis: in 1989 in Swindon and Oxfordshire, affecting 5,000 people (15), and in 1993 in Milwaukee, affecting 400,000 people (16). The magnitude of these outbreaks helped emphasize the role of contaminated drinking water in spreading *Cryptosporidium* and led to research on the identification and treatment of oocyst contamination of water supplies (17). *Cryptosporidium* continues to be a cause of sporadic outbreaks associated with public water and swimming facilities (18).

In recent years, *Cryptosporidium* has been identified as a major cause of diarrhea in children in developing regions. This finding can be attributed to two important studies: GEMS (Global Enteric Multicenter Study, (19)) and the MAL-ED (Malnutrition and Enteric Disease) study (20, 21). GEMS was a 3-year prospective study with over 20,000 child participants (aged 0-59 months) from seven sites in Africa and Asia. Children with moderate-to-severe diarrhea were enrolled along with age-matched controls. Fecal samples were collected at enrollment to identify potential enteropathogens. MAL-ED was a birth cohort study with eight sites in Africa, Asia, and South America. Children were enrolled at birth and diarrheal episodes were identified through frequent home visits and fecal sample collection up till the child became two years of age. GEMS found *Cryptosporidium* to be the second and third leading pathogen identified in diarrhea in infants (0-11 months) and toddlers (12-23 months), respectively, behind Rotavirus and *Shigella* spp. Surprisingly, *Cryptosporidium* was a major pathogen at all sites visited independent of HIV prevalence. MAL-ED found *Cryptosporidium* to be the fifth and seventh leading cause of diarrhea in infants and toddlers, respectively. Both studies used the same commercial immunoassay to identify *Cryptosporidium* in the fecal samples. The difference in their findings could be due to the different sites of the studies as well as the fact that GEMS

enrolled patients with moderate to severe diarrhea only, while MAL-ED captured all cases of diarrhea, including mild disease that did not require hospitalization or administration of intravenous fluids.

The GEMS and MAL-ED studies have drawn attention to the global burden of *Cryptosporidium*. Other studies have directly linked *Cryptosporidium* to childhood malnutrition (22, 23), growth faltering (24), and mortality (25), and it is generally known that diarrhea is a major cause of child mortality worldwide (26) and malnutrition and diarrhea have a reciprocal relationship (27). As a widespread gastrointestinal pathogen, *Cryptosporidium* therefore plays a significant role in childhood malnutrition and mortality. Based on the GEMS data, the number of pediatric diarrhea cases annually attributable to *Cryptosporidium* in sub-Saharan Africa and Asia is estimated to be ~7.6 million with ~200,000 deaths (2). These numbers have caused a renewed research interest in *Cryptosporidium* biology and a reexamination of the lack of treatment options for the disease (28). The one drug approved for *Cryptosporidium* infection by the FDA is nitazoxanide and while this drug shortens disease duration in healthy patients (29), it has limited effectiveness in malnourished children (30) and no effectiveness in immunosuppressed patients (31), the two patient populations that most need treatment. Recently, multiple new candidates have emerged for cryptosporidiosis therapy, notably bumped kinase inhibitors of *C. parvum* calcium-dependent protein kinase 1 (32), a PI(4) kinase inhibitor (33), and a repurposed leprosy drug, clofazimine (34). These drugs have shown promise in animal studies and will hopefully prove to be effective in humans in upcoming clinical trials.

Life cycle of *Cryptosporidium*

Cryptosporidium has a complex life cycle consisting of asexual and sexual stages that culminate in oocyst formation (see figure 1.1). Unlike related parasites *Toxoplasma* and *Plasmodium*, *Cryptosporidium*'s life cycle is completed within a single host. Humans and other animals become infected when they ingest oocysts, which excyst as they travel through the stomach and small intestine. Excystation occurs in response to a variety of factors, including temperature change and bile salt exposure (35). In the duodenum and ileum, each oocyst releases 4 sporozoites, which infect intestinal epithelial cells and transform into trophozoites, initiating the asexual phase of the life cycle (merogony). Trophozoites develop into type 1 meronts, which contain 8 merozoites. These merozoites are released and go on to infect more epithelial cells, where they can initiate another round of merogony, or become type II meronts, which are thought to initiate the sexual phase of the life cycle (gametogony). Type II meronts contain 4 merozoites; when these merozoites are released, they invade epithelial cells and are hypothesized to become either micro- or macrogamonts. There is no concrete proof of this, but it is clear by electron microscopy that there is a distinct life cycle stage with 4 merozoites (36). Microgamonts contain 16 parasites, which are released to fertilize macrogamonts, initiating oocyst development. Sporulation (sporozoite formation) occurs within the host cell, after which the oocyst is released into the intestinal lumen. Endogenous sporulation is unusual for a coccidian parasite; other coccidians like *Toxoplasma*, sporulate outside of the host in the environment.

Amazingly, Tyzzer's original publication on the discovery of *C. parvum* defined many basic features of the parasite life cycle that still hold true today (8) with some modifications. Tyzzer proposed a single round of schizogony (asexual merogony), and it was later discovered that type I meronts undergo multiple rounds of asexual replication, and there is also a separate

type II meront stage (36) that precedes sexual development. Additionally, while Tyzzer only identified one type of oocyst, there have been several reports of both "thick-" and "thin-walled" oocysts forming *in vivo* (36, 37). By transmission electron microscopy, thick-walled oocysts have an inner and outer wall that surround the sporozoites; these walls enable the oocyst to travel through the intestine unaltered and be excreted in the feces. Thin-walled oocysts have only one membrane, in addition to the host-derived parasitophorous vacuole membrane, surrounding the sporozoites and are hypothesized to rupture easily within the host intestine, starting another round of infection. Unlike thick-walled oocysts, thin-walled oocysts are not found in the feces. Thin-walled oocysts have been proposed to be the source of autoinfection that enables *Cryptosporidium* to grow for weeks and months in immunocompromised patients (36).

When *Cryptosporidium* infects a host cell, it does not invade the host cytoplasm like other apicomplexans; instead the parasite establishes itself in a "intracellular but extracytosolic" location in the apical region of the cell. After the parasite attaches itself to a cell, it actively invades (38) and becomes encapsulated by the host cell membrane, forming a parasitophorous vacuole or "sac" in the microvillous region of the enteric epithelial cell (39). The parasite membrane and host-derived vacuole membrane fuse at the base of the parasite (40) at the "zone of attachment", the region that separates the parasite from the host cell cytoplasm. This region contains a membranous structure with extensive folds that is the feeder organelle of the parasite (36, 41). It has been hypothesized that the feeder organelle membrane regulates nutrient uptake from the host cell cytoplasm (42) and is likely the location for the numerous nutrient transporters found in the *Cryptosporidium* genome (43, 44).

This unusual relationship with the host cell has caused discussion about *Cryptosporidium*'s grouping with the coccidia, a subclass of apicomplexans that includes other

pathogens like *Toxoplasma* and *Sarcocystis* (45). The "epicellular" location of *Cryptosporidium* is like that of gregarines, another group of apicomplexans distantly related to *Toxoplasma* and *Plasmodium*. Gregarines are intestinal parasites of invertebrates; they attach to the apical side of the host cell and take up the host's cytoplasm through a specialized feeding organelle. This process appears superficially similar to how *Cryptosporidium* gains its nutrients from the host, however, *Cryptosporidium*, unlike the gregarines, becomes overlaid by the host cell membrane during the infection process. There is genetic evidence from 18S small subunit ribosomal RNA sequencing that *Cryptosporidium* arose from a common alveolate ancestor shared with gregarines, forming a separate clade from the other major apicomplexan clade containing the coccidia (46). In addition to its unusual relationship with the host cell, *Cryptosporidium* is also atypical for a coccidian due to its autoinfective, thin-walled oocyst, lack of sporocyst within the oocyst, and its resistance to anticoccidial drugs (47). *Cryptosporidium* was originally grouped with the coccidia due to its similar life cycle, however, it is possible that *Cryptosporidium* is more distantly related to the coccidia then what was initially thought. It is important to keep this in mind when attempting to make inferences about *Cryptosporidium*'s biology from what we know about coccidian parasites in general.

Animal models of cryptosporidiosis

In general, there is no "simple" animal model for studying *Cryptosporidium* infection. The most clinically significant *Cryptosporidium* species are *C. parvum* and *C. hominis*, which do not cause productive oocyst shedding in adult immunocompetent mice (48, 49). There are two mouse-specific *Cryptosporidium* species, *C. muris* and *C. tyzzeri*, but there has been no significant interest in using one of these species as a model pathogen in mouse infections. *C.*

muris was identified by Tyzzer in the early 1900s and it infects the stomach (6) and not the small intestine. *C. tyzzeri* was more recently identified and appears to have a similar life cycle to *C. parvum* (50); it is possible that in future studies this parasite could be used as an animal model of disease, similar to mouse-specific *Plasmodium* species such as *P. berghei*.

Unlike adult mice, neonatal mice are susceptible to *C. parvum* (51-53). Specifically nursing mice are susceptible; mice that are 7-8 days old are the most consistent in terms of infection outcome (53). Weaned mice can become susceptible if they are given a protein-deficient diet in a model of malnutrition (54, 55), modeling the increased susceptibility to infection seen in malnourished children (56, 57). While both immunocompetent and genetically immunocompromised neonatal mice are susceptible, only immunocompromised mice develop prolonged infections (58-60). The neonatal mouse model has been used to assess the efficacy of anticryptosporidial agents *in vivo* (32, 61) and also to study the parasite life cycle (36, 62).

Adult mice are only susceptible to *C. parvum* if they are immunocompromised. SCID mice develop chronic infections with prolonged oocyst shedding and extraintestinal involvement, mimicking what is seen in AIDS patients (63, 64). Interferon-γ knockout mice are another model used to study cryptosporidiosis (65) and were recently used to develop a genetic system for *C. parvum* (66) and also evaluate new treatment candidates, such as a PI(4)K inhibitor (33) and bumped-kinase inhibitors (32). Immunocompromised mice are probably the most "accessible" of the different animal models available to study *C. parvum*, however, these models do not recapitulate one major aspect of human cryptosporidiosis: diarrhea. Therefore, it is difficult to study symptom alleviation in drug treatment studies using mice. Piglet and neonatal calf models develop the watery diarrhea and dehydration seen in human cases (67-69) and can be used to

study the efficacy of different treatment candidates (33, 67, 70); however, these large animal models are only routinely used by a few specialized labs.

C. parvum has all the above animal model options available; the options for *C. hominis*, the *Cryptosporidium* species that most commonly infects humans (2-4), are much more limited. *C. hominis* cannot infect mice but can infect guinea pigs, piglets and calves (71-73). Guinea pigs are not used frequently but have been used to test the efficacy of different drugs (74, 75). Gnotobiotic piglets are used by the Tzipori lab to passage the *C. hominis* TU502 strain, originally isolated from a child with diarrhea in sub-Saharan Africa (71); *C. hominis* oocysts can be obtained from piglets and used for challenge studies (76). The piglet model can also be used to evaluate drug efficacy against *C. hominis* (70, 77). Since a calf model has not been created, the piglet model is currently the only *in vivo* model for *C. hominis*; like the large animal models for *C. parvum*, it is only routinely used in very specialized labs and is not easily available to all researchers.

Cell culture models for *Cryptosporidium*

To date, no systems claiming continuous cultivation or complete life cycle development of *Cryptosporidium* have been independently verified. Therefore, most *in vitro* studies rely on cell culture platforms that support 2-3 days of growth, which rapidly declines as the parasite enters the sexual part of its life cycle. These cell culture platforms are mainly cancer cell lines of different origins. Most *in vitro* studies are done with *C. parvum* instead of *C. hominis* due to the limited availability of *C. hominis* oocysts. A brief overview of some of these *in vitro* systems is below.

C. parvum growth has been described in undifferentiated and differentiated HT-29 cells (human colorectal adenocarcinoma line), with growth being 5 to 6-fold better in differentiated cells, but still declining by day 5 post-infection (78). MDCK cells have been reported to be support asexual and sexual development of *C. parvum*, but not oocyst development (79). The MDCK model has been adapted by Arrowood and colleagues to investigate potential anticryptosporidial treatments (80-82). Upton and colleagues have developed a model using HCT-8 cells (human ileocecal adenocarcinoma line) (83-85). One group improved upon this model by finding that *C. parvum* infection lasted longer in "starved" cells in which the cell growth medium was not renewed for 7-14 days (86). HCT-8 cells have been used to investigate the interaction between *C. parvum* and host cells (87, 88), as well as define the *C. parvum* transcriptome during infection (89). Caco-2 cells (human adenocarcinoma cell line) have also been used to study *C. parvum* infection (44, 90, 91).

Complete development of *Cryptosporidium* in a cell-free culture system has been reported (92), but the results have not been replicated (93). It has been suggested the original images of developing *C. parvum* in axenic culture were misinterpreted and were likely budding yeast or another contaminant (94). At this time, axenic culture has not been used to evaluate drug efficacy against *Cryptosporidium* or any other investigation into parasite biology.

Recently, there have been three new models published claiming to support complete life cycle development of *C. parvum in vitro* (95-97); these models use adenocarcinoma lines but modify the cell culture platform to potentially support better *C. parvum* growth. For example, one system utilizes a hollow fiber cartridge with circulating medium to support HCT-8 cell growth (95). Within the cartridge, HCT-8 cells form monolayers around "lumens" and the composition of the medium inside and outside the lumen can be controlled separately. The

authors found that *C. parvum* grew optimally when the apical side of the HCT-8 cells was in a low redox environment, mimicking the low oxygen environment of the gut. The medium was also altered to include lipids that may be required for *Cryptosporidium* growth (98, 99). The authors found that this system sustained parasite growth for weeks, potentially months, and produced oocysts that were infectious to HCT-8 cells and immunocompromised mice. While this system is promising, it is unclear how reliable it is because it has not yet been replicated in another lab. The authors also claim to observe oocyst development in 24 hours in normal HCT-8 culture, something that is biologically improbable, considering the typical length of the complete *C. parvum* life cycle (3-6 days). Additionally, all perturbations to the system were done serially, instead of in parallel, to determine the optimal medium composition for *C. parvum* growth; for example, if two lipid mixes were tested, one mix was tested in the hollow fiber for 2 weeks, and then washed out, and the new mix was added after that. Oocyst development was then compared from the two time periods. This experimental design is likely out of necessity because the hollow fiber system is expensive and it is not practical to have multiple systems running to test each variable individually. However, this means that the final medium composition and recirculation settings the authors arrived at are not thoroughly tested. If the system can be replicated in another lab, it would be a great system for producing oocysts *in vitro* and possibly long-term drug experiments, but not necessarily a good system for any kind of biological investigation into the parasite. The monolayers on the hollow fibers cannot be accessed easily; to do any kind of microscopy or collect samples for RNA/DNA, the cartridge needs to be opened, which permanently ends the experiment. So, while this system has potential, its future role in *Cryptosporidium* investigation is unclear.

Another recently developed cell platform also utilizes a 3D scaffold to recreate the intestinal environment. This system relies on silk scaffolds with a hollow lumen; the lumen is populated with Caco-2 and HT29-MTX cells and the porous bulk space of the scaffold contains primary human intestinal myofibroblasts (H-InMyoFibs) (96, 100). Each cell type has a role: Caco-2 cells are "enterocyte-like"; HT29-MTX cells secrete mucus, replicating an important aspect of the intestinal environment; H-InMyoFibs secrete various growth factors and cytokines that help support cell viability. The 3D scaffold also enables the creation of an oxygen gradient across the cells in the lumen, mimicking the low oxygen environment of the intestine (100). This system, like the hollow fiber system, supported *C. parvum* growth and oocyst development. Additionally, infectious material from one scaffold could be propagated to another scaffold for at least three passages, potentially enabling continuous culture. This study did have some caveats; for example, parasite growth was measured by 18S RNA levels, which remained stable over a 15-day period but did not show any amplification from the day 1 values, making it unclear how much parasite growth was happening. Also, the evidence for passaged infection was only presented as microscopy, there was no quantitative data showing the level of infection for each passage. If the system can support continuous passage, it would greatly facilitate genetic modification of *C. parvum*, which is currently possible but requires the use of animal to generate infectious transgenic oocysts (66). However, the system does rely on specialized equipment to create the porous silk scaffolds, so it is unclear how easily the system can be set up in a new lab. Like the hollow fiber system, this platform has promise if the results can be replicated by other researchers.

The most recently published system is simpler than the other two systems; it only relies on the COLO-680N cell line, which is a human squamous cell carcinoma line derived from the

esophagus (97). This line has not previously been tested for its ability to support *C. parvum* growth. The authors found that COLO cells supported *C. parvum* oocyst development, and that oocysts purified from cell culture could be used to infect fresh cell cultures, thereby propagating the infection (97). Additionally, infected COLO cells could be frozen by traditional cryopreservation methods, thawed at a later date, and oocyst production would begin again within three days. This development is especially interesting because currently there is no way to preserve *Cryptosporidium* oocysts, requiring researchers to continually purify oocysts from animal sources in order to maintain viable stocks. This system, if replicable, would be the easiest for other labs to adopt, since it requires no special equipment or growth medium. However, the study has several caveats: like the hollow fiber study, the authors report oocyst development by HCT-8 cells, something that has not been seen by other researchers; also, the evidence for propagation is the presence of *C. parvum* 18S RNA, shown as a cDNA band in a gel – there is no quantitative PCR. There are also no low magnification images of infected cell cultures to demonstrate the density of infection, only small images showing individual parasites. This system could be a great boon to the *Cryptosporidium* research community if it can be reproduced by other labs; it is an inexpensive and accessible system that would facilitate many kinds of studies.

Since *Cryptosporidium* was first recognized as a public health threat in the 1980s (101, 102), there have been claims of complete life cycle development and continuous propagation *in vitro* and *ex vivo* (37, 103, 104), but no system has proven to be reproducible. The three new systems described here have unique advantages and disadvantages and could all have a role in enabling new lines of investigation into *Cryptosporidium*. However, their true utility cannot be determined until their results are replicated by other hands. The lack of an *in vitro* culture system

has hindered *Cryptosporidium* for the past several decades but hopefully the renewed interest in cryptosporidiosis (28) will instigate a reexamination of the approach to developing a cell culture platform for this parasite.

Anti-*Cryptosporidium* antibodies

The various obstacles stalling *Cryptosporidium* research (difficult animal models, lack of culture system) has led to a general absence of tools for investigators. For example, there are very few anti-*Cryptosporidium* antibodies publicly available, making microscopy-based studies difficult. For a lab beginning to investigate *Cryptosporidium*, it can take a significant amount of time to understand the progression of the parasite life cycle *in vitro* without markers designating specific life cycle stages. Currently, the only published "visual maps" of the parasite life cycle are based on electron microscopy (36) or bright field images (105), or, most commonly, authors enumerate different life cycle stages without providing any images (86).

There are two commercially available antibodies that many researchers rely on: Sporo-Glo™ and Crypt-a-Glo™ (Waterborne, Inc); the former is a rat polyclonal antibody raised against sporozoites that broadly recognizes all life cycle stages, the latter is a mouse monoclonal antibody raised against oocyst wall proteins that recognizes oocysts. Sporo-glo™ is very useful due to its broad reactivity and is used in many microscopy-based inhibitor studies (88, 106, 107). However, it has limited usefulness in enabling the researcher to detect specific life cycle stages without familiarity of other stage markers, such as size, nuclei number, and timing of appearance. Crypt-a-glo™ is primarily intended as a tool to detect oocyst contamination of water supplies, but it has also been used to evaluate the ability of different cell culture systems to produce oocysts (96, 97).

Antibodies that have been made against *Cryptosporidium* have been raised against extracellular stages (sporozoites, oocysts) or specific recombinant proteins. The former approach has aided in the discovery of proteins that likely have a role in parasite motility and invasion. For example, 4E9 is a monoclonal antibody raised against fixed whole sporozoites that can block *C. parvum* sporozoite attachment and invasion (108). It also shows reactivity against material shed by sporozoites during gliding motility (108). By western blot, 4E9 recognizes two glycoproteins, gp40 and GP900. After the identification of gp40 by 4E9, researchers cloned and sequenced the gene encoding gp40 (109) and discovered the gene also encoded a previously-identified protein, gp15 (110, 111), that is also hypothesized to be involved in parasite motility. Without an accessible genetics system, it is difficult to investigate the role of gp40 and gp15 in *C. parvum* further, but these antibody-based studies have been successful in identifying the two proteins as important targets. 4E9 has also been useful in assessing *C. parvum* life cycle progression in a novel cell culture platform (96).

Antibodies against specific recombinant proteins have been made to investigate the function of various proteins during the parasite life cycle. Usually these studies follow one of two approaches: identifying a gene of interest, then creating the recombinant protein and specific antibody (44), or identifying a protein of interest first by affinity chromatography (112). CpABC, a putative transporter of large organic anions, was identified using the first approach (44); antisera to recombinant CpABC localized it to the host-parasite interface, providing additional evidence that this interface is the location of the parasite "feeder organelle" (44). Gal-affinity chromatography has been used to identify lectins on the sporozoite surface; purification of one of these lectins led to the identification of the p30 gene and protein (112). Antisera to p30 revealed that it can associate with the previously mentioned gp40 and GP900 proteins (112), suggesting it

has a role in parasite motility. Both of these approaches to gene/protein function discovery have led to important findings about *C. parvum* biology, but as said above, it is difficult to pursue further studies without an accessible genetics system.

Antibodies raised against whole parasites and recombinant proteins have been very useful to the *Cryptosporidium* field, but there is room for improvement in terms of identifying life cycle markers. This gap in knowledge may be due in part to the fact that it has been impossible to make antibodies against intracellular stages specifically; the adenocarcinoma cell lines that support *C. parvum* growth are all human-derived, so immunization of mice with infected cellular material would lead to the creation of host-specific antibodies. In order to create novel antibodies against intracellular parasite stages, it will be necessary to identify a murine cell line that supports robust parasite growth.

Advancements in intestinal stem cell culture

The epithelial lining of the small intestine is organized into crypts and villi; the lining turns over every 3-5 days in the mouse, a process driven by cell proliferation in the crypts and balanced by apoptosis at the villi (113). Self-renewing stem cells, identified by expression of *LGR5* (114), a GPCR (115, 116) that is part of the Wnt signaling pathway (117), are located at the crypt base (114, 118). These stem cells produce rapidly dividing transit-amplifying cells that give rise to all the differentiated cell types of the intestine, which migrate up the crypt-villus axis (113).

In the last decade it has become possible to propagate intestinal stem cells *in vitro* due to advancements in understanding the growth requirements of the intestinal epithelium. Specifically, Wnt signaling is necessary for crypt proliferation (119), overexpression of Noggin

drives expansion of crypt numbers (120), and isolated intestinal epithelial cells will undergo anoikis if cell-cell and cell-matrix contacts are disrupted (121). The first two discoveries led to the inclusion of different growth factors, such as Wnt3a, noggin, and R-spondin 3 (Wnt agonist), in the medium used to grow stem cells (122-125) and the latter finding led researchers to using Matrigel, a mix of basement membrane proteins extracted from the EHS mouse sarcoma, as a growth substrate in order to prevent apoptosis (122, 125).

There are various platforms available to propagate stem cells which differ in terms of medium composition and whether the cells are grown as organoids or spheroids. Organoids are a mix of stem cells and differentiated cells and are grown in medium containing Wnt3a, R-spondin 1, and Noggin (122). Spheroids are enriched for stem cells and are grown in medium containing Wnt3a, R-spondin-3, and Noggin (125, 126). Systemic doses of R-spondin 1 induce crypt cell proliferation in mice (127), but R-spondin 3 is expressed by intestinal mesenchymal cells (125, 128) and therefore may be the more relevant R-spondin family member for intestinal stem cells, partially explaining the difference in the two culture systems. In both cases, the Wnts and R-spondins enhance canonical Wnt signaling, which is necessary for self-renewal of stem cells (129) and noggin, a BMP signaling inhibitor (120), has been found to be necessary to passage small intestinal organoids *in vitro* (122).

Initially, the growth factors required for stem cell proliferation had to be added to the medium separately, as recombinant proteins, making the medium very expensive (122). The creation of the L-WRN cell line, which secretes biologically active Wnt3a, R-spondin 3, and noggin (125), made this method unnecessary. The L-WRN line is a modification of the L-Wnt3a line, an L cell (neuroendocrine cell found in small intestine) line modified to secrete Wnt3a

(130). The L-WRN cell line can be used to create “conditioned medium” containing the required factors; this medium is then used to propagate intestinal stem cells as spheroids (125, 126).

Primary cell monolayers can be derived from spheroids in order to study intestinal function in a 2D model. Spheroids are trypsinized and plated onto a transwell membrane coated with Matrigel; L-WRN conditioned medium is removed and replaced with growth medium lacking stem cell growth factors in order to induce cell differentiation (131). These monolayers are polarized and contain the major intestinal epithelial lineages such as enterocytes and secretory cells (enteroendocrine, goblet, Paneth). These monolayers lose their proliferative potential and therefore only maintain viability for about 2-3 days. This system can be used to study aspects of intestinal function, such as IgA transcytosis across the epithelial cell layer (131).

In the last several years, a new method for creating primary intestinal monolayers from spheroids has been developed. This system differs from the above method in three major ways: inclusion of a feeder cell layer in addition to the Matrigel coating, continuous exposure to stem cell growth factors, and the creation of an air-liquid interface (ALI) at the surface of the cells (132). In this system, spheroids are trypsinized and plated onto the feeder cell layer in a Matrigel-coated transwell. The monolayer is grown in medium containing stem cell growth factors such as R-spondin 1 and Noggin. After 7 days of growth, the medium in the top chamber is removed, creating the ALI. This triggers a dramatic differentiation of the cells, leading to development of enterocytes and other differentiated cells such as goblet cells; there is even formation of structures resembling crypts (132). The mechanism behind ALI inducing differentiation is unclear, however, ALI has historically been used to improve differentiation of airway tract epithelial monolayers (133-135). ALI has recently been used in intestinal epithelial cell culture, causing major metabolic changes and also upregulation of markers associated with

cell differentiation (136, 137). Monolayers with ALI maintain viability for weeks because a portion of the monolayer continues to proliferate, replacing cells as they undergo apoptosis (132). This long-term proliferation is likely due to maintaining the cells in stem cell growth medium. The differentiation status and long-term viability of these monolayers makes them a great candidate for modeling the intestinal environment.

Aim and scope of thesis

The central aim of this thesis was to use the recent advancements in stem cell culture to develop a platform for *C. parvum* growth and development *in vitro*. The majority of cell culture systems currently used to study *Cryptosporidium* infection rely on cancer cell lines that do not resemble the intestinal epithelial cell the parasite encounters *in vivo*. The use of transformed cell lines likely explains why attempts to achieve propagation or complete life cycle development of *C. parvum in vitro* have failed. Recent systems claiming continuous culture and oocyst development also use cancer cell lines (HCT-8 or COLO-680N) to serve as "enterocytes" (95-97); the reproducibility of these systems has yet to be demonstrated. A primary cell culture system with intestinal epithelial cells would provide a great model for investigating *C. parvum*'s interactions with the host cell, and potentially support complete life development.

Propagating intestinal stem cells as spheroids using L-WRN conditioned medium was first developed using mouse cells (125, 126) and then later adapted to human cells (138). These stem cells can be induced to differentiate into enterocytes and secretory cells by plating them on transwell membranes and changing the medium composition (131, 138). The mouse and human monolayers created using this method only survive 3 or 6 days, respectively (131, 138). The viability of these monolayers could be improved by incorporating aspects of the model described by Wang *et al* (132), which creates primary monolayers that continue to proliferate for weeks. This model uses medium containing stem cell growth factors and creates an air-liquid interface at the surface of cells to induce differentiation. The main aim of this thesis was to test monolayers developed using this method for their ability to support *C. parvum* growth and oocyst development.

Even though adult, non-immunocompromised mice are resistant to *C. parvum* infection, this thesis focused on monolayers created using stem cells isolated from the small intestine of adult C57BL/6 mice. We hypothesized that murine monolayers would be susceptible to infection because they lack the cellular and humoral immunity of the whole animal. Additionally, creating a platform for robust *C. parvum* growth in mouse cells would potentially enable us to create novel antibodies against intracellular stages of *C. parvum* by immunizing mice with infected cells, something not previously possible.

An *in vitro* culture system that has the major lineages of the intestinal epithelium as well as long-term viability could be the key to unlocking *Cryptosporidium* development *in vitro*. Developing and characterizing this system would support future investigation into *Cryptosporidium* biology, such as host-receptor interactions, role of metabolism in infection, and the efficacy of potential treatment options. Additionally, if this system could be used to generate novel antibodies against different life cycle stages, it would be filling in a major reagent gap in the field. Essentially, this thesis aims to create two tools for *Cryptosporidium* research: a platform for growth and unique antibodies against all life cycle stages.

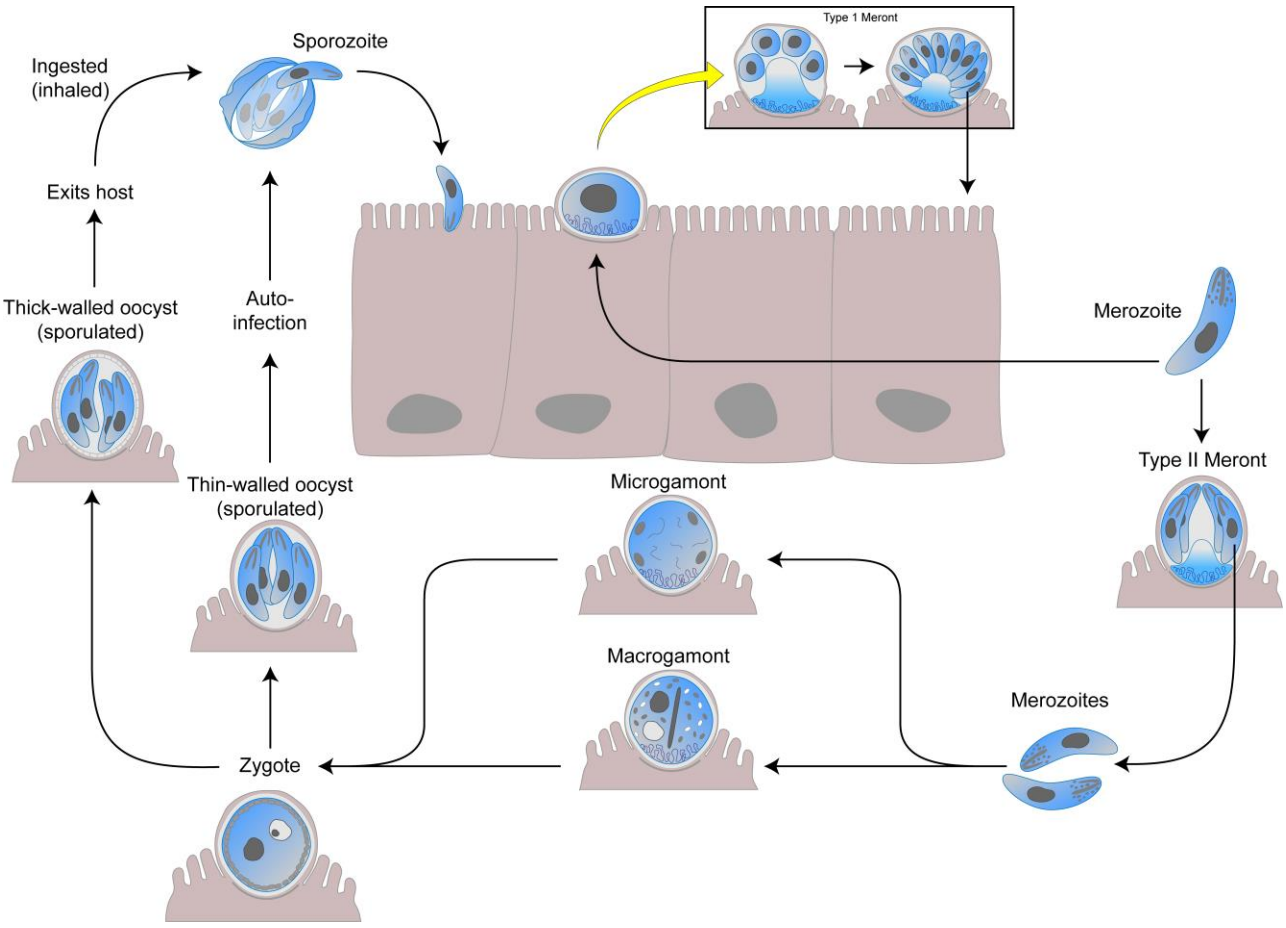

Figure 1.1. Life cycle of *Cryptosporidium parvum*.

Cartoon depicting the life cycle of *C. parvum* (courtesy of Laura Kyro, reproduced with permission). A host becomes infected when they ingest oocysts. The oocysts travel through the stomach and excyst in the small intestine, releasing 4 sporozoites. The sporozoites invade the epithelial cells of the intestinal lining and develop into trophozoites, residing in a host membrane-enclosed vacuole in an "intracellular but extracytoplasmic" niche in the apical region of the cell. Trophozoites develop into type I meronts, which contain 8 merozoites when mature. The merozoites are released and they can either initiate another round of asexual development by becoming trophozoites or initiate the sexual part of the life cycle by becoming type II meronts.

Mature type II meronts contain 4 merozoites, these are released and become micro- or macrogamonts. Microgamonts fertilize macrogamonts, which develop into zygotes and eventually thin- or thick-walled oocysts. Thin-walled oocysts are believed to rupture within the intestine, initiating another round of infection, while thick-walled oocysts exit the host to spread the infection.

Chapter 2

Monoclonal antibodies to intracellular stages of *Cryptosporidium parvum* define life cycle progression *in vitro*

Preface

GW and KLVD optimized mIEC culture system for *C. parvum* infection. GW, SR, QW, and JB generated and characterized the hybridomas. SR subcloned the hybridomas. GW, SR, and LFJ performed immunofluorescence staining analysis, TBK, MSK, and KLVD provided key biological reagents and advice; TSS and LDS provided advice and supervision; GW and LDS wrote the paper with input from all authors.

This chapter has previously been published:

Wilke, G.*, Ravindran, S.*, Funkhouser-Jones, L.*, Barks, J., Wang, Q., VanDussen, K.L., Stappenbeck, T.S., Kuhlenschmidt, T.B., Kuhlenschmidt, M.S., Sibley, L.D. (2018). Monoclonal antibodies to intracellular stages of *Cryptosporidium parvum* define life cycle progression *in vitro*. *mSphere*. pii: e00124-18. Print 2018 Jun 27.

* equal contribution

Summary

Among the obstacles hindering *Cryptosporidium* research is the lack of an *in vitro* culture system that supports complete life development and propagation. This major barrier has led to shortage of widely available anti-*Cryptosporidium* antibodies, and a lack of markers for staging developmental progression. Previously developed antibodies against *Cryptosporidium* were raised against extracellular stages or recombinant proteins, leading to antibodies with limited reactivity across the parasite life cycle. Here we sought to create antibodies that recognize novel epitopes that could be used to define intracellular development. We identified a mouse epithelial cell line that supported *C. parvum* growth, enabling immunization of mice with infected cells to create a bank of monoclonal antibodies (mAbs) against intracellular parasite stages while avoiding the development of host-specific antibodies. From this bank, we identified 12 antibodies with a range of reactivity across the parasite life cycle. Importantly, we identified specific mAbs that can distinguish different life cycle stages, such as trophozoites, merozoites, type I vs. II meronts and macrogamonts. These mAbs provide valuable tools for the *Cryptosporidium* research community and will facilitate future investigation into parasite biology.

Introduction

Cryptosporidium is a genus of protozoan parasites that causes diarrheal disease (cryptosporidiosis) in humans and other animals. Over 20 species are recognized, but the majority of human cases is caused by *C. parvum* or *C. hominis* (1). For decades, *Cryptosporidium* was mainly recognized as a cause of chronic diarrhea in patients immunocompromised from HIV/AIDS (139). However, an investigation into the etiologies of diarrheal illnesses in children in Africa and South Asia found that *Cryptosporidium* is second only to rotavirus as a cause of diarrhea in infants in these regions (19). Since diarrheal disease is a significant cause of child mortality (26), this discovery has led to increased interest in cryptosporidiosis and a reexamination of the barriers to studying *Cryptosporidium* (28). The main obstacle hindering research on this parasite is that it cannot be propagated *in vitro* and instead must be passaged through large animals such as calves to generate infectious oocysts. *C. parvum* can also infect mice, although susceptible mouse models are limited to immunodeficient (140) or neonatal animals (141). Current cell culture models rely on human adenocarcinoma cell lines (e.g. Caco-2, HCT-8) that do not support complete life cycle development (142). Without the ability to propagate, clonal lines cannot be established and *in vitro* studies are restricted to studying limited rounds of asexual replication and incomplete sexual development. Genetic manipulation is possible if the parasites are passed through immunocompromised mice (66), however it is not feasible to examine the cellular basis of complex phenotypes without a parallel *in vitro* system for development.

Cryptosporidium has a complex life cycle consisting of both an asexual phase (merogony) and a sexual phase (gametogony) that culminates in oocyst formation (143). There are a limited number of antibodies that identify different life cycle stages of *Cryptosporidium*,

especially intracellular stages. In part, this limitation is due to the fact that antibodies have typically been generated against extracellular stages such as oocysts (144) and sporozoites (108), and many of these recognize widely conserved epitopes found in intracellular stages (145). For example, it has been reported that epitopes shared on gp60, a glycoprotein involved in parasite adhesion to host cells, and its processed components of gp15 and gp45, are expressed on both sporozoites and merozoites (110, 111, 146). Antibodies have also been made against specific proteins (44, 112, 146); however this method of antibody production does not typically allow for the discovery of novel antigens. Additionally, many antibodies previously raised against *Cryptosporidium* were made in rabbits (44, 146, 147), which is a non-renewable source of antibody. Collectively, these available reagents do not allow the specific life cycle stages to be clearly delineated with unique markers, confounding attempts to track development during *in vitro* growth.

Our goal was to create a mouse hybridoma bank against *Cryptosporidium* to provide reagents to easily identify life stages, discover new antigens and provide a renewable reagent source. One barrier to making antibodies against intracellular stages of *Cryptosporidium* is that there is no mouse cell line that supports robust parasite growth (142). Although human adenocarcinoma lines allow for limited intracellular growth, immunizing with culture material derived from such heterologous sources would likely generate many host-specific antibodies. Here, we tested primary murine ileal epithelial cells (IECs) and found that *C. parvum* underwent efficient amplification in these cells. The use of mouse IECs allowed us to immunize mice with infected cell lysates without the risk of generating host-specific antibodies. Using this strategy, we created a hybridoma bank expressing novel monoclonal antibodies (mAbs) against intracellular parasite stages. By examining the timing of expression and patterns of staining, we

identified antibodies with distinctive reactivity against specific life cycle stages, such as trophozoites, merozoites, type I and II meronts, and macrogamonts. Collectively, this "antibody toolkit" should lead to a deeper understanding of parasite biology and foster efforts to define conditions for complete development and propagation *in vitro*.

Results and discussion

Establishing a mouse hybridoma bank against C. parvum

We initially sought to identify a mouse cell type that would support robust parasite growth *in vitro*. It has been reported that bovine and human isolates of *Cryptosporidium* will grow in mouse L929 fibroblasts (148) and peritoneal macrophages (149), but these cell types are not commonly infected *in vivo.* Instead, *Cryptosporidium* spp. primarily grows in the epithelial cells of the small intestine (150). Recent developments have shown that mouse intestinal stem cells can be maintained in culture as spheroids using media containing a cocktail of specific growth factors (126). When these stem cells are grown as monolayers on transwells, they develop into polarized epithelial monolayers that include enteroendocrine cells, Paneth cells, mucin-producing goblet cells, and enterocytes (131). As shown previously, these different lineages are present in the monolayers at rates similar to what is found in the mouse intestine (131). Such monolayers could provide a much more natural niche for growth of *C. parvum* than typical transformed cell lines. Consequently, we tested primary mouse ileal epithelial cells (mIECs) that were differentiated from intestinal stem cells for their ability to support *C. parvum* growth *in vitro*. *C. parvum* was able to achieve high levels of amplification over a 3-day period in mIECs grown in transwells as shown by qPCR (Figure 2.1).

Having successfully identified a mouse cell line that supported robust development of *C. parvum*, we immunized mice with infected mIEC lysates, performed a fusion, and screened the resulting hybridomas by microscopy to identify novel antibodies to *C. parvum*. Following sequential subcloning, individual monoclonal antibodies (mAbs) were screened on infected mIECs and HCT-8 cells to investigate their reactivity against different life cycle stages of *C. parvum*. To monitor *C. parvum* infection, we stained the monolayers with a rabbit polyclonal

antibody raised against the *Toxoplasma gondii* strain RH that was broadly cross-reactive to *C. parvum* antigens based on western blot (Figure 2.2). As shown in Figure 2.3, this anti-RH antibody (labeled "Cp" in figures) recognized both asexual and sexual stages of *C. parvum* by immunofluorescence (IFA).

Starting from a total of 31 mAbs, we identified 12 antibodies with distinctive staining patterns (Table 1). Other mAbs with positive reactivity showed similar patterns to those described here and therefore they were not pursued further. Overall, most mAbs reacted to multiple stages (see table 1, Figure 2.4, Figure 2.5), suggesting that they recognize epitopes that are expressed broadly across the intracellular life cycle. We identified one antibody, 1E12, that recognized every life stage, excluding oocysts (table 1, Figure 2.4, Figure 2.5). Based on its reactivity pattern, 1E12 recognizes an epitope associated with the membrane of all life cycle stages (figure 2.3). Due to its broad spectrum and membrane pattern of reactivity, 1E12 can be used to identify specific stages based on appearance, size, and number of nuclei. For example, 1E12 can be used to distinguished type I meronts, which have 4 nuclei but a single cytoplasmic mass (figure 2.3B), from type II meronts, which have four nuclei, but have separated into 4 distinct merozoites (figure 2.3D). MAb 1E12 also stains the surface of type I merozoites (figure 2.3C), allowing mature type I meronts to be clearly distinguished from immature type I meronts. MAb 1E12 also recognized the membrane of macrogamonts (figure 2.3E) and one end of the small microgametocytes within the microgamont (figure 2.3F).

MAb 1E12 has great utility as a "pan-crypto" antibody; it can be used to easily assess the ability of different cell culture platforms to support *Cryptosporidium* growth as it recognized all the major stages, which are distinguishable by their surface morphology. Other antibodies identified through the screen did not have this broad reactivity but rather identified specific life

cycle stages in distinguishable patterns, making them useful for understanding life cycle progression in different culture systems. These antibodies are described in detail below.

mAb 1B6 recognizes the oocyst outer wall

Only one antibody from the hybridoma library was specific for a single stage; mAb 1B6 only recognized oocysts and did not show any reactivity towards asexual (Figure 2.4, Figure 2.5) or sexual stages (table 1). MAb 1B6 detected residual oocysts from the inoculum that were present in mIECs (Figure 2.4). MAb 1B6 stained the oocyst wall in a continuous pattern (Figure 2.6), similar to Crypt-a-glo^{TM}, a commercial reagent that is an oocyst-specific monoclonal antibody (Waterborne Inc.) (151). MAb 1B6 equally recognized oocysts that were either left unstimulated or stimulated to excyst (Figure 2.6), suggesting it recognizes an epitope on the outer wall of the oocyst. MAb 1B6 preferentially stained bleached oocysts (figure 2.6), a process that removes the outer veil (152). Based on this result, it is likely that bleach treatment removes the veil and exposes the 1B6 epitope on the outer wall. Interestingly, 1B6 did not stain macrogamonts (table 1), unlike the previously described mAb OW50, which also reacts to an outer oocyst wall protein, and stains wall-forming bodies in mature macrogamonts (153).

mAbs 1B5 and 1F9 have distinctive trophozoite-specific patterns

Although many of the antibodies generated here react to multiple life cycle stages, they still provide markers for defining development due to the unique patterns of staining they detect in specific stages. For example, mAbs 1B5 and 1F9 detect a distinctive “doughnut-shaped” pattern in trophozoites during the initial stages of asexual development (Figure 2.7C, E). Although both mAbs have a circular staining pattern on trophozoites, 1B5 staining has a smooth,

continuous appearance while 1F9 is punctate, implying the two antibodies recognize different epitopes. While 1F9 did not show reactivity by western blot, 1B5 recognized a 230 kDa product in sporozoites (Figure 2.2).

When images of trophozoites were acquired by laser scanning confocal microscopy and the Z-stacks were rendered in 3D, the resulting images revealed that the epitope recognized by 1B5 is mostly confined to the base of the parasite where it contacts the host cell, while 1F9 staining begins at the base and extends up the side of the vacuole or parasite membrane (Figure 2.7D, F). Because these antibodies have a polarized recognition pattern in sporozoites (Figure 2.8), their targets likely relocalize following invasion to this interface during initial trophozoite growth.

The host-parasite interface is where the host cytoskeleton is reorganized into an actin-rich pedestal during intracellular development (154-156). When infected HCT-8 cells were stained with fluorescently labeled phalloidin to visualize this actin pedestal, labeling with 1B5 and 1F9 revealed that both mAbs formed a ring around the nascent pedestal in trophozoites (Figure 2.9A). Examination of Z-slices generated by laser scanning confocal microscopy revealed that the ring formed by 1B5 is within the same plane as the pedestal, whereas the 1F9-labeled ring is positioned above the pedestal (Figure 2.9A). As trophozoites develop into meronts, the epitopes recognized by 1B5 and 1F9 redistributed, leading to more diffuse labeling that was no longer confined to the base of the parasite (Figure 2.9B, table 1, Figure 2.4).

The host-parasite interface is also the site where the parasite elaborates a membrane-rich feeder organelle (157) (Figure 2.7A). The nature of this feeder organelle is uncertain, although the genomes of *C. parvum* (43) and *C. hominis* (158) contain a large number of transporters and it has been speculated that this interface is responsible for transport of nutrients from the host

(159). Consistent with this, a *C. parvum* ATP-binding cassette protein that shares features with transporters has previously been localized to this interface (44). Attempts to localize the epitopes recognized by 1B5 or 1F9 using immunoelectron microscopy were not successful, however, based on their localization pattern in trophozoites by fluorescent microscopy, it is possible that the targets recognized by either mAb are involved in the reorganization of the host cytoskeleton and the generation of the feeder organelle. Hence, these mAbs may facilitate future investigation into these two developmental processes.

mAb 5E3 recognizes mature type I merozoites in a polarized manner

Moving forward in the parasite life cycle, the parasite progresses through asexual development to replicate mitotically and generate 8 mature merozoites within type I meronts (Figure 2.10A). Transmission electron microscopy reveals that the apical end of merozoites in mature type I meronts is characterized by many small secretory vesicles corresponding to micronemes and cross-sections of rhoptries (Figure 2.10B, C), similar to what is seen in sporozoites (160). Four mAbs (1A5, 1A12, 5E3, 5F7) recognized both type I and type II merozoites in a distinctive polarized pattern reminiscent of this apical specialization (Table 1) and these mAbs, along with others, also stain the apical end of sporozoites (Figure 2.8). An example of this polarized staining pattern is shown for 5E3 staining of fully developed merozoites in mature type I meronts (Figure 2.10E, F, Figure 2.5). mAb 5E3 was also able to recognize immature type I meronts, where the epitope is fainter and distributed along the membrane (Table 1) from mature type I meronts that contain 8 merozoites, which demonstrate strong polarized staining (Figure 2.5). Three-dimensional rendering of Z-stacks acquired by laser scanning confocal microscopy revealed that the epitope recognized by 5E3 is concentrated at one

end of the parasite (Figure 2.10E, F). This polarized pattern is similar to that of a previously published mouse monoclonal 4E9, which stains the apical end of sporozoites and also recognizes trails of protein shed by the sporozoite during gliding motility (108). Attempts to label the apical end of sporozoites directly with 5E3 by immunoelectron microscopy were unsuccessful, but based on its recognition pattern by fluorescence microscopy, it is likely that mAb 5E3, and other antibodies that stain in a highly polarized pattern (Table 1), recognize components of apical secretory organelles, which are implicated in host cell attachment and invasion (161, 162).

Antibodies that distinguish type I from type II meronts

The life cycle of *Cryptosporidium* spp. proceeds through two rounds of merogony, the first of which culminates in eight merozoites (type I), while the second terminates with four merozoites (type II) (157). Because the type I merogony cycle also proceeds through a 4 nuclear stage, it can be difficult to distinguish these immature type I stages from mature type II stages based on the number of nuclei alone. To identify antibodies that recognize type II meronts, we established a method to reliably distinguish type II meronts, which contain 4 nuclei within mature merozoites, from "early stage" or immature type I meronts, which can also contain 4 nuclei. To distinguish between these stages, we pulse-labeled parasites growing in HCT-8 cells using EdU, which labels replicating DNA (66), and detected incorporation fluorescently using click labeling (see methods). By adding EdU in specific intervals after infection, we identified actively replicating stages that were further defined by nuclear morphology and number. Type II meronts were most commonly detected from 30-32 hr post-infection. When EdU was added during this 2 hr interval, type II meronts were identified by the presence of 4 nuclei that lacked

EdU positivity, as they were mature and no longer replicating, whereas 4 nuclei type I meronts were EdU positive because they were still actively replicating (Figure 2.11).

Based on differential EdU labeling, we identified several antibodies that recognized type II meronts with different staining patterns (Table 1). For example, mAb 1A5 did not stain immature type 1 meronts (Figure 2.11A) but did stain mature type I (Figure 2.11B) and type II (Figure 2.11C) meronts. Because of this pattern of reactivity, mAb 1A5 can be used to positively identify type II meronts from immature type I meronts, which also contain 4 nuclei. By western blot, 1A5 recognized a 125 kDa band (Figure 2.2) and this protein serves as a marker of mature merozoites, whether they are type I or II.

Despite their superficial similarity, merozoites produced by these two rounds of merogony have different fates. Type I merozoites are thought to reinitiate multiple rounds of asexual replication, while type II merozoites are thought to give rise to gamonts (143). Unfortunately we did not identify any mAbs that only stain type II meronts, nor have such reagents been described previously, although differences have been detected by ultrastructure (157). Consequently, the ability to track type II meronts using mAbs like 1A5 combined with EdU staining provides a convenient means of monitoring development of stages that are committed to undergo sexual development.

Antibodies that distinguish sexual stage development

Merozoites released by type II meronts are thought to give rise to micro- and macrogamonts, which eventually undergo fertilization to form oocysts, although this last step does not occur efficiently *in vitro*. The majority of mAbs studied here did not recognize sexual stages, with two exceptions (table 1). For example, mAbs 1A5 and 1B5 broadly stain asexual

stages but fail to stain either micro- or macrogamonts (table 1). The membrane-reactive mAb 1E12 did stain the membranes of both microgamonts and macrogamonts (figure 2.3, table 1), although the staining of macrogamonts did not provide a unique recognition pattern that differentiated it from asexual stages such as meronts. In contrast, mAb 4D8 showed a characteristic "V" (figure 2.12C) or line pattern (figure 2.12D) in macrogamonts (table 1), a reactivity pattern not reported in any published studies with other *Cryptosporidium* antibodies. When examined by transmission electron microscopy, macrogamonts were found to contain a prominent striated fiber running through the center of the cytoplasm (figure 2.12B). This striated fiber is not seen in all thin sections, possibly explaining why some electron microscopy studies of *in vivo* infection do not mention the fiber at all (157) and only one published study contains an image of a macrogamont with a fiber, although it is not described in detail (163). Attempts to label the fiber directly with 4D8 by immunoelectron microscopy were not successful, so while we cannot definitively say 4D8 recognizes this structure, it seems highly likely based on its appearance. The molecular nature of this striated fiber is also uncertain, as the streamlined genome of *C. parvum* contains homologs for tubulin, actin, and several actin-related proteins (http://cryptoDB.org). The genome also contains orthologues of articulins, which are known in other apicomplexans as inner membrane complex proteins (IMCs) (164), although they are not annotated as such in *C. parvum* (http://cryptoDB.org). The striated fiber observed in macrogamonts does not resemble microtubules that are typically found apically, or the meshwork of IMC proteins that are localized under the membrane of motile stages (164). Hence, this striated fiber may represent a novel assemblage of actin filaments, or a novel cytoskeletal element that imparts some form of structural integrity within macrogamonts. Currently, macrogamonts are recognized by their size and diffuse nucleus. In contrast, the staining pattern

of 4D8 provides definitive marker for this stage based on the strongly striated pattern, while it stains other stages much more diffusely (Figure 2.5).

We did not identify any antibodies that specifically stain microgamonts, although they are recognizable by their many small nuclei, which number 16 in mature microgamonts (figure 2.12E). These small, replicating nuclei were easily visualized using a commercially available anti-phospho-histone H3 antibody (figure 2.12G), which stains DNA during mitosis (165), or through the incorporation of EdU during DNA replication (figure 2.12H).

Conclusions

Previous studies on the development of *C. parvum* in vitro have been hampered both by the lack of an efficient *in vitro* system for propagation and lack of specific reagents to stage development. We have taken advantage of developments in stem cell biology to propagate *C. parvum* in mouse IECs, which more closely resemble the intestinal cells that support growth *in vivo* compared to adenocarcinoma cell lines. Although attempts to achieve complete development of *C. parvum* in mIECs are ongoing, here we have used this system to generate antigens for production of novel mAbs to intracellular stages. This approach has been effective at generating reagents that define stage-specific patterns of expression, which greatly enhances our ability to define specific stages during *in vitro* growth. Collectively these reagents should be useful for future studies to 1) define developmental progression during *in vitro* culture, 2) identify conditions necessary to support complete development *in vitro*, and 3) pinpoint the stages that are susceptible to chemotherapy, thereby supporting efforts at target identification.

Materials and methods

Ethics Statement

Animal studies were conducted according to the U.S.A. Public Health Service Policy on Humane Care and Use of Laboratory Animals. Animals were maintained in an Association for Assessment and Accreditation of Laboratory Animal Care – approved facilities. Animal studies were approved by the Institutional Animal Studies Committee at the School of Medicine, Washington University in St. Louis, protocol number 20170163.

Adenocarcinoma cell culture

Human ileocecal adenocarcinoma cells (HCT-8; CCL-244^{TM} ATCC) were maintained in RPMI-1640 medium (Gibco, ATCC modification) supplemented with 10% FBS. Human colorectal adenocarcinoma cells (Caco-2; HTB-37^{TM} ATCC) were maintained in Minimum Essential Medium (Corning CellGro) supplemented with 20% FBS. Cell lines were tested for the presence of mycoplasma and confirmed negative with the e-Myco plus Mycoplasma PCR Detection Kit (Boca Scientific).

3D spheroid cell culture

Primary ileal epithelial stem cells isolated from 8-10 week old C57BL/6 mice were obtained from the laboratory of Dr. Thad Stappenbeck, Washington University in St. Louis. Ileal stem cells were expanded and maintained as 3D spheroid cultures in Matrigel (BD Biosciences), as described previously (125). Spheroid cultures were grown in 50% L-WRN conditioned medium (CM) containing 10 μm Y-27632 (ROCK inhibitor; Tocris Bioscience). The medium was changed every 2 days and the cells were passaged every 3 days in a 1:6 split.

Formation of transwell monolayers

To form monolayers, spheroids from 3-day-old stem cell cultures were recovered from Matrigel and dissociated with trypsin as described previously (131). Transwells (polyester membrane, 0.4 µm pore; Corning Costar) were prepared for cell seeding by coating the upper compartment with 100 µl of 1:40 dilution of Matrigel for 20 min at 37°C. Excess Matrigel was aspirated off the membrane and approximately $2x10^5$ cells, diluted in 100 ul CM with 10 µm Y-27632, were seeded onto the coated membrane. Media (700 µl of CM with Y-27632) was added to the bottom compartment of the transwell. About 24 hr after seeding, the media in the top and bottom compartments of the transwell was changed to 0% CM referred to as "primary medium" (consisting of advanced DMEM/F12 containing 20% fetal bovine serum, 100 U of penicillin, 0.1 mg/ml streptomycin, and 2 mM L-glutamine; Sigma). Monolayers were infected with oocysts 24 hr after seeding.

Oocyst preparation and excystation

Oocysts were provided by the Kuhlenschmidt lab (University of Illinois at Urbana Champaign). The AUCP-1 isolate of *C. parvum* was maintained in male Holstein calves and oocysts were purified as described previously (107). Oocysts were stored at 4°C in 50 mM Tris-10 mM EDTA, pH 7.2. Before infection, $1x10^8$ purified oocysts were diluted into 1 ml of Dulbecco's Phosphate Buffered Saline (DPBS; Corning Cellgro) and treated with 1 ml of 40% bleach (commercial laundry bleach containing 8.25% sodium hypochlorite) for 10 min on ice. Oocysts were then washed 4 times in DPBS containing 1% (wt/vol) bovine serum albumin (BSA; Sigma) and resuspended in 1 ml DPBS with 1% BSA. For some experiments, oocysts were excysted

prior to infection by incubating the oocysts with 0.75% sodium taurocholate (w/v; Sigma) at 37°C for 60 min. Excysted oocysts were washed once with cell media prior to adding to cells.

For sporozoite and oocyst labeling experiments, coverslips were coated with Poly-L-Lysine (PLL, Sigma) overnight at room temperature. After aspirating the PLL and allowing the coverslips to dry, unexcysted oocysts or a mixture of excysted oocysts and sporozoites were added to the coverslips and allowed to settle for 20 min. Unbleached oocysts were washed three times with sterile DPBS before being plated onto coverslips. The oocysts or sporozoites were fixed in 4% formaldehyde, permeabilized with 0.05% saponin (except where stated) and stained.

Growth of C. parvum in transwell mIEC monolayers

At 24 hr after plating, mIECs were infected with $2x10^6$ oocysts diluted in primary medium added to the top compartment of the transwell. Media was changed in the top and bottom compartments of the transwell daily during infection. To measure *C. parvum* growth in infected monolayers, the media in the top compartment was removed and 50 µl of buffer (5 mM Tris/HCl, pH 8.5) containing 50 µg/ml proteinase K (Sigma) was added. Cells were scraped into the lysis buffer using a pipette tip and the lysate was transferred to a PCR tube and incubated at 37°C for 60 min, 56°C for 60 min, and 95°C for 10 min. Two µl of the lysate was used as a template in the qPCR reaction with SYBR Green PCR Master Mix (Applied Biosystems). Reactions were performed on a Stratagene MX3000P qRT-PCR system with the following amplification conditions: initial denaturation at 95°C for 10 min and 45 cycles of denaturation at 95°C for 5 seconds, annealing at 55°C for 10 seconds, and extension at 72°C for 30 seconds. Primer sequences targeting C. *parvum* GAPDH were as follows: forward primer 5’ AAGGACTGGAGAGCAGGAAG 3’ and

reverse primer 5’ AAAGCTGGGATGACCTTACC 3’. A standard curve for *C. parvum* genomic DNA was generated by lysing a known number of oocysts and creating a dilution series.

Antigen preparation

About 48 hr post-infection, medium in the top compartment of the infected transwells was removed. Groups of 10 transwells were lysed in 100 µl of NP-40 lysis buffer (150 mM sodium chloride, 1% NP-40, 50 mM Tris pH 8.0) with protease inhibitor cocktail (Roche Diagnostics). Protein concentration of lysate was checked by BCA assay (Thermo Scientific) and adjusted to 1 mg/ml and stored at -20°C. Antigen was emulsified with TiterMax Classic Adjuvant (Sigma) in a 1:1 ratio prior to injecting into mice.

Mouse immunization

Five 8-10 week old female inbred BALB/c mice (Charles River Laboratories) were immunized with 6 injections of antigen over 2 weeks. Mice were injected in the same footpad every 3 or 4 days. The first two injections consisted of a 1:1 emulsion of antigen and adjuvant, the remaining 4 injections consisted of antigen only. Each injection was 20 µl in volume; when using antigen/adjuvant mix, the mice received 10 µg of antigen, when using antigen alone, the mice received 20 µg of antigen. Seventeen days after the initial injection, the mice were sacrificed and the popliteal lymph nodes draining the injected footpads were isolated and kept in serum-free medium on ice until fusion.

Hybridoma fusion and screening

The popliteal lymph nodes cells were fused with myeloma cells (P3X63Ag8.653) at a 5:1 ratio with polyethylene glycol (PEG)-1500 (Sigma Aldrich) following standard procedures by the Washington University Hybridoma Center (166). Supernatants were harvested for screening when the cells were 50% confluent (about 2 weeks after fusion). Hybridomas were screened for reactivity against *C. parvum* grown in Caco-2 cells plated on 96-well plates (Greiner Bio-One). Monolayers were fixed with 4% formaldehyde (Polysciences), permeabilized with 0.05% saponin (Sigma) and blocked with a solution containing 0.05% saponin, 5% normal goat serum and 5% FBS. Hybridoma supernatants were added to the wells in addition to a solution containing anti-RH antibody (rabbit polyclonal sera raised against *Toxoplasma gondii* strain RH; WU 1047, Covance) at 1:1000 dilution and 0.02% saponin. After 1 hr incubation, cells were washed and then stained with secondary antibodies conjugated to Alexa Fluor dyes (Thermofisher) diluted in 0.01% saponin solution. Positive hybridomas were expanded in Iscoves' medium (Sigma) supplemented with 20% FBS, cryopreserved in culture medium supplemented with 10% DMSO, and stored in liquid nitrogen.

Hybridoma subcloning and expansion

Positive hybridomas were taken through two rounds of subcloning by single-cell limiting dilution to ensure clonality. At each stage, the hybridoma suicide supernatants (collected when overgrowth of cells results in a decrease in viability to 20%) were screened for reactivity. Hybridomas were weaned in a step-wise manner into 10% FBS before being transferred into a CELLine flask (Wheaton) for concentrated monoclonal antibody production. The isotype identification for the hybridomas was done with the Pierce Rapid Isotyping Kit (ThermoFisher).

Some of the hybridoma isotyping results were confirmed with the Hybridoma Core at Washington University or Rapid Mouse Immunoglobulin Isotyping kit (Antagen).

Immunofluorescence analysis of C. parvum in mIECs

mIECs grown on transwells were infected with $1x10^6$ oocysts 24 hr after plating. After 4 hr, monolayers were washed with DPBS and the media in the top transwell compartment was replaced. Monolayers were fixed 24 hr post infection, permeabilized and blocked as described above. Both primary (hybridoma supernatants listed in Table 1) and secondary antibodies (anti-IgG or anti-IgM) conjugated to Alexa Fluor dyes, (Thermofisher) were diluted in 0.01% saponin solution for staining. Samples were stained with Hoechst (Thermofisher) and the membrane was cut out from the transwell insert and mounted with Prolong Diamond Antifade Mountant (Thermofisher). Imaging was done on a Zeiss Axioskop Mot Plus fluorescence microscope equipped with a 100x, 1.4 N.A. Zeiss Plan Apochromat oil objective and an AxioCam MRm monochrome digital camera. Exposure times for each antibody were established based on optimal auto exposure times for the most intensely staining stages and then maintained consistently for all stages for a given antibody. Images were acquired using Axiovision software (Carl Zeiss Inc.).

Immunofluorescence analysis of C. parvum in HCT-8 cells

HCT-8 cells grown on coverslips were infected 24 hr post-seeding with $1x10^6$ oocysts per well and fixed at 24 hr post-infection for asexual stages or 48-72 hr post-infection for sexual stages then stained for IFA as described above. To identify type II meronts, cells were infected with $1x10^6$ excysted oocysts per well then incubated with 10 µM EdU for two hours starting 30 hr

post-infection before fixation and permeabilized as described above. Cells were then treated with the Click-iT Plus EdU Alexa Fluor 488 Imaging kit (Thermofisher) for 30 min, then stained with mouse monoclonal antibodies and rabbit anti-RH to detect *C. parvum*, followed by secondary antibodies conjugated to Alexa Fluor dyes (Thermofisher). Cells were stained with Hoechst and mounted as described previously. To detect individual microgametocyte nuclei, infected HCT-8 cells were either stained with anti-phosphohistone H3 (Cell Signaling Technology; 1:200) or treated with 10 µM EdU for two hours starting 46 hr post-infection before fixing and staining as described above. To detect host actin, infected HCT-8 cells were fixed and permeabilized as described above, and then incubated with Alexa Fluor 488 phalloidin (Thermo Fisher) for 20 min before proceeding with antibody staining, as described above. Epifluorescent images were acquired as described for the mIECs. For confocal images, infected monolayers were prepared as described and then viewed with a Zeiss LSM880 laser scanning confocal microscope (Carl Zeiss Inc.) equipped with a 63X, 1.4 N.A. Zeiss Plan Apochromat oil objective and a GaAsP detector. ZEN 2.1 Black Edition software was used to obtain Z-stacks through the entire height of the parasites with confocal Z-slices of 0.230 µm. Three-dimensional images were generated using the visualization module of Volocity version 6.3 (Improvision).

Western blot analysis

Oocysts and sporozoites were lysed in 1% NP-40 lysis buffer containing protease inhibitor cocktail (Roche Diagnostics). Oocysts were bleached prior to lysis. Sporozoites were prepared from excysted oocysts that were filtered through a 1 µm filter (Whatman) to remove unexcysted oocysts and excysted oocyst shells. Samples were lysed on ice for 30 min with occasional vortexing and then centrifuged at 14,000 for 3 min; the supernatant was moved to a new tube and

frozen at -20°C. Prior to use, lysates were thawed and reduced using DTT (dithiothreitol) at a final concentration of 100 mM. Samples were resolved on a 10% SDS-PAGE gel then transferred to a nitrocellulose membrane, blocked with the Odyssey blocking buffer (LI-COR). Anti-RH antibody was used at a concentration of 1:500. A secondary goat anti-mouse IR dye 800CW (LI-COR) was used at a concentration of 1:10,000. Samples were imaged with a LI-COR Odyssey imaging system.

For detection with monoclonal antibodies, sporozoite samples obtained after oocyst excystation were lysed in sample buffer and boiled for 5 min at 95ºC. They were then centrifuged at 14,000 g for 1 min and the supernatant was used for loading. Samples were resolved on a 10% SDS-PAGE gel, transferred to a nitrocellulose membrane and blocked with 5% BSA. Monoclonal antibodies against *C. parvum* were used at 1:250 and secondary goat anti-mouse conjugated to horse-radish peroxidase (HRP) was used at 1:10,000. Signal detection was done using the Amersham ECL prime western kit (GE Health care). Among the antibodies highlighted here, we were only able to detect reliable signals in sporozoites for two of them (i.e. 1B5 and 1A5).

Transmission electron microscopy

For ultrastructural analyses, infected mIECs on transwell membranes or trypsinized HCT-8 monolayers were fixed in a freshly prepared mixture of 1% glutaraldehyde (Polysciences, Inc) and 1% osmium tetroxide (Polysciences, Inc.) in 50 mM phosphate buffer at 4ºC for 30 min. Samples were then rinsed multiple times in cold dH_20 prior to en bloc staining with 1% aqueous uranyl acetate (Ted Pella Inc.) at 4ºC for 3 hr. Transwell membranes were removed from insert using a scalpel. Following several rinses in dH_20, samples were dehydrated in a graded series of

ethanol and embedded in Eponate 12 resin (Ted Pella, Inc.). Sections of 95 nm were cut with a Leica Ultracut UCT ultramicrotome (Leica Microsystems, Inc.), stained with uranyl acetate and lead citrate, and viewed on a JEOL 1200 EX transmission electron microscope (JEOL USA, Inc.) equipped with an AMT 8-megapixel digital camera and AMT Image Capture Engine V602 software (Advanced Microscopy Techniques).

Acknowledgements

Supported by a Grand Challenges Grant from the Bill and Melinda Gates Foundation (OPP1098828, OPP1139330). K. L. VanDussen was supported by a K01 from the NIH (DK109081). G. Wilke and L. Funkhouser-Jones were partially supported by an Institutional Training Grant to Washington University (AI007172). The monoclonal lines derived in this paper were isolated from hybridomas created by Misha Hart and Paul Schjetnan under the guidance of Kathy Sheehan in the Washington University Hybridoma Facility, which is supported by the Facility of Rheumatic Diseases Core Center (NIH P30AR048335). We thank Dr. Wandy Beatty of the Microbiology Imaging Facility for electron microscopy processing. We thank Drs. Michael Arrowood and Honorine Ward for reagents and helpful advice on antibody staining. The life cycle stage cartoons used in this publication were created by Laura Kyro. All of the antibodies described here are available for research use and interested parties should contact the corresponding author to arrange transfer of materials.

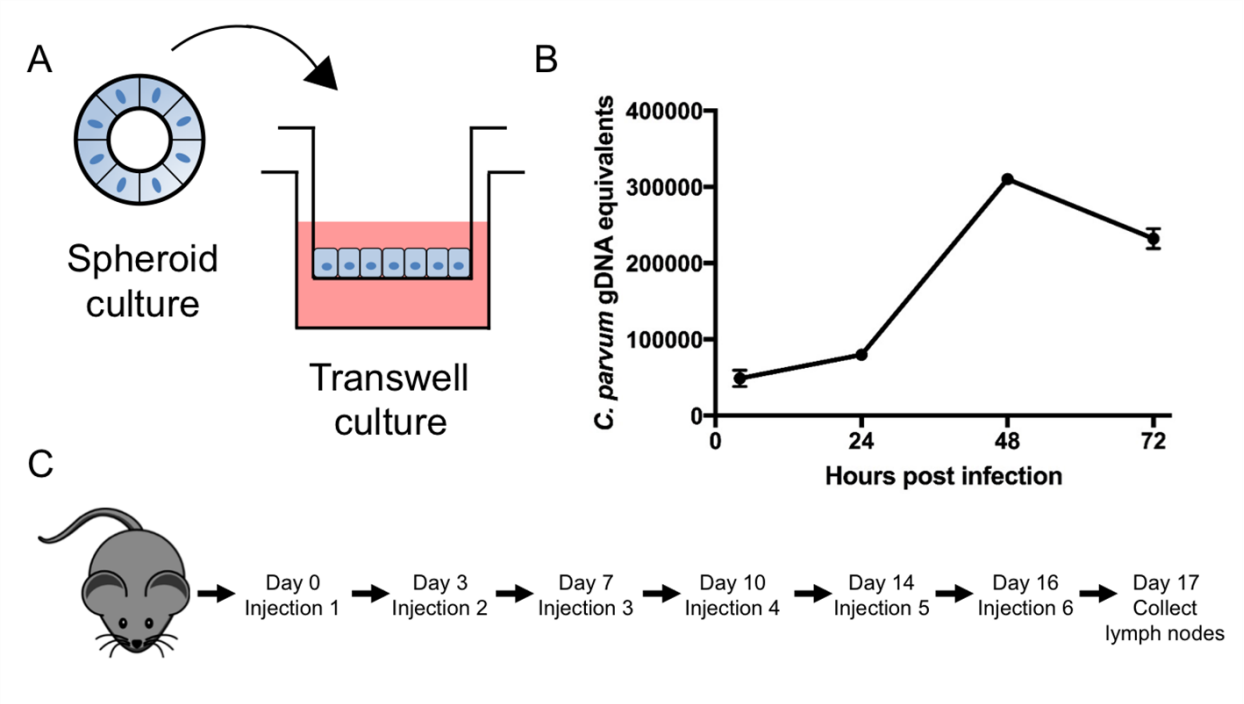

Figure 2.1. Infecting primary mouse ileal epithelial cells (mIECs) and immunization of mice.

A) Mouse intestinal stem cells were passaged as spheroids. To establish monolayers, spheroids were trypsinized and the cells seeded onto transwell membranes.

B) Twenty-four hr after plating the monolayer, the cells were infected with oocysts and samples were harvested at intervals to isolate genomic DNA for estimation of growth by qPCR. Data shown is from one experiment but is representative of the growth seen in 3 or more experiments. N = 3 transwells at each time point. Mean ± S.D.

C) Five mice were immunized with infected mIEC lysates, obtained at 48 hr post-infection, following a series of 6 footpad injections over 2 weeks. Seventeen days after the initial injection, the mice were sacrificed and the popliteal lymph nodes were isolated.

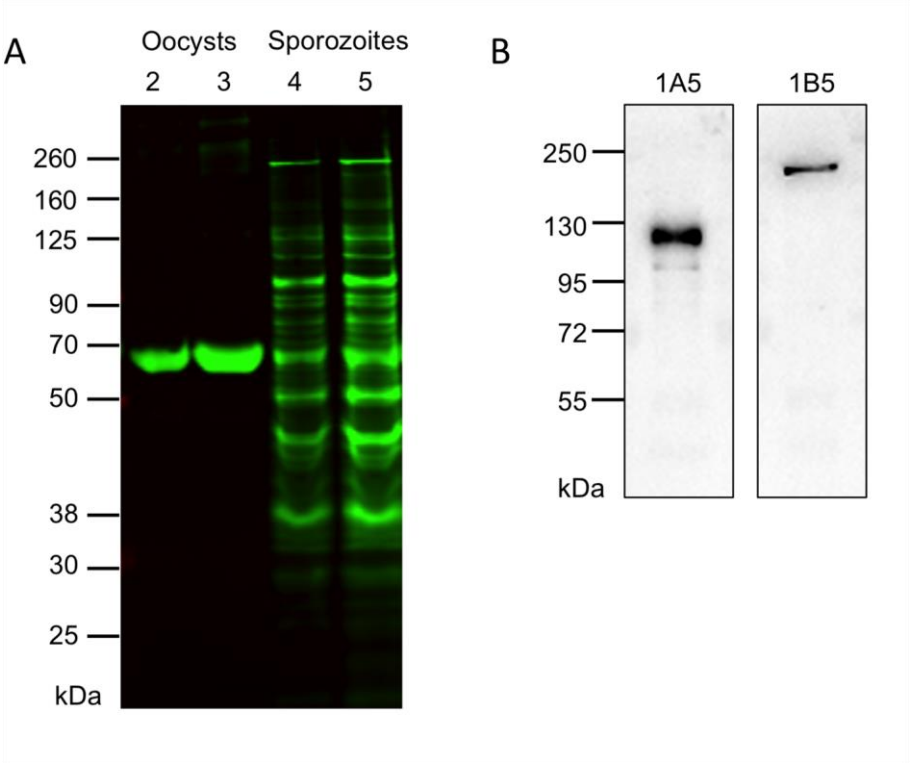

Figure 2.2. Antibody reactivity by western blot.

A) Western blot analysis of samples separated by SDS-PAGE. Loading of samples: oocyst at $1x10^4$ (lane 2) and $2x10^4$ (lane 3), sporozoites at $1x10^6$ (lane 4) and $2x10^6$ (lane 5). The blot was probed with anti-RH antibody at 1:500 and goat anti-rabbit IR dye 800CW was used at a 1:10,000 dilution.

B) Western blot analysis of samples separated by 10% SDS-PAGE. Each lane was loaded with $4x10^6$ sporozoites. The blot was probed with the respective monoclonal antibodies at 1:250 each and a secondary goat anti-mouse HRP at 1:10,000. Detection was done with an ECL prime western kit at an exposure time of 2 min.

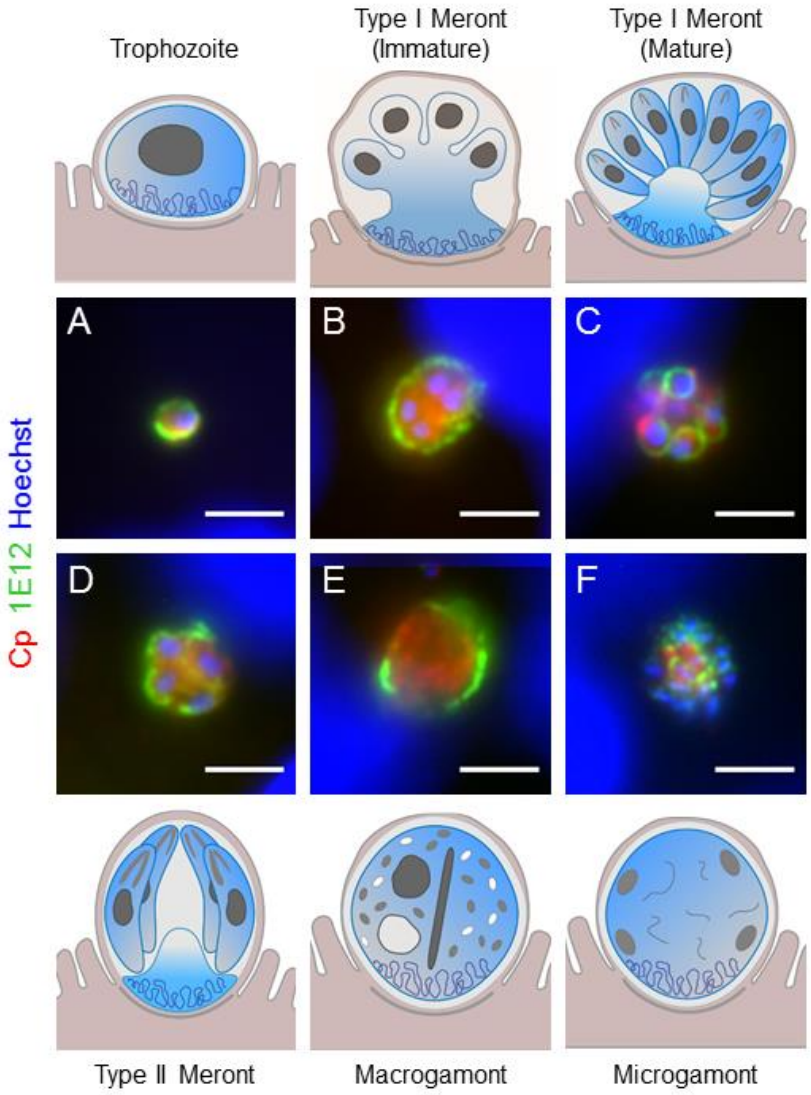

Figure 2.3. mAb 1E12 recognizes the parasite membrane of all life cycle stages.

Cartoons depicting life cycle stages (courtesy of Laura Kyro, reproduced with permission) are shown above or below their respective fluorescent images. Infected HCT-8 cells were fixed and stained with mAb 1E12 (green), rabbit anti-RH (Cp, red) to detect *C. parvum*, and Hoechst to detect DNA. Samples from 4 hr post-infection were used to image trophozoites (A) and immature (B) and mature type I meronts (C), 32 hr post-infection for type II meronts (D), or 48 hr post-infection for macrogamonts (E) and microgamonts (F). Scale bars = 3 µm.

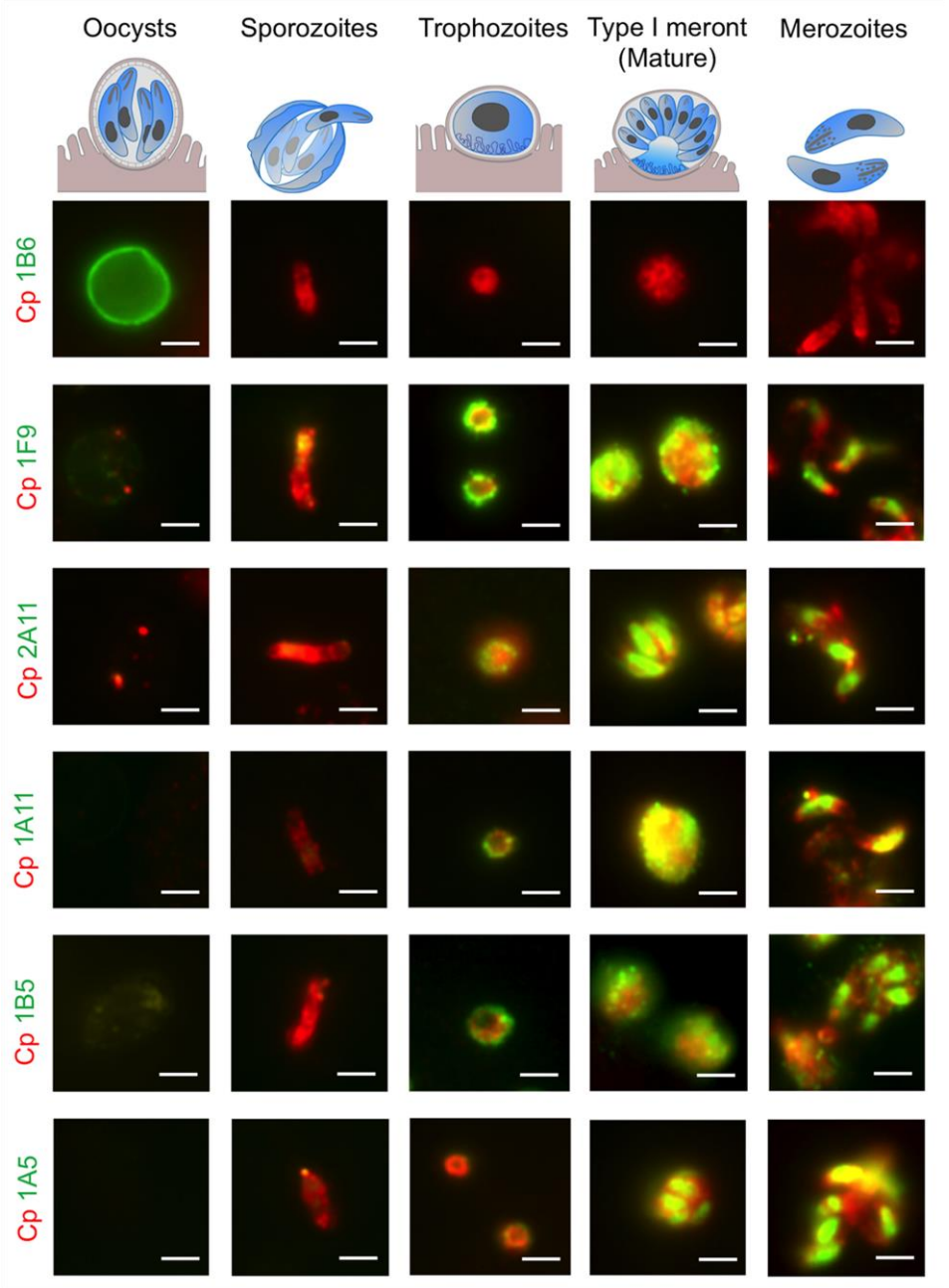

Figure 2.4. Staining patterns of monoclonal antibodies in infected mIECs.

mIECs were infected with *C. parvum* oocysts and fixed 24 hours after infection. Cells were stained with the specified mouse mAbs and rabbit-anti-RH to detect *C. parvum* (Cp). Secondary antibodies used were goat anti-mouse Alexa Fluor 488 and goat anti-rabbit Alexa Fluor 594. Scale bar = 5 µm.

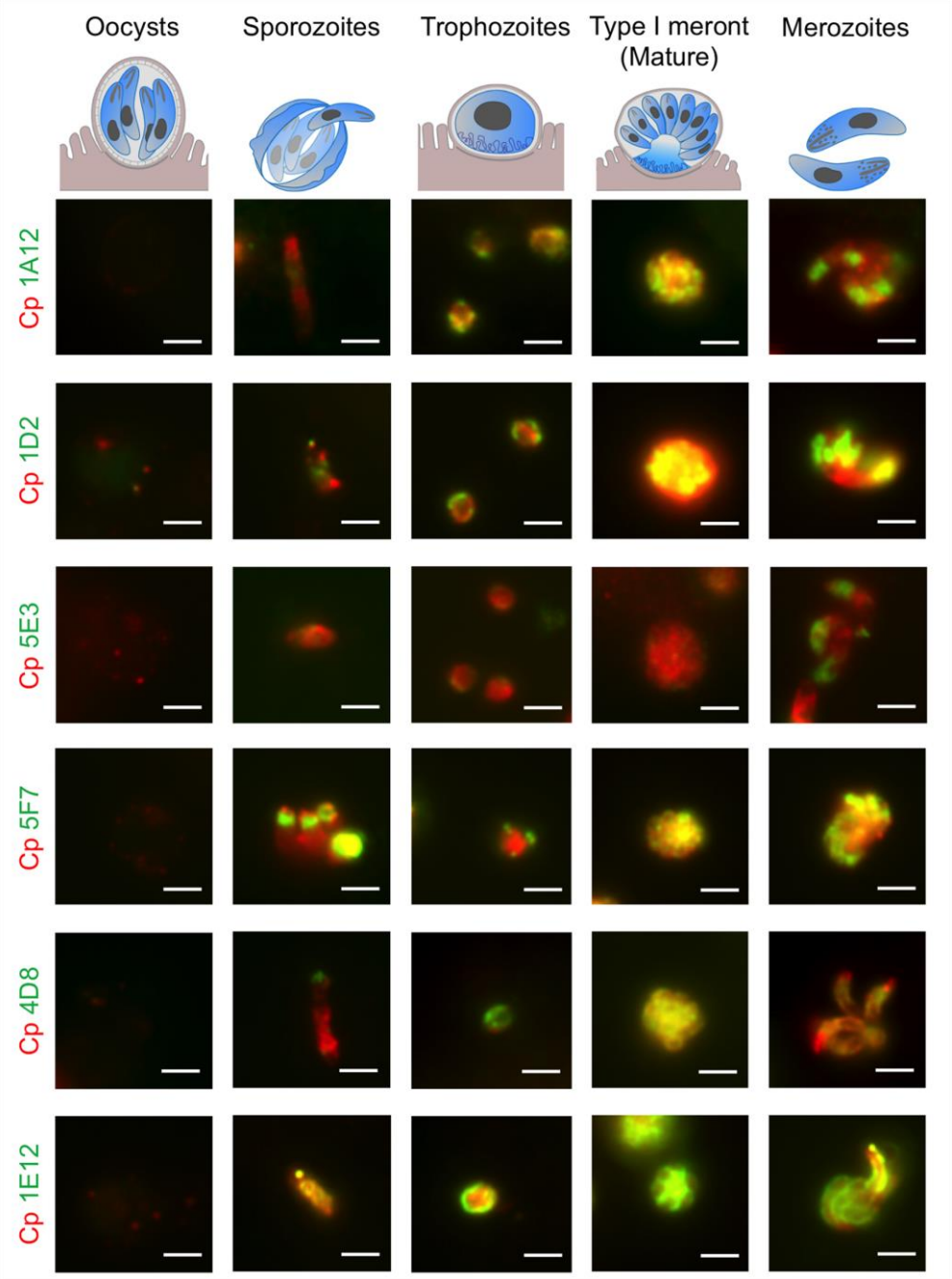

Figure 2.5. Staining patterns of monoclonal antibodies in infected mIECs.

mIECs were infected with *C. parvum* oocysts and fixed 24 hours after infection. Cells were stained with the specified mouse mAbs and rabbit-anti-RH to detect *C. parvum* (Cp). Secondary antibodies used were goat anti-mouse Alexa Fluor 488 and goat anti-rabbit Alexa Fluor 594. Scale bar = 5 µm.

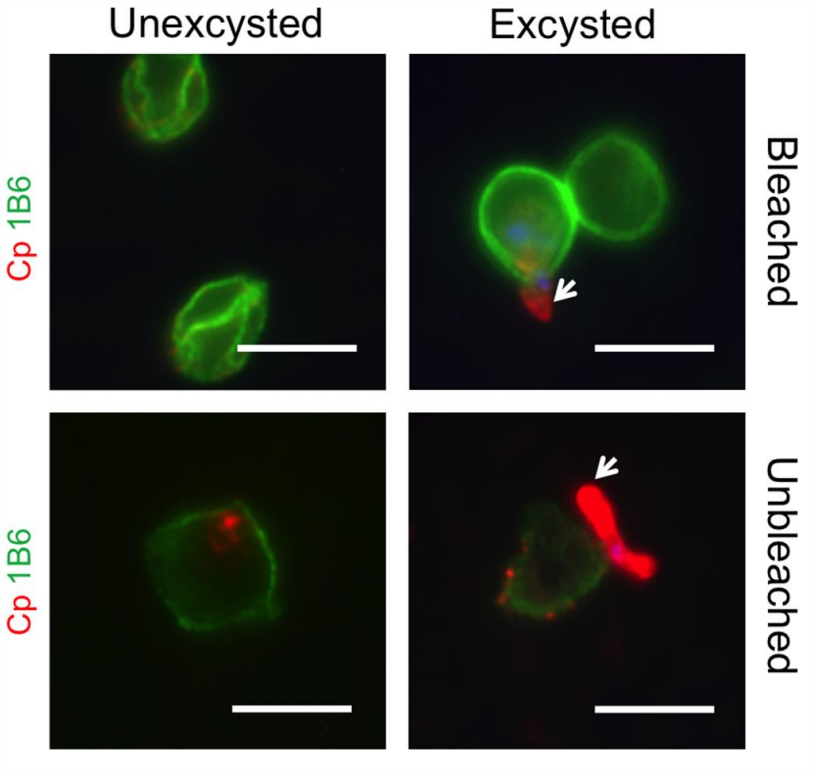

Figure 2.6. mAb 1B6 stains the outer oocyst wall.

Oocysts were either left unbleached or bleached for 10 min in a 40% bleach solution, and then were either left unexcysted, or excysted in a 0.75% sodium taurocholate solution for 60 min at 37°C. Oocysts were then plated on coverslips coated with poly-L-lysine. Samples were fixed and stained with 1B6 (green) and rabbit-anti-RH (Cp, red) to detect *C. parvum.* Arrows indicate sporozoites. Scale bars = 5 µm.

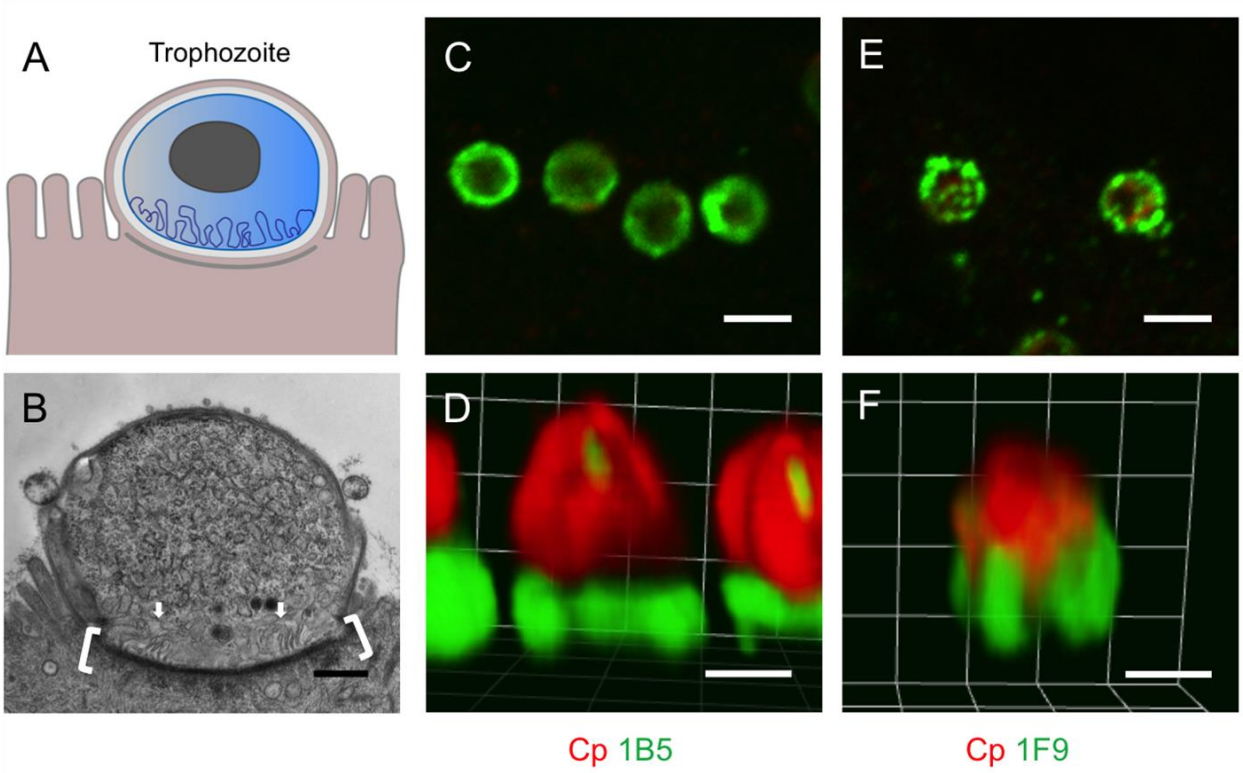

Figure 2.7. Antibodies that recognize unique patterns in trophozoites.

A) Cartoon representing the trophozoite stage.

B) Transmission electron micrograph of trophozoite growing in mIEC, 24 hr post-infection. The actin-rich host cell cytoskeleton is denoted by brackets. The membrane-rich feeder organelle is indicated by arrows. Scale bar = 500 nm.

C, D,) Pattern of staining with mAb 1B5 (green) and rabbit-anti-RH (Cp, red) to detect *C. parvum.*

E, F) Pattern of staining for mAb 1F9 and rabbit-anti-RH (Cp, red) to detect *C. parvum.* For C-F, HCT-8 cells were infected with oocysts and fixed and stained 24 hr post-infection. C and E show single Z-slices acquired by laser scanning confocal microscopy, D and F show 3D rendering of a full Z-stack. Scale bars in C and E = 2 µm. Scale bars in D and F = 1 µm.

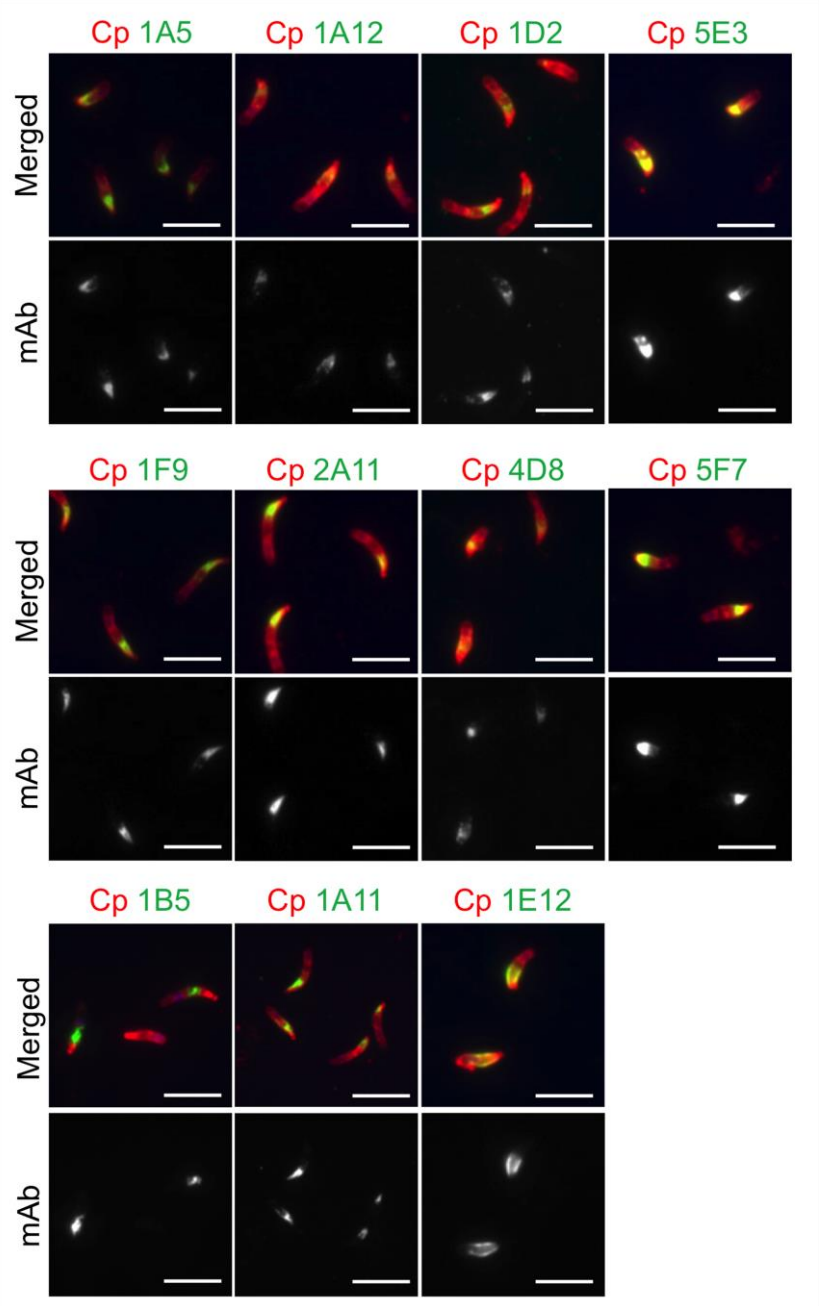

Figure 2.8. Monoclonal antibodies that recognize sporozoites.

Oocysts were excysted and plated onto PLL-coated coverslips. Sporozoites were fixed and stained with the specified mouse mAbs and rabbit-anti-RH to detect *C. parvum* (Cp). For 1B5 staining, samples were permeabilized with 0.1% Triton X-100. Secondary antibodies used were goat anti-mouse Alexa Fluor 488 and goat anti-rabbit Alexa Fluor 594. Scale bar = 5 µm.

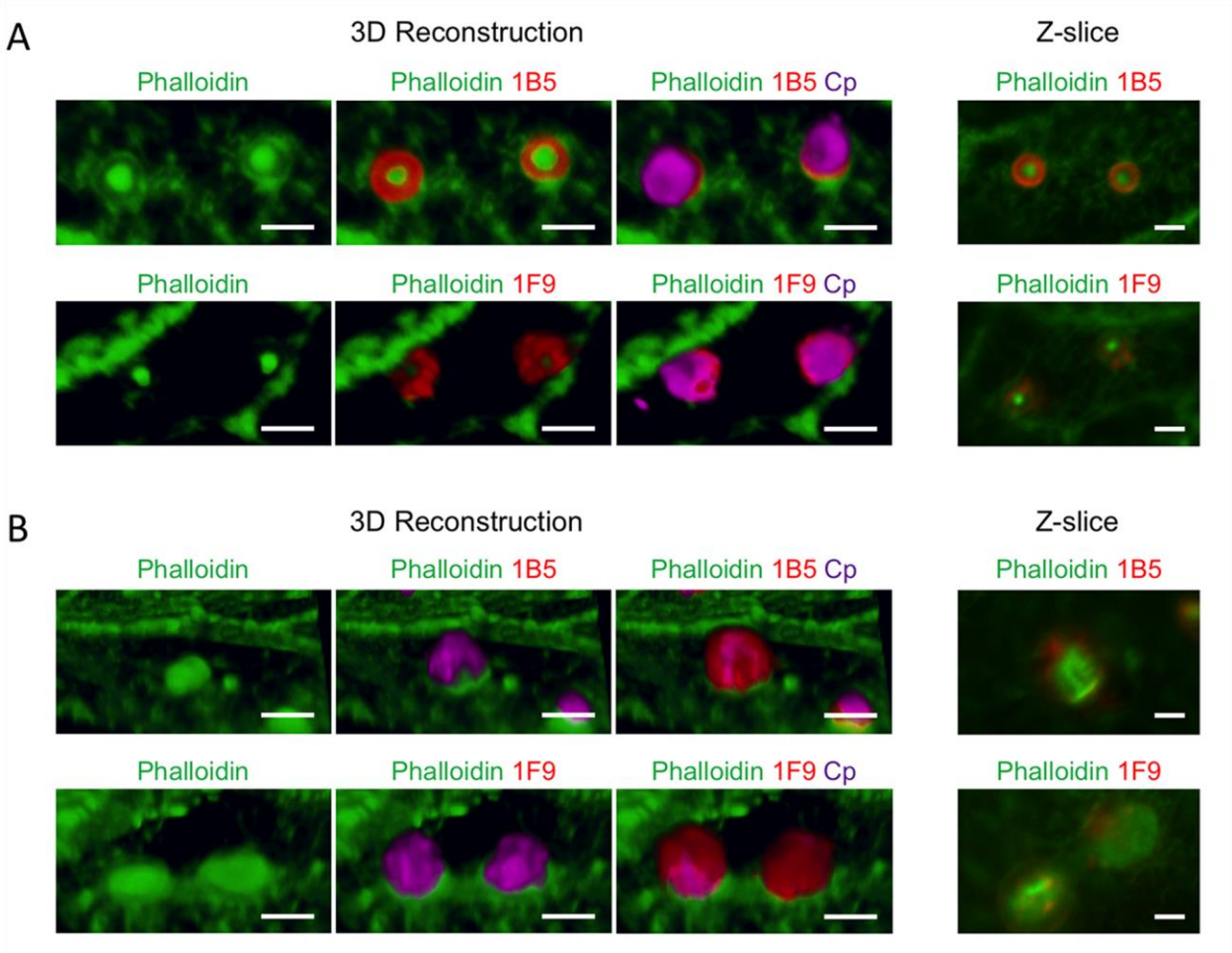

Figure 2.9. Distribution of 1B5 and 1F9 staining in trophozoites and meronts relative to the actin pedestal.

A) HCT-8 cells were infected with oocysts and fixed 2 hr post infection to detect trophozoites. Cells were stained with phalloidin, mAbs 1F9 or 1B5, and rabbit-anti-RH to detect *C. parvum* (Cp). Secondary antibodies used were goat anti-mouse Alexa Fluor 555 and goat anti-rabbit Alexa Fluor 647. First panel is the 3D rendered images from a Z-stack acquired by laser scanning confocal microscopy; additional image is a single Z-slice from the Z-stack. Scale bar = 3 µm.

B) HCT-8 cells were infected with oocysts and fixed 24 hr post infection to detect meronts. Cells were stained with phalloidin, 1F9 or 1B5, and rabbit-anti-RH to detect *C. parvum* (Cp). Secondary antibodies used were the same as for (A). First panel is the 3D rendered images from a Z-stack acquired by laser scanning confocal microscopy; additional image is a single Z-slice from the Z-stack. Scale bar = 3 µm.

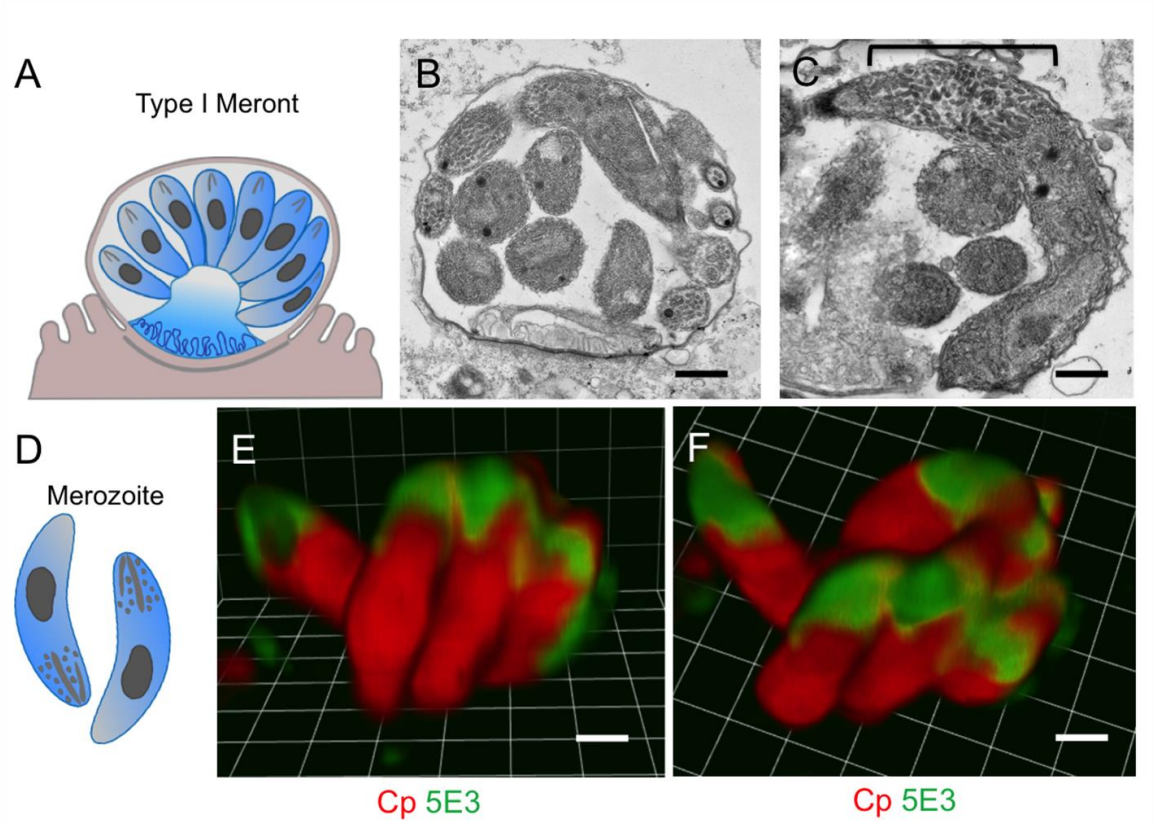

Figure 2.10. mAb 5E3 recognizes the apical end of merozoites.

A, D) Cartoons representing Type I meront and merozoite, respectively.

B, C) Transmission electron micrograph of a mature meront in HCT-8 cells 24 hr post-infection. Brackets denote micronemes at the apical end of merozoite. Scale bar = 500 nm.

E, F) HCT-8 cells were infected with oocysts and fixed at 24 hr post-infection and stained with mAb 5E3 (green) and rabbit-anti-RH (Cp, red) to detect *C. parvum*. Side (E) and top view (F) images of 3D rendered images from a Z-stack acquired by laser scanning confocal microscopy. Scale bars = 1 µm.

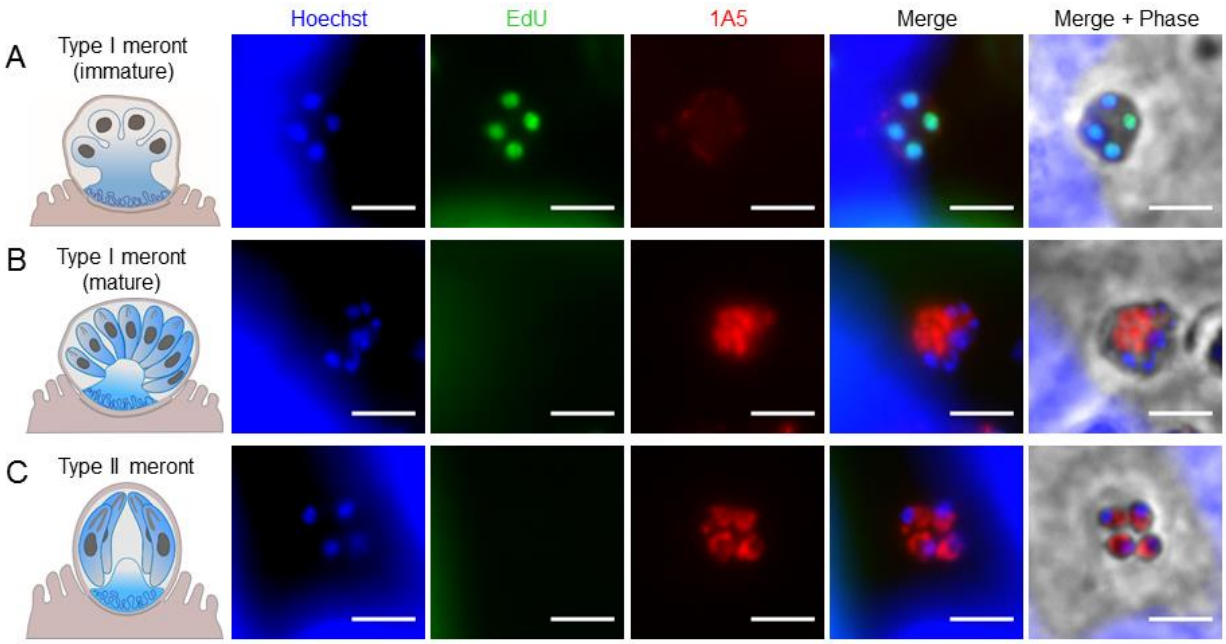

Figure 2.11. mAb 1A5 recognizes mature Type I and Type II meronts but not immature Type I meronts.

A) Staining of immature type I meronts defined by four EdU-positive nuclei and lack of defined merozoites by phase contrast (Merge + Phase).

B) Staining of mature type I meronts defined by a lack of EdU staining and presence of defined merozoites by phase contrast microscopy (Merge + Phase).

C) Staining of type II meronts as defined by four nuclei that lack EdU staining as well as the presence of 4 individual merozoites by phase contrast microscopy (Merge + Phase).

Infected HCT-8 cells were incubated with the thymidine analog EdU for two hours starting 30 hr post-infection then were fixed and treated with an EdU Click-It 488 labeling kit (green) and stained with mAb 1A5 (red) and Hoechst DNA stain (blue). Scale bar = 3 µm.

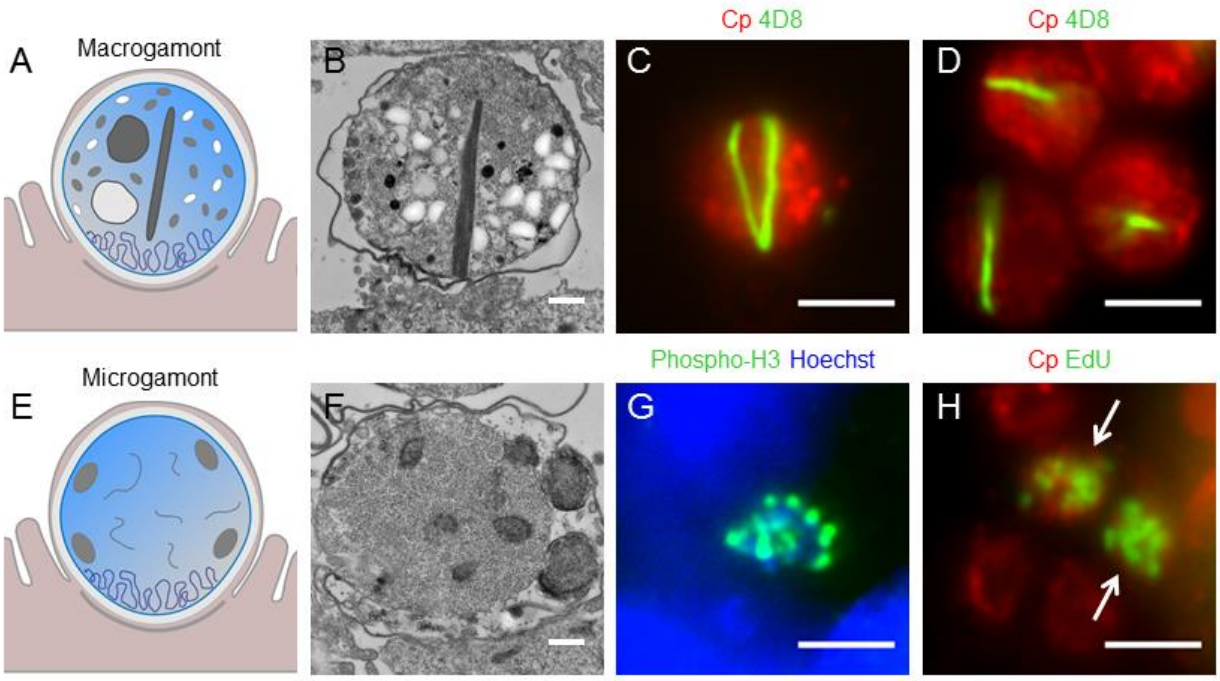

Figure 2.12. Antibodies with reactivity to *C. parvum* sexual stages.

A, E) Cartoon representing macrogamont and microgamont, respectively.

B) Transmission electron micrograph of macrogamont within an HCT-8 cell 48 hr post-infection. Scale bar = 5 µm.

C, D) Infected HCT-8 cells were fixed and stained 72 hr post-infection with rabbit-anti-RH (Cp, red) to detect *C. parvum* and mAb 4D8 (green). Scale bars = 3 µm.

F) Transmission electron micrograph of microgamont within an HCT-8 cell 48 hr post-infection.

G) Infected HCT-8 cells were fixed and stained 72 hr post-infection with an anti-phospho-histone H3 (Ser10) antibody (green). Scale bar = 3 µm.

H) Infected HCT-8 cells were incubated with the thymidine analog EdU for two hours starting 46 hr post-infection before fixation. Cells were treated with an EdU Click-It 488 labeling kit (green) to detect microgametocyte nuclei undergoing replication (arrows) and stained with rabbit-anti-RH (Cp, red) to detect *C. parvum.* Scale bar = 3 µm.

Table 1. Staining patterns of mouse monoclonal antibodies against *C. parvum*.[a]

Hybridoma	Isotype	Oocyst	Sporozoite	Trophozoite	Type I meront	Type I Merozoite	Type II meront	Macrogamont	Microgamont
1B6	IgG1	Outer wall							
1F9	IgG1		Polarized	Ring	Punctate	Cytoplasmic			
2A11	IgG2a		Polarized	Membrane	Cytoplasmic	Cytoplasmic			
1A11	IgG2b		Polarized	Membrane	Cytoplasmic	Cytoplasmic			
1B5	IgG2b		Central	Ring	Cytoplasmic	Cytoplasmic			
1A5	IgG1		Polarized	Membrane	Polarized	Polarized	Polarized		
1A12	IgG2b		Polarized	Punctate	Punctate	Polarized	Polarized		
1D2	IgG1		Polarized	Membrane	Cytoplasmic	Cytoplasmic	Cytoplasmic		
5E3	IgG1		Polarized	Membrane	Membrane	Polarized	Polarized		
5F7	IgG2a		Polarized	Punctate	Punctate	Polarized	Polarized		
4D8	IgM		Polarized	Variable	Variable	Cytoplasmic	Punctate	"V" Shape	
1E12	IgG1		Membrane	Membrane	Membrane	Membrane	Membrane	Membrane	Membrane

[a] Staining patterns are based on reactivity to infected mIECs (Fig. S 2,3) and infected HCT-8 cells (images in mains figures) and reactivity on sporozoites (Fig. S4). The colors denote strength of reactivity with dark green corresponding to string staining and light green reflecting weaker, positive staining. Blank cells indicate no reactivity.

Chapter 3

Complete life cycle development of

Cryptosporidium parvum in vitro

Preface

The first complete draft of this chapter was written by GW. Comments from LDS were incorporated into the final version presented here. GW designed and performed the majority of experiments, analyzed the data, and generated the figures. LFJ contributed data (figure 3.7A, C) and advice. YW, TSS, TBK, MSK, and WW provided key biological reagents and advice. SR provided technical support. LDS supervised the studies and contributed to the design and analysis of the experiments.

This chapter is intended for publication and is in progress:

Wilke, G., Funkhouser-Jones, L., Wang, Y., Ravindran, S., Wang, Q., Stappenbeck, T.S., Kuhlenschmidt, T.B., Kuhlenschmidt, M.S., Witola, W., Sibley, L.D. Complete life cycle development of *C. parvum in vitro*.

Summary

Recent investigation into the etiology of pediatric diarrhea in Africa and southeast Asia identified *Cryptosporidium* as a frequent infection in patients studied. *Cryptosporidium* has long been recognized as an opportunistic infection in immunocompromised patients, but its importance in global health was underestimated until now. There are no effective treatments for cryptosporidiosis in immunocompromised or malnourished patients, the two populations most affected by the disease. The lack of treatment options is due to the many barriers hindering investigation into *Cryptosporidium* biology, such as difficult animal models, genetic tools that rely on passage through an animal, and lack of accessible systems that support complete development *in vitro*. We describe here a cell culture platform that enables complete life cycle development and long-term growth of *C. parvum in vitro*. Primary intestinal epithelial cell monolayers, derived from stem cell spheroids, were grown on transwells in medium containing stem cell growth factors. The cells were induced to differentiate by removing the medium from the top chamber of the transwell, creating an "air-liquid interface". These monolayers supported *C. parvum* replication over several weeks and produced viable oocysts. These oocysts incorporated EdU added to the culture medium, indicating they were produced *de novo*. Oocysts were recovered from bleached cell monolayers and used to productively infect mice. This system will be a valuable tool for investigating the complete parasite life cycle *in vitro* and understanding host-parasite interactions in a model that replicates the intestinal environment.

Introduction

Cryptosporidium is a gastrointestinal parasite that causes long-term illness in immunocompromised patients (139) and contributes to malnourishment and impaired growth in children in low- to middle-income countries (24). For years, investigation into the biology of *Cryptosporidium* has been stalled due to the intractability of the parasite: it lacks a continuous culture system and molecular genetic tools. The latter has recently experienced a breakthrough with the successful genetic modification of *C. parvum* using the CRISPR/Cas9 system (66). However, stable transgenic parasites still cannot be selected for or propagated *in vitro* due to the lack of robust cell culture platforms, making it difficult to create and maintain lines, as well as study genes that are required for life cycle completion. Adenocarcinoma cell lines such as HCT-8 can support 2-3 days of growth, but when the parasite reaches the sexual part of its life cycle, it stops before oocyst formation (83). There have been recent reports of systems enabling complete life development and passage *in vitro* (95, 96), but these systems require specialized equipment and are not easily scalable. Additionally, these systems use HCT-8 cells, which do not resemble the intestinal epithelial cells *Cryptosporidium* infects *in vivo*. Another recent report of continuous culture *in vitro* utilized a different cancer cell line, COLO-680N (97); however, this result has not been validated by another lab.

It is possible to create primary intestinal cell cultures that replicate aspects of the gut environment (131, 138). These cultures are grown as monolayers on transwells and are derived from intestinal stem cell spheroids (125, 126). These monolayers can support robust *C. parvum* growth over a 3-day period and were essential in creating a novel library of monoclonal antibodies against intracellular stages of the parasite (167). However, *C. parvum* cannot

complete its life cycle in this system, likely due to the limited lifespan of the monolayers, which only last a few days.

A recent report described a method for creating primary intestinal monolayers that maintained viability for weeks (132). This system also derived cells from spheroids and used transwells but incorporated a feeder cell layer and an "air-liquid interface" (ALI) in the top chamber of the transwell. The ALI induced dramatic differentiation of the cells into enterocytes and secretory cells of the gut, as well as the formation of structures resembling crypts. Additionally, the cells were grown in medium containing stem cell growth factors, leading to the maintenance of a population of cells that continually proliferated, replacing terminally differentiated cells as they died. The latter modification likely explains the long-term viability of these monolayers.

The differentiation status and long lifespan makes ALI monolayers an ideal candidate for supporting complete life cycle development of *C. parvum*. Here, we describe long-term growth of *C. parvum* and oocyst development *in vitro* in the ALI system.

Results

ALI monolayers support long-term C. parvum infection

The recently published ALI system (132) was modified to be compatible with the spheroid system we had previously used to generate primary monolayers for *C. parvum* infection (167). There were three primary changes needed to adapt the system. First, stem cells for establishing ALI monolayers were obtained from a spheroid line isolated from the mouse ileum (126) instead of a human fetal line. Second, the medium used to grow the ALI monolayers was switched to L-WRN conditioned medium (126) from the original medium used in the publication (SCM-6F8 medium). SCM-6F8 medium contains a cocktail of recombinant growth factors; using L-WRN conditioned medium allows us to bypass the need to purchase each growth factor individually. Finally, mouse ileal stem cells were expanded as spheroids (126) and plated onto a feeder cell layer of irradiated fibroblasts in a transwell coated with Matrigel. Cells were maintained in conditioned medium and allowed to proliferate for 7 days before removing the medium from the top part of the chamber to create the ALI culture (figure 3.1A). Within days of the initiation of ALI, the monolayer began to undergo differentiation into enterocyte and secretory cell lineages found in the small intestine, such as goblet cells (data not shown).

To determine if ALI monolayers supported *C. parvum* growth, we infected monolayers with oocysts and tracked parasite growth using qPCR to measure parasite genomic DNA equivalents. We found *C. parvum* numbers increased for at least 20 days post infection (figure 3.1B), amplifying ~ 70-fold from the initial infection. This high parasite burden did not appear to affect monolayer viability, however, because qPCR of mouse genomic DNA equivalents showed that host cell numbers increased over the same period (figure 3.1B). Additionally, visual

inspection of the infected transwells did not show signs of barrier breakdown such as leakage of medium into the top chamber (data not shown). H&E-stained sections of ALI monolayers showed a continuous monolayer of cells with height comparable to that found *in vivo*, a strong sign of cellular differentiation (168) (figure 3.1C, 3.2). Electron microscopy of infected monolayers revealed the presence of a brush border on the apical side of the cells (figure 3.2). In IHC-stained sections as well as electron microscopy images, *C. parvum* vacuoles were easily visualized growing at the apical end of the cell (36) (figure 3.1C, 3.2).

All developmental stages of C. parvum can be found in ALI monolayers

We utilized a recently described panel of mAbs (167) to examine the life cycle development of *C. parvum* in the ALI cultures. Fluorescent microscopy of infected monolayers confirmed the appearance of asexual life cycle stages of *C. parvum*. mAb 1B5 detected trophozoites by their distinct donut-shaped pattern (167) (figure 3.1D). Trophozoites were also detected by electron microscopy (figure 3.3A). Type I and II meronts were identified by mAb 1A5, which stains mature merozoites within meronts in a polarized manner (167) (figure 3.1D). Type II meronts are distinguished from immature type I meronts, which also contain 4 nuclei, because 1A5 does not have polarized staining in immature type I meronts (167). Type I and II meronts were also differentiated in electron microscopy images. Type I meronts had round vacuoles with 8 merozoites (figure 3.3B, C) while type II meronts had taller, narrower vacuoles with 4 merozoites (figure 3.4A).

Sexual stages of *C. parvum* appeared by day 2 post-infection and were abundant in the ALI cultures. Microgamonts were identified by their multiple tiny nuclei and membrane staining pattern by pan-Cp, which recognized the developing septations between microgamonts within

the parasitophorous vacuole (figure 3.1D). Microgamonts were also identified by electron microscopy as vacuoles containing multiple small bullet-shaped parasites (figure 3.4C, D). Interestingly, microgamonts were recognized by Crypt-a-Glo™ (Waterborne, Inc) (figure 3.6A) and OW50 (153) (data not shown), mAbs that both recognize oocyst wall proteins. These mAbs stained the surface of early macrogamonts and then the individual membranes around each microgamont in late and extracellular microgamonts. These Crypt-a-Glo™-positive structures were confirmed to be replicating parasites by adding EdU, a thymidine analog that is incorporated into replicating DNA, to the cell culture medium, (figure 3.6B). This recognition of microgamonts by oocyst wall-specific mAbs has not been reported previously and we did not observe this phenomenon in infected HCT-8 cells (data not shown).

Macrogamonts were identified by the presence of wall-forming bodies (WFBs, clusters of oocyst wall proteins (36, 169)), which are recognized by both Crypt-a-glo™ (figure 3.1D) and OW50 (data not shown). Macrogamonts could also be identified by electron microscopy, which revealed the numerous lipid and glycogen vacuoles within the parasite cytoplasm, as well as the striated fiber previously observed to be present in macrogamonts (167) (figure 3.4B). In some macrogamonts, the WFBs coalesced into a ring (figure 3.1D); we termed these "late-stage" macrogamonts because the WFBs appeared to be organizing in preparation for oocyst formation. This ring-like structure of WFBs has not previously been reported in other cell culture systems. We potentially identified this stage by electron microscopy; some macrogamonts had numerous small vesicles lined up against the parasite membrane (figure 3.5A, B), which resembles the pattern of WFBs seen by fluorescent microscopy. We could not identify a similar observation in other published electron microscopy studies of *C. parvum* growth *in vitro* or *in vivo*.

Robust C. parvum growth requires ALI and initiation of cell differentiation and proliferation

To confirm that the ALI was required for *C. parvum* growth, we infected "submerged" transwells (monolayers without an ALI) as well as transwells 3 days after initiation of ALI. *C. parvum* grew significantly better over a 3-day period in the ALI transwells compared to the submerged transwells (figure 3.7A). Interestingly, host cell viability during infection was improved in the ALI transwells compared to the submerged transwells, despite the high level of infection in the former (figure 3.7A).

After the ALI is established in this culture system, the cells begin to differentiate into terminal lineages such as goblet cells. To determine if cell differentiation was required for *C. parvum* growth, we infected transwells on day 0 of ALI initiation and day 3 post-ALI initiation, when monolayers begin to show signs of differentiation (data not shown). *C. parvum* grew significantly better in the transwells infected 3 days after ALI initiation compared to the day 0 group (figure 3.7B). Similar to the ALI vs. no ALI experiment, host cell viability during infection was improved in the transwells infected on day 3 (figure 3.7B).

From these two types of experiments, it appeared that improved host cell viability and proliferation were tied to *C. parvum* growth. To visualize cell proliferation during infection, we infected submerged transwells and transwells 3 days after ALI initiation; on day 2 post-infection, we added EdU to the medium in the bottom chamber of the transwells for an 8-hour pulse. Microscopy showed higher numbers of both *C. parvum* and proliferating cells in the transwells infected 3 days after ALI initiation (figure 3.7C) compared to the submerged transwells. The EdU microscopy in addition to the qPCR of mouse genomic equivalents supports the presence of dividing cells within the ALI monolayers, something the previous primary cell transwell system lacked (131, 167).

ALI monolayers support oocyst development

The continued amplification of parasite numbers over 20 days suggested that *C. parvum* may be undergoing multiple rounds of its life cycle in the ALI system, which implies the production of oocysts *in vitro*. When we were investigating the possibility of oocyst development *in vitro* in ALI culture, a report was published claiming oocyst development in a cancer cell line, COLO-680N (97). When we attempted to replicate these results, we identified a potential issue with interpreting the presence of oocysts in cultures: they may represent input from the inoculum rather than newly produced structures. In our experiments, COLO-680N monolayers infected with oocysts showed very little parasite growth over a 10-day period compared to HCT-8 cells (figure 3.8A). However, oocyst counts over the same time period revealed that oocysts were present on each day examined (figure 3.8B). Fluorescence microscopy showed almost equivalent numbers of oocysts in COLO-680N monolayers at day 1 and 10 post-infection (figure 3.8C). Since there was very little parasite growth and the total number of oocysts in the culture did not increase over time (figure 3.8B), it appears that the oocysts from the initial inoculum bound tightly to the monolayer and remained there for the duration of the experiment, and there was no *in vitro*-production of oocysts. It is possible that in the original publication, the presence of oocysts at later time points was misconstrued as production of oocysts. Similarly one of the earliest studies claiming oocyst production *in vitro* was later found to be incorrect due to misinterpretation of the appearance of input oocysts (103).

Based on the above findings, when we began investigating oocyst production in ALI culture, we wanted to avoid mis-identifying input oocysts as new oocysts. Monolayers can be infected with oocysts that have been excysted to release the sporozoites; the excysted oocysts can

be filtered to remove the oocyst shells, leaving behind only sporozoites. We tested different filter pore sizes to remove oocysts from excysted sporozoites. We found that filters with a 3 µm pore size were insufficient to completely remove oocysts from sporozoites, it was necessary to use a 1 µm pore size to completely remove input oocyst contamination from sporozoites (figure 3.8D). When COLO-680N cells were infected with 1 µm-filtered sporozoites, there was no sign of oocyst development (figure 3.8E), again suggesting that the "oocyst production" reported in this line was due to input oocysts that remained stuck to the monolayers.

In order to determine if oocysts were being produced in the ALI monolayers, we infected the cells with excysted sporozoites that had been passed through filters with a 1 µm pore size to remove unexcysted oocysts and oocyst shells. To visualize oocyst development, we stained the monolayers with Crypt-a-glo™ and counted the number of oocysts per field. We found that oocysts began to appear by day 3 and that there was variation in the number of oocysts seen on each day, suggesting the possibility of cycles of oocyst formation occurring (figure 3.9A). The oocysts produced were numerous and easily visible, as seen in the example low magnification image in figure 3.9B, taken at day 10 post-infection.

To confirm the oocysts observed by staining were indeed newly produced in culture, we added EdU to the culture medium overnight and then looked for EdU incorporation into the oocysts. We found EdU-positive oocysts in the monolayers (figure 3.9C), confirming the oocysts were produced *in vitro* and not the result of possible contamination from the original inoculum. It has been shown previously that *C. parvum* oocysts bind the GalNAc-binding lectin *Maclura pomifera* agglutinin (MPA) and the fucose-binding lectin *Ulex europaeus* agglutinin I (UEA-1) (170). To confirm that the *in vitro*-produced oocysts shared these characteristics, we isolated the oocysts from the ALI monolayers by bleaching the monolayers to remove cell debris and plating

the remaining material on poly-L-lysine-coated coverslips. We stained the material with the MPA and UEA-1 and observed lectin-positive oocysts (figure 3.9D), confirming the oocysts shared this phenotype with *in vivo*-produced oocysts.

One interesting observation related to the oocyst production *in vitro* was unusual reactivity patterns in the ALI culture with the 4D8 mAb, which recognizes several life cycle stages but is most useful for identifying macrogamonts (167). In infected ALI cultures, 4D8 revealed its typical "V" or line reactivity pattern in macrogamonts (figure 3.10A), but it also stained very long lines that were not associated with any parasite (figure 3.10B, C). These long lines were not seen in infected HCT-8 cultures (data not shown). These lines resemble "trails" of protein left behind during gliding motility, which have been observed with *C. parvum* sporozoites with other mAbs (108). 4D8 recognizes *C. parvum* sporozoites in a polarized manner (figure 3.10D), suggesting it might recognize a protein that is stored in apical secretory organelles, which play a role in host cell attachment and invasion (161, 162). It is possible these 4D8 "trails" seen in ALI cultures are left behind by sporozoites as they traverse the monolayer after oocyst excystation.

Oocysts produced in vitro are infectious to mice

To confirm the oocysts produced *in vitro* were viable and capable of infection, we infected ALI monolayers with filtered sporozoites and then bleached the monolayers on days 1 and 3 post infection and used this material to infect mice. *C. parvum* oocysts are resistant to bleach treatment (171) and oocysts purified from calves are normally treated with bleach to remove surface contamination prior to using the oocysts in cell culture. We hypothesized that on day 1, only asexual/intracellular stages of *C. parvum* are present, which are not resistant to

bleach treatment; but that by day 3, oocysts are present, which should survive the bleach treatment and be able to productively infect the mice.

We confirmed oocyst development in the ALI cultures (figure 3.11A) and also confirmed the presence of oocysts in the material after bleaching (figure 3.11A). Oocysts resembled *in vivo*-produced oocysts: they were recognized by both pan-Cp and Crypt-a-Glo^{TM} and appeared to contain sporozoites (figure 3.11B). Ifngr1$^{-/-}$ mice, which are susceptible to *C. parvum* (unpublished), were orally gavaged with bleached material from day 1 and day 3 cultures. Mice that received day 1 material survived for the duration of the experiment, while mice that received day 3 material had 100% mortality by day 12 post-gavage (figure 3.11C). We collected pellets from both groups of mice to measure levels of *C. parvum* DNA, a proxy for oocyst shedding. We found that the animals that received the day 3 bleached material began shedding oocysts by day 5 post-gavage, the number of oocysts increased almost two logs before the animals died. Animals that received day 1 material did not show any evidence of oocyst shedding above the background signal in the assay. We observed similar results in a repeat experiment (figure 3.12). Intestinal tissue sections from mice that received the day 1 and day 3 material showed robust infection by anti-*C. parvum* IHC in the latter but no sign of infection in the former (figure 3.11D).

Discussion

Development of novel therapeutics for cryptosporidiosis and investigation into the pathogenesis of the disease have been slowed by the lack of *in vitro* models that support complete *C. parvum* development in a system that resembles the intestinal environment. Such systems are necessary for furthering our understanding of the parasite and how it interacts with the host, which will help guide innovative approaches to treatment.

In this report, we demonstrated that primary intestinal epithelial cell monolayers with an ALI supported *C. parvum* growth for at least 20 days. We identified all life cycle stages of *C. parvum* in the monolayers, including oocysts. Oocysts appeared by day 3 post-infection and resembled *in vivo*-derived oocysts by microscopy. The oocysts also incorporated EdU, signifying they are produced *in vitro*. This is a novel finding since EdU incorporation to validate oocyst production *in vitro* has not been utilized by other systems claiming complete oocyst development (95-97). Additionally, we carefully controlled for oocyst contamination in the input inoculum by testing different filter pore sizes and found that the pore size most commonly used (3 μm) was insufficient to remove oocysts from sporozoites and 1 μm was necessary. Between the EdU incorporation and complete removal of contaminating oocysts, we are confident that *C. parvum* is completing its life cycle in the ALI monolayers. Additionally, we showed that the *in vitro*-produced oocysts were viable by demonstrating they were infectious to mice and caused robust oocyst shedding.

The ALI system has several features that likely contribute to its ability to enable long-term *C. parvum* growth and complete life cycle development *in vitro*. The monolayers are grown in medium containing factors that support stem cell growth, which likely maintains a population of stem cells in the monolayer that continually give rise to differentiated cell types. In a previous

iteration of our primary intestinal cell culture system, the monolayers were grown in medium lacking stem cell growth factors; the cells lost their proliferative potential and the monolayers only lasted a few days (131). This system only supported 2-3 days of parasite growth before the monolayers collapsed (167). In ALI monolayers, we observed many dividing cells in the presence of infection, visualized by EdU incorporation. Apoptosis occurs during *C. parvum* infection both *in vivo* (172) and *in vitro* (173, 174), so the proliferative capacity of the ALI monolayer likely allows continual replacement of dying infected cells at a rate that enables constant parasite growth without compromising monolayer integrity. Additionally, the inclusion of a feeder cell layer, something the previous primary cell culture system lacked, likely creates a temporary extracellular matrix that supports initial stem cell growth before the cells can start making their own matrix proteins, ensuring a robust monolayer.

In addition to the self-renewing ability, the ALI monolayers contain the major differentiated cell types of the intestinal epithelium. These differentiated cells appear after the introduction of the ALI in this culture system. The mechanism for how ALI induces cellular differentiation is unknown, but ALI has been used in airway tract epithelial cell culture for many years to enhance cell differentiation (133-135). It has also recently been applied to intestinal epithelial cell culture, leading to increased expression of markers associated with cell differentiation, significant changes in cell metabolism, and increased monolayer longevity (132, 136, 137). The development of all intestinal lineages that we see in our ALI cultures likely creates a great facsimile of the gut environment for *C. parvum*. Though *C. parvum* infection does not appear to be restricted to a specific cell type in the intestine because parasitophorous vacuoles are seen along the length of the villus in various animal models (175-177) and even in the base of the crypt in the neonatal mouse model (172). So, while we cannot pinpoint a specific

cell type that is required for *C. parvum* growth, the cells of the ALI monolayer likely generally resemble the cells *C. parvum* encounters *in vivo* in terms of metabolism, differentiation state, surface expression of different receptors, etc. The primary cells may deliver the right signals to *C. parvum* to turn on expression of genes involved in fertilization, meiosis, and oocyst wall development, leading to complete life cycle development *in vitro*. These signals may be lacking in cell culture systems that rely on adenocarcinoma cell lines. Further studies are needed to identify differences in gene expression in *C. parvum* in different culture systems.

The gene expression program triggered in the parasite by interaction with the primary cells could also explain the novel microscopic findings we observed in this system. We saw evidence of oocyst wall protein expression by microgamonts, since two mAbs that recognize oocyst wall proteins (OW50 and Crypt-a-Glo^{TM}) reacted to microgamonts, something not seen in adenocarcinoma cell models. There is no previous report of this in the literature, and it is a difficult observation to explain. It is possible that the antibodies are cross-reacting to a surface protein expressed by microgamonts that is involved in a receptor-ligand interaction with macrogamonts. This surface protein could be critical for fertilization, explaining why its expression is not seen in adenocarcinoma cell cultures.

Another interesting microscopic finding in the ALI system was the appearance of what we termed “late-stage macrogamonts”, which had WFBs organized in a circular pattern, as if preparing for oocyst formation. This life cycle stage does not appear in HCT-8 cultures, which do contain macrogamonts, but their WFBs are spread throughout the parasite cytoplasm without any apparent organization. The WFB “ring” could represent the step after fertilization of the macrogamont by the microgamont, explaining why it is not seen in culture systems that do not support oocyst development. This life cycle stage could be further investigated by live-imaging

fluorescently tagged parasites in ALI culture to see if WFB ring formation coincides with fertilization. If this is the case, these "late-stage macrogamonts" are actually zygotes, a life cycle stage that has been difficult to identify *in vitro* and *in vivo*.

In addition to the WFB rings, another interesting microscopic finding we observed in ALI culture was the unusual reactivity pattern of mAb 4D8; it recognized long "trials" of protein that were not clearly associated with any parasite. mAb 4D8 recognizes many life cycle stages but most notably has a line or V-shaped reactivity pattern in macrogamonts and a polarized reactivity pattern in sporozoites. As mentioned earlier, the 4D8-positive trails could be proteins shed during gliding motility by the sporozoite. This would explain why the trails are not seen in other cell culture systems, since they do not support oocyst/sporozoite development.

There have been two recent reports of systems that enable complete *C. parvum* development and propagation *in vitro* (95, 96). One system utilizes hollow fiber technology to mimic the intestine by having separately controlled apical and basolateral compartments with different redox and nutrient conditions (95). While this system can produce oocysts for months at a time, it is a difficult system to scale up for testing a variety of growth conditions or drug screening purposes. It is also not well-suited to studies that require multiple time points for microscopy or RNA/DNA collection, since the hollow fiber must be opened and thereby destroyed to obtain a sample, terminating the experiment. Another system employs a bioengineered silk 3D intestinal model to grow *C. parvum* (96); this system is more easily scalable than the hollow fiber system but relies on specialized equipment to make the silk scaffolds. Both systems use adenocarcinoma cell lines, which do not accurately replicate the cell types *C. parvum* encounters *in vivo*, making them poor models for studying host-parasite interactions.

The ALI system described here relies on commercially available transwells and reagents, so it can easily be adapted for small-scale drug studies, as well as other types of experiments testing multiple conditions in parallel where many samples are required for microscopy, gene expression analysis, etc. The system builds upon previously published methods for propagating intestinal stem cells as spheroids (126) and growing primary intestinal epithelial cells as monolayers on transwells (131, 132, 138), so it has a strong foundation as a model of the intestinal environment. *C. parvum* encounters the same differentiated cells in the ALI monolayers that it infects *in vivo,* making this system a great candidate for examining host-parasite interactions. Additionally, this system is very amenable to microscopy studies, which will facilitate investigation into the processes behind fertilization, meiosis, etc., which could not previously be studied *in vitro*.

There are limitations to the ALI system: efforts to propagate *C. parvum* using ALI monolayers are ongoing, and the amount of oocysts produced by the monolayers is too small to replace standard methods of producing oocysts *in vivo*. However, the system could potentially be used to select for transgenic parasites *in vitro* before amplification in the mouse, bypassing the need for surgery to infect mice with transgenic parasites (66). Additionally, the long-term growth and complete life cycle development *in vitro* makes the system very useful for investigating drug mechanism and effect – for example, determining if a drug is static or cidal, and what specific life cycle stage is targeted. We believe this system is an accessible model of the gut environment and will enable innovative studies into *Cryptosporidium* biology and its interaction with the host.

Materials and methods

Ethics Statement

Animal studies were conducted according to the U.S.A. Public Health Service Policy on Humane Care and Use of Laboratory Animals. Animals were maintained in an Association for Assessment and Accreditation of Laboratory Animal Care – approved facilities. Animal studies were approved by the Institutional Animal Studies Committee at the School of Medicine, Washington University in St. Louis.

3D spheroid cell culture

Primary ileal epithelial stem cells isolated from 8-10 week old C57BL/6 mice were obtained from the laboratory of Dr. Thad Stappenbeck, Washington University in St. Louis. Ileal stem cells were expanded and maintained as 3D spheroid cultures in Matrigel (BD Biosciences), as described previously (125). Spheroid cultures were grown in 50% L-WRN conditioned medium (CM) containing 10 µm Y-27632 (ROCK inhibitor; Tocris Bioscience). Cells were cultured at 37°C in a 5% CO_2 incubator. The medium was changed every 2 days and the cells were passaged every 3 days in a 1:6 split.

Irradiating fibroblasts and seeding feeder cell layer

Mouse fibroblast cells (NIH/3T3; CRL-1658^{TM} ATCC) were maintained in Dulbecco's Modified Eagle's Medium (DMEM; ATCC, 30-2002) with 10% FBS (Sigma) and penicillin/streptomycin (Sigma). Cells were cultured at 37°C in a 5% CO_2 incubator. Cells were passaged every 3 days

in a 1:5 split. For irradiation, cells were trypsinized, suspended in growth medium and irradiated at 3000 rads using the Small Animal Radiation Research Platform (SARRP, Xstrahl). After irradiation, cell viability was assessed with Trypan Blue staining (Thermo Fisher), cells were quantified and aliquoted in freezing medium (growth medium with 30% FBS and 5% DMSO). Irradiated cells were kept at -80°C for short-term use (weeks) and in liquid nitrogen for long-term use (months). In order to create feeder cell layers, transwells (polyester membrane, 0.4 µm pore; Corning Costar) were coated with Matrigel (Corning) diluted 1:10 in cold PBS. After incubating at 37°C for 15-20 min, excess Matrigel solution was aspirated immediately before adding irradiated 3T3 (i3T3) cells. i3T3 cells were thawed, resuspended in growth medium, and seeded onto transwells at 8x10^4 cells/transwell. Growth medium was added to the top and bottom of the transwell.

Seeding epithelial cell monolayers and creating ALI

To form monolayers, spheroids from 3-day-old stem cell cultures were recovered from Matrigel and dissociated with trypsin as described previously (131). Cells were quantified, suspended in 50% CM with 10 µm Y-27632, and plated onto i3T3 monolayers that were seeded 24 hours previously. Cells were seeded at 5x10^4/transwell. 3T3 growth medium was removed from bottom of transwells and replaced with 50% CM with 10 µm Y-27632. Medium was replaced in the top and bottom compartments of the transwell every other day. After 7 days, the medium in the top compartment was removed to create the ALI. Medium in the bottom compartment of the transwell continued to be changed every other day. Liquid/mucus that appeared in top compartment was removed every other day.

Oocyst preparation and excystation

Oocysts were provided by the Kuhlenschmidt or Witola laboratories (University of Illinois at Urbana Champaign). The AUCP-1 isolate of *C. parvum* was maintained in male Holstein calves and oocysts were purified as described previously (107). Oocysts were stored at 4°C in 50 mM Tris-10 mM EDTA, pH 7.2. Before infection, $1x10^8$ purified oocysts were diluted into 1 ml of Dulbecco's Phosphate Buffered Saline (DPBS; Corning Cellgro) and treated with 1 ml of 40% bleach (commercial laundry bleach containing 8.25% sodium hypochlorite) for 10 min on ice. Oocysts were then washed 4 times in DPBS containing 1% (wt/vol) bovine serum albumin (BSA; Sigma) and resuspended in 1 ml DPBS with 1% BSA. For some experiments, oocysts were excysted prior to infection by incubating the oocysts with 0.75% sodium taurocholate (w/v; Sigma) in DPBS at 37°C for 60 min. If required, excysted oocysts were filtered through a membrane with 1 μm pore size (Whatman, VWR International) to remove oocysts from sporozoites. Sporozoites were spun down at 1250 x g for 3 min and then resuspended in 50% CM prior to adding to ALI monolayers.

Infecting ALI monolayers and measuring C. parvum growth and host cell viability by qPCR

Oocysts or filtered sporozoites were added to monolayers in 30 μl volume. After 3 hr, monolayers were washed twice with DPBS. The Qiagen QIAamp kit was used to collect DNA from the infected transwells. Briefly, 100 μl Buffer ATL (provided by kit) was added to monolayer; cells were scraped into buffer using a blunt pipette tip. Lysed cells were incubated in Buffer ATL and proteinase K (both reagents provided by kit) at 56°C for 3-24 hr before proceeding with the rest of the protocol. Purified DNA was diluted 1:10 with H_2O before adding

to qPCR reaction mix. Two µl of the diluted DNA was used as a template in the qPCR reaction with TB Green™ Advantage® qPCR premix (Takara, Clontech). Primer sequences targeting C. *parvum* GAPDH were as follows: forward primer 5' CGGATGGCCATACCTGTGAG 3' and reverse primer 5' GAAGATGCGCTGGGAACAAC 3'. A standard curve for *C. parvum* genomic DNA was generated by purifying DNA from a known number of oocysts and creating a dilution series. Primer sequences targeting mouse GAPDH were as follows: forward primer 5' GCCATGAGTGGACCCTTCTT 3' and reverse primer 5' GAAAACACGGGGGCAATGAG 3'. A standard curve for mouse genomic DNA was generated by purifying DNA from a known number of mouse ileal stem cells and creating a dilution series. Reactions were performed on a QuantStudio 3 Real-Time PCR System (Thermo Fisher) with the following amplification conditions: priming at 95°C for 2 min then 40 cycles of denaturing at 95°C for 10 sec, annealing at 60°C for 20 sec, extension at 72°C for 30 sec. Genomic DNA equivalents present in each sample were determined by the QuantStudio Design & Analysis software.

Development of pan-Cp antibody

Antigen for the pan-Cp polyclonal antisera was generated by excysting 8x10^8 bleached oocysts in 0.75% sodium taurocholate at 37°C for 1 hour; excysted oocysts were then freeze-thawed 6 times (3 min on dry ice mixed with ethanol, then 3 min at 37°C). Sample was sent to Covance for immunization. One rabbit was injected subcutaneously with 250 mg antigen with Freund's Complete Adjuvant (FCA) then boosted three times at 21-day intervals with 125 mg antigen in Freund's Incomplete Adjuvant (FIA).

Fluorescent microscopy

Transwells were moved to a new 24-well plate; DPBS was added to bottom chamber. Monolayers were fixed by adding 100 µl 4% formaldehyde (Polysciences) for 10-15 min. Cells were washed twice with DPBS and then permeabilized with DPBS containing 1% BSA and 0.1% Triton X-100 (Sigma) for 20 min. Primary and secondary antibodies were diluted in this "permeabilization buffer" for staining. Cells were incubated with primary antibody for 60 min at room temperature. Antibodies were used at different concentrations; 1B5 and 1A5 (purified mouse mAbs) were used at 1:500 , pan Cp (rabbit pAb) was used at 1:1000, Crypt-a-glo™ (mouse mAb, Waterborne, Inc) was used at 1 drop per 2 transwells, and 4D8 (hybridoma supernatant) was used at 1:5. After primary antibody incubation, transwells were washed twice with PBS and then incubated with secondary antibodies conjugated to Alexa Fluor dyes (Thermofisher) for 60 min at room temperature. Secondary antibodies were used at 1:1000 concentration. Samples were stained with Hoechst (Thermofisher) and the membrane was cut out from the transwell insert using a scalpel and mounted with Prolong Diamond Antifade Mountant (Thermofisher).

For lectin staining of bleached ALI monolayers, bleached material was pipetted onto coverslip in 24-well plate (150-200 µl total volume per well), allowed to settle for 30 min, then fixed and permeabilized as above and then stained with specified lectin for 30 minutes, followed by pan Cp staining for 60 min and secondary antibody staining for 60 min. Lectins used were FITA-conjugated *Maclura pomifera* (MPA) lectin (E Y Laboratories, F-3901-1) and FITC-conjugated *Ulex europaeus* (UEA-1) lectin (E Y Laboratories, F-2201-2), both used at 100 µg/ml.

For EdU staining, 10 μM EdU was added to medium in the bottom chamber of the transwell. After a defined time period, the transwell was fixed with 4% formaldehyde and permeabilized as above. EdU was labeled with the Click-iT Plus EdU Alexa Fluor 488 (Invitrogen, C10637) or 594 (Invitrogen, C10339) Imaging Kit. Primary and secondary antibody staining were done after EdU labeling.

Imaging was done on a Zeiss Axioskop Mot Plus fluorescence microscope equipped with a 100x, 1.4 N.A. Zeiss Plan Apochromat oil objective and an AxioCam MRm monochrome digital camera. Images were acquired using Axiovision software (Carl Zeiss Inc.).

Transwell sections

Transwells were moved to a new plate; 4% formaldehyde added to the top and bottom chambers. After 20 min, the cells were washed 3 times in 70% ethanol in both the top and bottom chambers, and then incubated in 70% ethanol for 20 min. The transwell membranes were cut from the insert using a scalpel and embedded in 1% agar and then processed for paraffin embedding. For hematoxylin and eosin staining and immunohistochemistry, five μm thick transverse sections were cut and processed for staining following standard procedures of the Digestive Disease Research Core Center (DDRC, Washington University in St. Louis). Sections were imaged using a Zeiss Observer.D1 inverted wide-field fluorescence microscope with Axiocam 503 dual B/W and color camera.

Electron microscopy

For ultrastructural analyses, ALI cultures were fixed in a freshly prepared mixture of 1% glutaraldehyde (Polysciences, Inc) and 1% osmium tetroxide (Polysciences, Inc.) in 50 mM phosphate buffer at 4ºC for 30 min. Samples were then rinsed multiple times in cold dH_20 prior to en bloc staining with 1% aqueous uranyl acetate (Ted Pella Inc.) at 4ºC for 3 hr. Transwell membranes were removed from insert using a scalpel. Following several rinses in dH_20, samples were dehydrated in a graded series of ethanol and embedded in Eponate 12 resin (Ted Pella, Inc.). Sections of 95 nm were cut with a Leica Ultracut UCT ultramicrotome (Leica Microsystems, Inc.), stained with uranyl acetate and lead citrate, and viewed on a JEOL 1200 EX transmission electron microscope (JEOL USA, Inc.) equipped with an AMT 8-megapixel digital camera and AMT Image Capture Engine V602 software (Advanced Microscopy Techniques).

COLO-680N and HCT-8 cell culture

Human ileocecal adenocarcinoma cells (HCT-8; CCL-244™ ATCC) were maintained in RPMI-1640 medium (Gibco, ATCC modification) supplemented with 10% FBS. Human esophageal squamous cell carcinoma cells (COLO-680N, CLS Cell Line Services) were maintained in RPMI-1640 medium (Sigma, R8758) supplemented with 10% FBS. Cell lines were tested for the presence of mycoplasma and confirmed negative with the e-Myco plus Mycoplasma PCR Detection Kit (Boca Scientific). For infection studies, cells were plated in 96-well plates for DNA collection or 24-well plates with coverslips for microscopy studies. DNA was purified using method described above and microscopy also performed as described above.

Bleaching ALI monolayers for microscopy and animal infection

ALI monolayers were infected on day 3 post top medium removal with filtered sporozoites. After 2 hr, monolayers were washed twice with DPBS. On days 1 and 3 post infection, monolayers were scraped into cold 40% bleach diluted in DPBS. Bleached material was combined into one Eppendorf tube. Monolayers were bleached on ice for 10-15 min before spinning down at maximum speed for 2 min. The supernatant was removed, the pellet resuspended in 1 ml cold DPBS, and centrifuged again. The bleached material was washed 5 times and then resuspended in the desired volume of cold DPBS.

Animal infection and pellet DNA extraction

Female 8- to 10-week-old Ifngr1$^{-/-}$ mice (Jackson Laboratories) were orally gavaged with 150 µl of bleached ALI material (equivalent to 4-5 transwells) from either day 1 or day 3 post-infection cultures. After gavaging, mice were housed separately for the duration of the experiment to avoid cross-infection. One mouse infected with bleached, day 1 ALI culture material was sacrificed on day 30 post-infection and one mouse infected with bleached, day 3 ALI culture material was sacrificed on day 9 post-infection in order to collect the small intestine for histology. Mouse pellets were collected every 2-3 days and the mice were monitored for signs of sickness. Mouse pellets were kept at -80°C until they were processed for DNA extraction, which was performed using the QIAamp DNA Stool Kit. Pellets were moved to Lysing Matrix E 2 ml tubes (MP Biomedicals) and 1.4 ml ASL Buffer (from Qiagen kit) was added. Samples were homogenized using the FastPrep-24^{TM} 5G High-Speed Homogenizer. The samples were then processed

according to the kit's directions. qPCR was used to quantify the number of *C. parvum* genomic DNA equivalents were present in the sample using the above primers and cycling protocol.

Acknowledgements

Supported by a Grand Challenges Grant from the Bill and Melinda Gates Foundation (OPP1098828, OPP1139330). G. Wilke and L. Funkhouser-Jones were partially supported by an Institutional Training Grant to Washington University (AI007172).

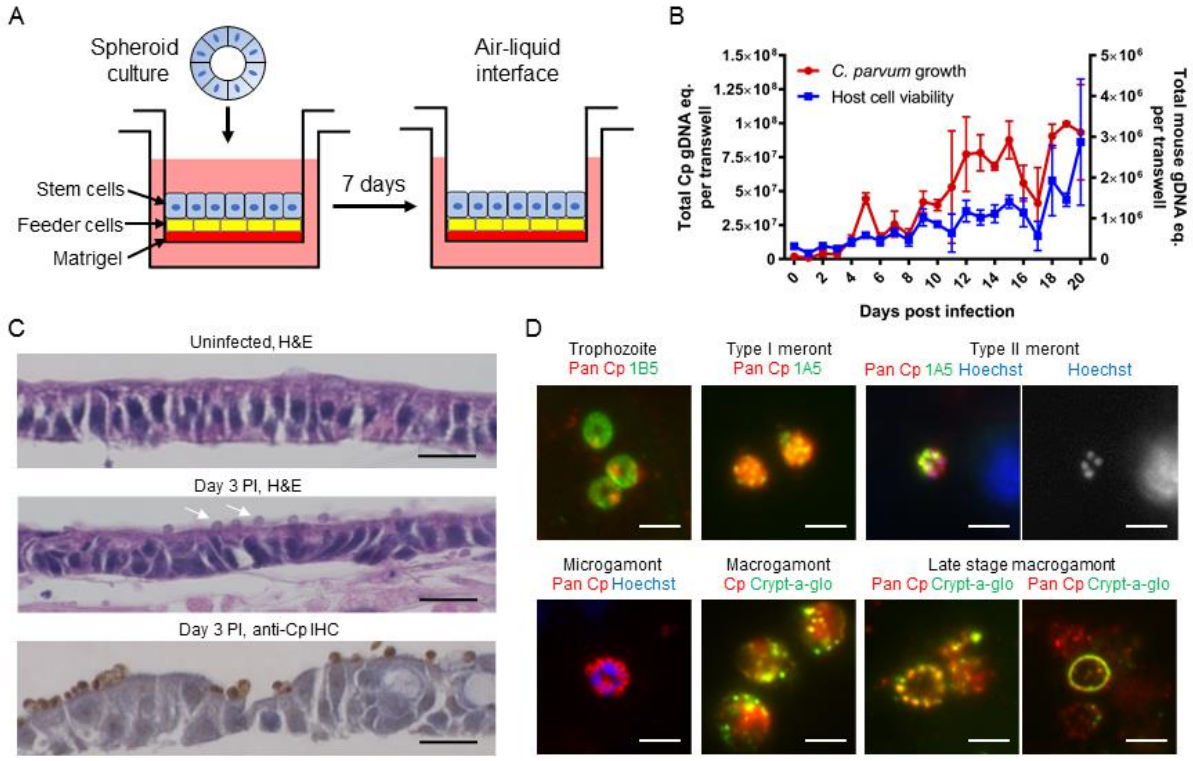

Figure 3.1. ALI cultures support robust *C. parvum* growth.

A) Cartoon depicting ALI culture method. Spheroids are trypsinized and plated on top of feeder cell and Matrigel layers. Monolayers are grown in 50% conditioned medium + 10 µM ROCK inhibitor. After 7 days, the medium in the top chamber of the transwell is removed to create the ALI.

B) ALI monolayers were infected 3 days post top medium removal with 2x10^5 oocysts. Monolayers were incubated with oocysts for 4 hr and then washed 3 times. DNA samples were collected daily. Graph depicts qPCR measuring *C. parvum* and mouse GAPDH equivalents (eq.) in DNA samples. Each data point represents the mean and standard deviation of two transwells.

C) Sections of uninfected and infected transwells stained with hematoxylin and eosin (H&E), or rabbit pAb Cp using immunohistochemistry. White arrows in middle panel are highlighting *C. parvum* vacuoles on the apical side of the cell. Scale bar = 20 µm.

D) Infected ALI transwells were fixed and stained with specified mouse mAb (1B5, 1A5, Crypt-a-glo^{TM}) and rabbit pAb Cp to detect *C. parvum*. Hoechst staining is shown for the type II meront to confirm the presence of 4 nuclei. Secondary antibodies used were goat anti-mouse Alexa Fluor 488 and goat anti-rabbit Alexa Fluor 568. Scale bar = 3 µm.

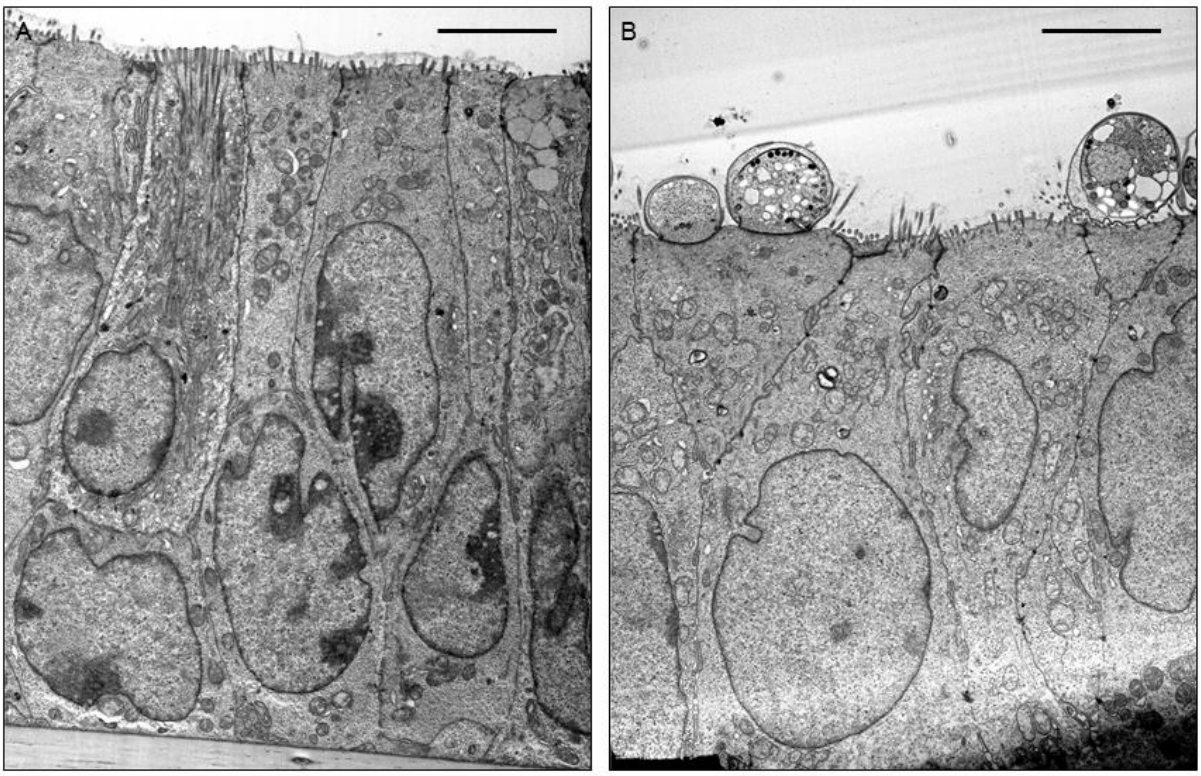

Figure 3.2. Electron microscopy images of ALI culture.

A) Uninfected region of ALI monolayer. Note cell height and presence of brush border. Scale bar = 5 μm.

B) Region of ALI monolayer with infected cells. Cell height and brush border are maintained in the presence of infection. Life cycle stages present in this image are early- and middle-stage macrogamonts. Scale bar = 5 μm.

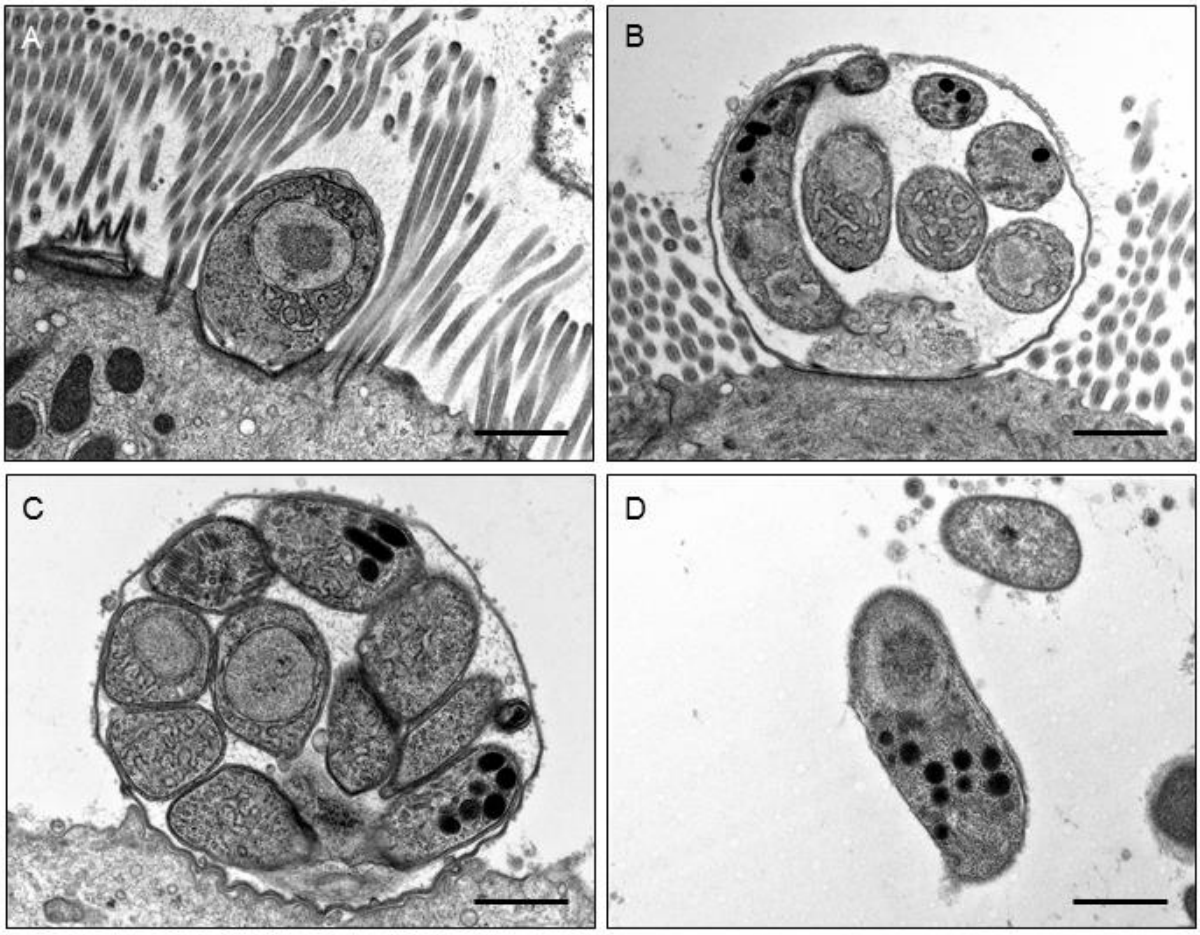

Figure 3.3. Electron microscopy images of asexual life cycle stages in ALI culture.

A) Trophozoite. Note disruption of brush border in the area of parasite attachment. Scale bar = 1 μm.

B, C) Type I meronts. Note multiple mature merozoites within the parasitophorous vacuole. Scale bar = 1 μm.

D) Extracellular merozoite. Scale bar = 1 μm.

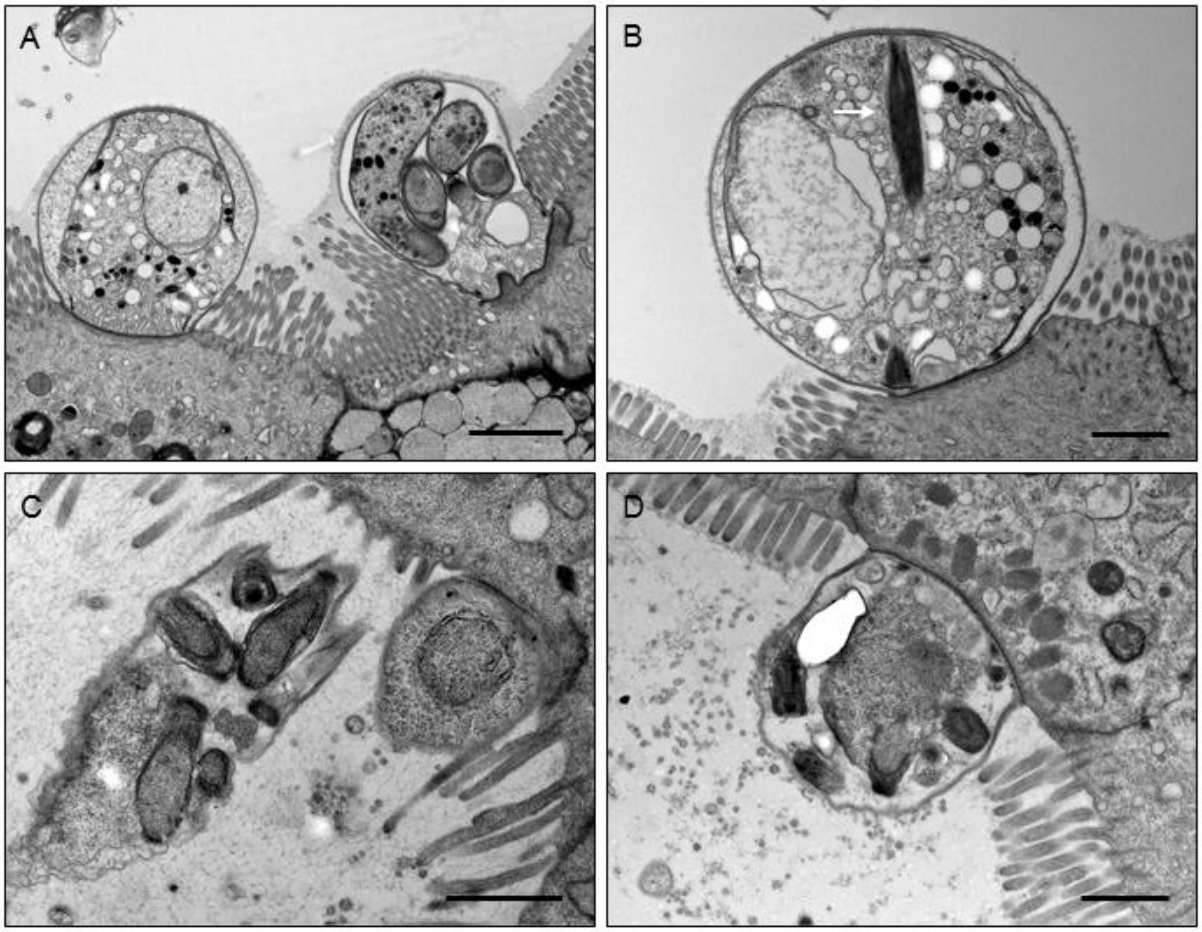

Figure 3.4. Electron microscopy images of sexual life cycle stages in ALI culture.

A) Macrogamont (right) and type II meront (left). Scale bar = 2 μm.

B) Macrogamont. Arrow is highlighting the presence of striated fiber. Scale bar = 1 μm.

C, D) Microgamonts. Note bullet-shaped parasites within vacuole. Scale bar = 1 μm.

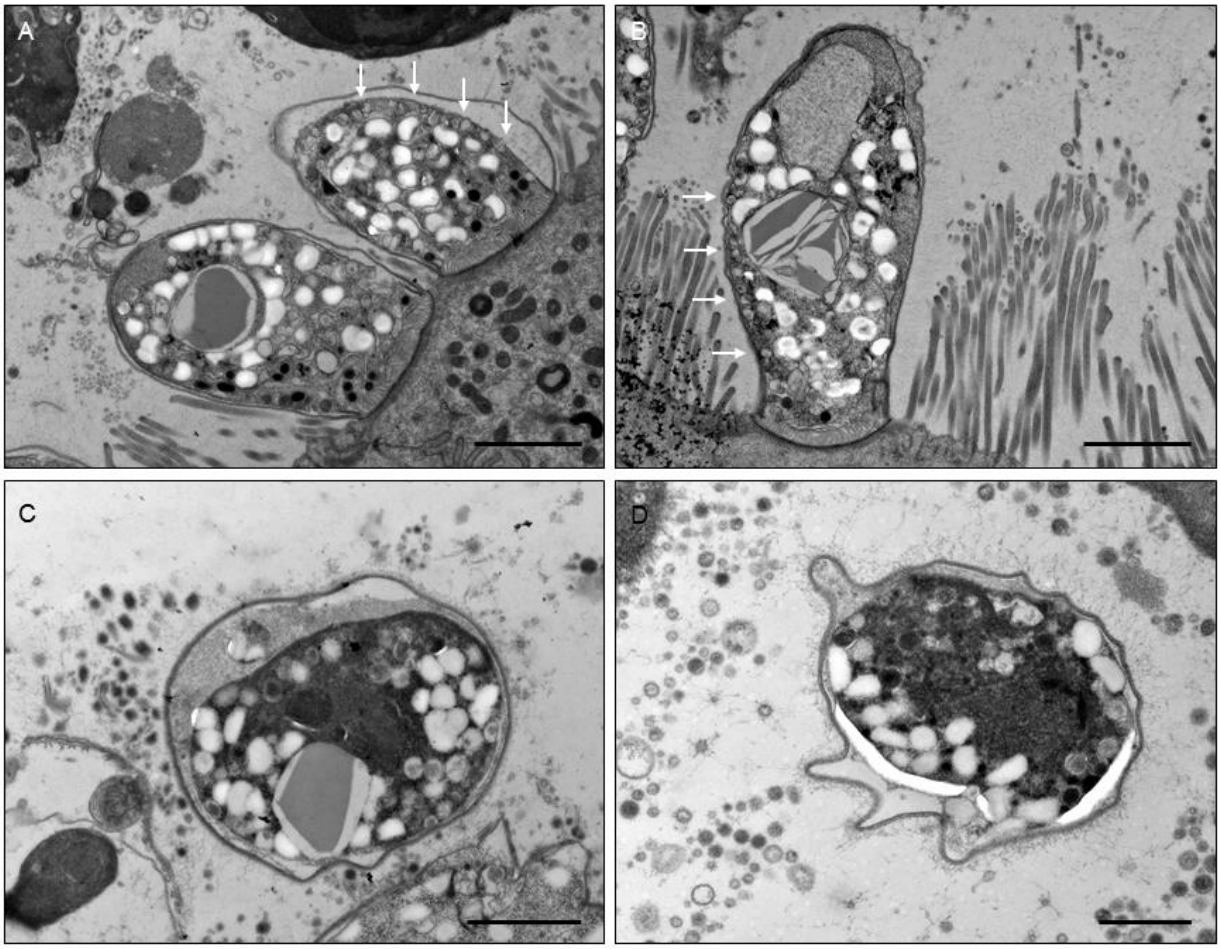

Figure 3.5. Electron microscopy images of late-stage macrogamonts and unsporulated oocysts in ALI culture.

A, B) Late-stage macrogamonts. Arrows pointing towards multiple vesicles lining up near the parasite surface. Scale bar = 2 μm.

C, D) Unsporulated oocysts. Note dense cytoplasm and the presence of a wall instead of vacuole membrane. Scale bar = 1 μm.

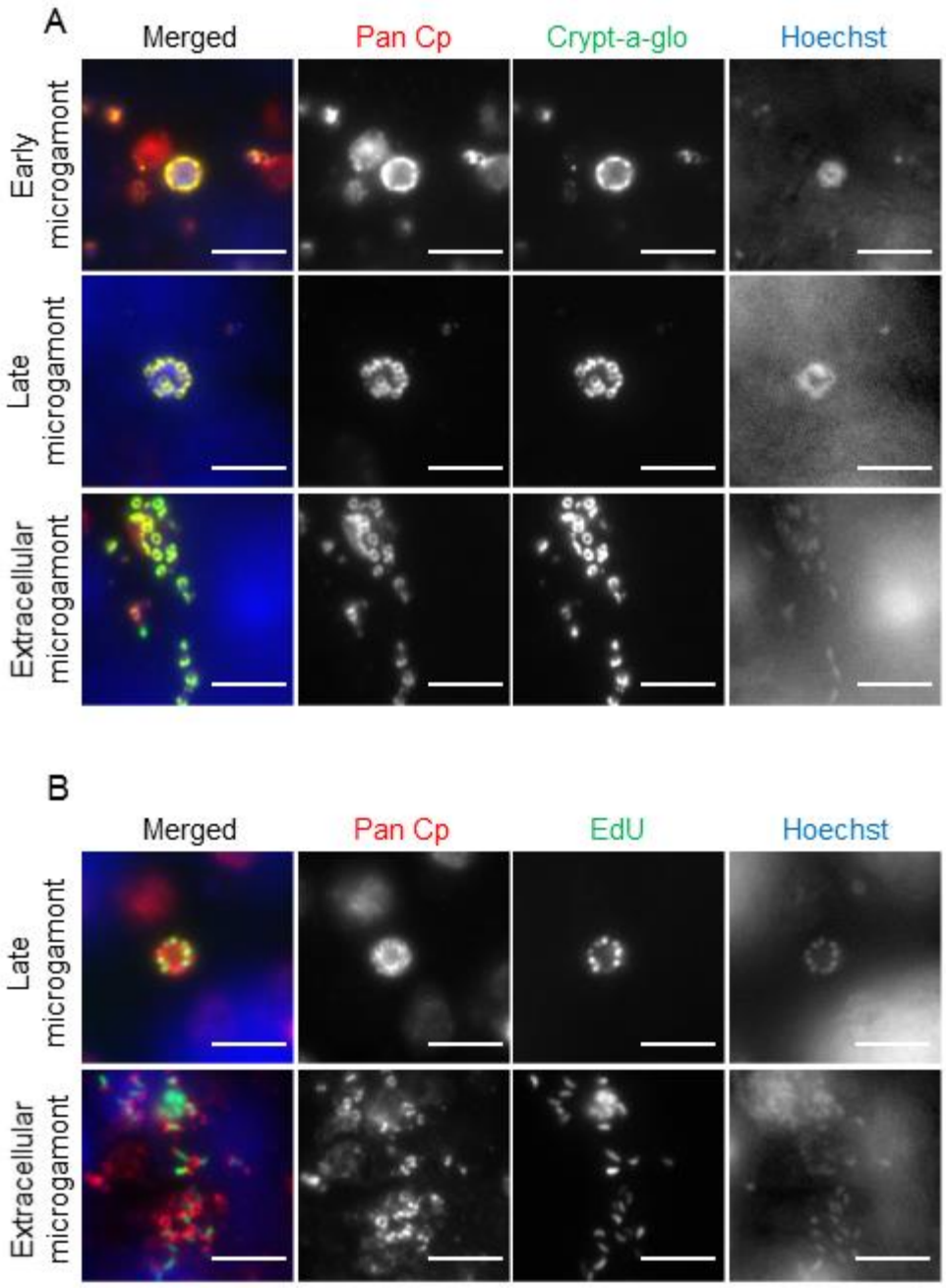

Figure 3.6. Microgamonts are recognized by Crypt-a-glo™ in ALI culture.

A) Transwells were infected with filtered sporozoites. On day 2 post-infection, transwells were fixed and stained with pan Cp, Crypt-a-glo™, and Hoechst. Secondary antibodies used were goat anti-rabbit 555. First row depicts early microgamonts, defined by their small size, multiple tiny

nuclei, and surface staining by pan Cp and Crypt-a-glo™. Second row depicts late microgamonts, which are identifiable by the rings forming around each nucleus, recognized by pan Cp and Crypt-a-glo, implying the formation of separate microgamonts. Third row depicts extracellular microgamonts that have been released from the parasitophorous vacuole. Scale bar = 5 μm.

B) Transwells were infected with filtered sporozoites. On day 1 post-infection, 10 μM EdU was added to the medium in the bottom chamber and left overnight. On day 2 post-infection, transwells were fixed and EdU labeled with click chemistry and microgamonts with pan Cp and Crypt-a-glo™. First row depicts late microgamonts and second row depicts extracellular microgamonts. Scale bar = 5 μm.

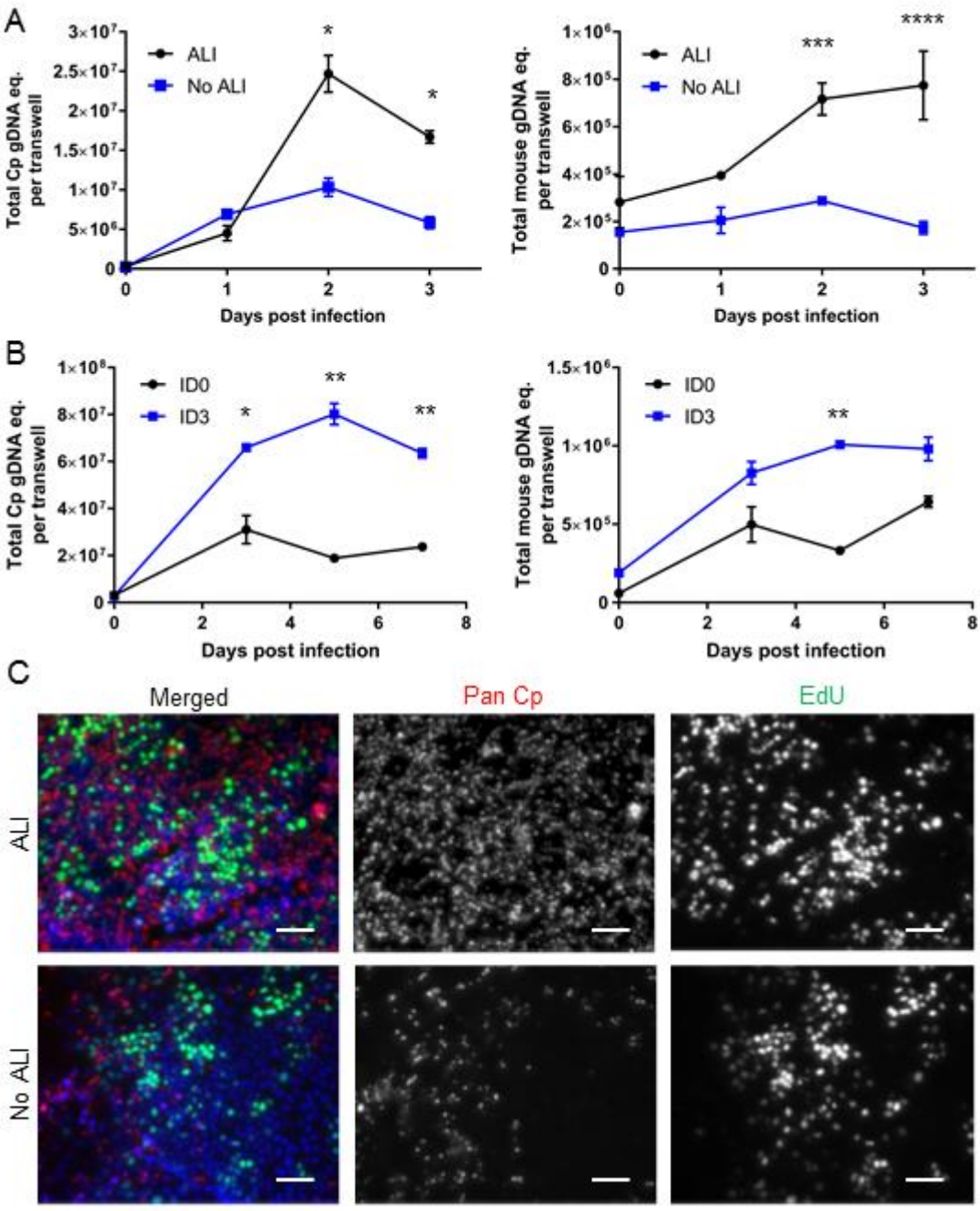

Figure 3.7. *C. parvum* growth in primary cell culture requires ALI and differentiated monolayers.

A) Top medium was removed from half of transwell to create "ALI" group; "no ALI" group continued to have top medium. Three days after the top medium was removed, both sets of

transwells were infected with 2x10^5 oocysts. Monolayers were incubated with oocysts for 4 hr and then washed 3 times. DNA samples were collected daily. Left graph depicts qPCR measuring *C. parvum* GAPDH in DNA samples; data is presented as *C. parvum* genomic DNA equivalents (Cp gDNA eq.). Right graph depicts qPCR measuring mouse GAPDH in DNA samples; data is presented as mouse genomic DNA equivalents (mouse gDNA eq.). * $P \leq 0.05$, *** $P \leq 0.001$, **** $P \leq 0.0001$.

B) Top medium was removed from transwells to create ALI. One group of transwells were infected the same day of top medium removal with 2x10^5 oocysts (ID0); the other group was infected 3 days post top medium removal with 2x10^5 oocysts (ID3). Monolayers were incubated with oocysts for 4 hr and then washed 3 times. DNA samples were collected daily. Left graph depicts qPCR measuring *C. parvum* GAPDH in DNA samples; data is presented as *C. parvum* genomic DNA equivalents (Cp gDNA eq.). Right graph depicts qPCR measuring mouse GAPDH in DNA samples; data is presented as mouse genomic DNA equivalents (mouse gDNA eq.). * $P \leq 0.05$, ** $P \leq 0.01$.

C) Top medium was removed from half of transwell to create “ALI” group; “no ALI” group continued to have top medium. Three days after the top medium was removed, both sets of transwells were infected with 2x10^5 oocysts. Monolayers were incubated with oocysts for 4 hr and then washed 3 times. On day 2 post infection, 10 µM EdU was added to the bottom chamber of both groups of transwells. After 8 hours, the transwells were fixed; EdU was labeled through a click-chemistry reaction, C. parvum was labeled with pan Cp, and host cell DNA was labeled with Hoechst. Secondary antibodies used were goat anti-rabbit Alexa Fluor 568. Scale bar = 50 µm.

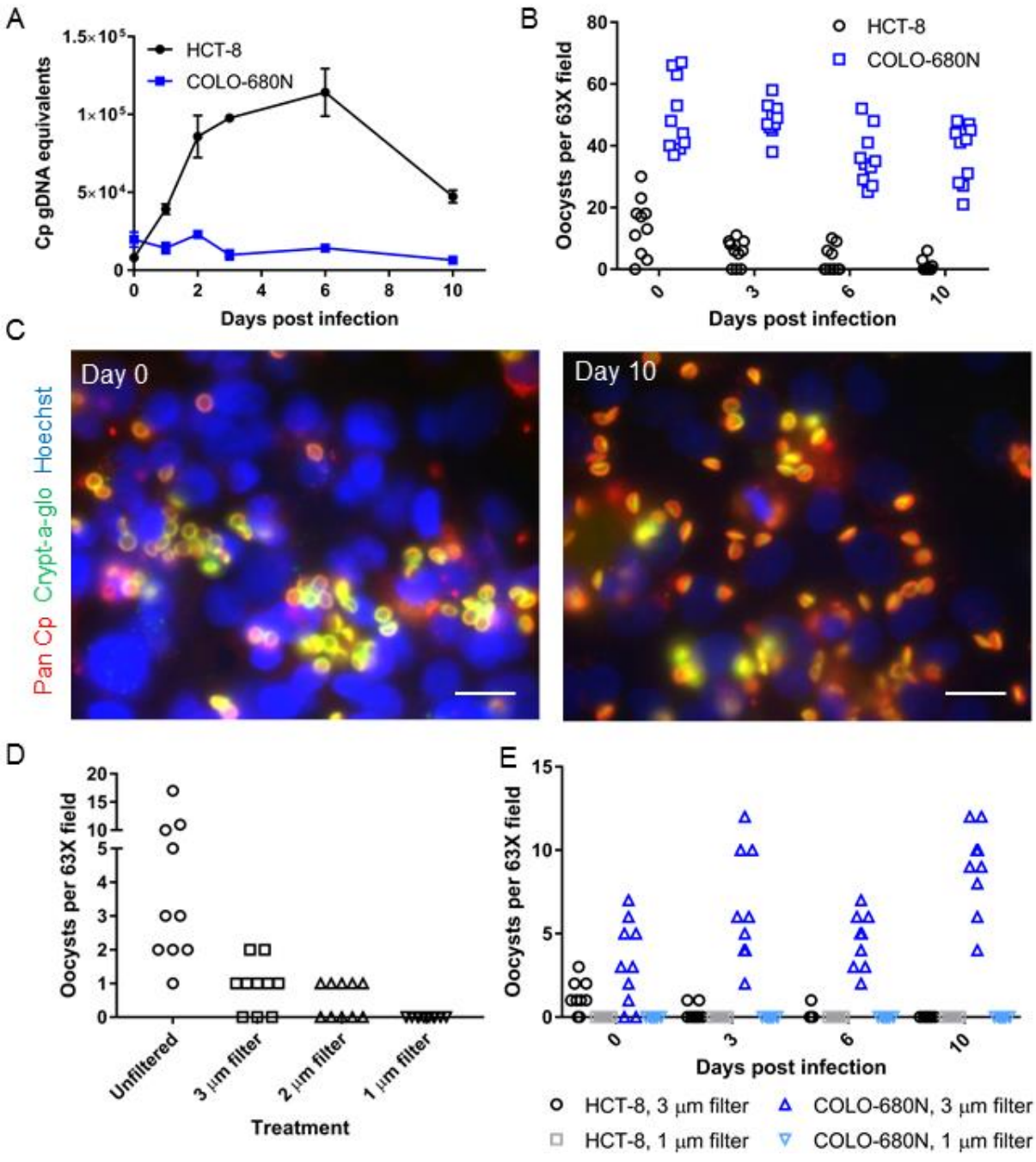

Figure 3.8. Testing COLO-680N line for ability to support *C. parvum* growth and oocyst development.

A) HCT-8 and COLO-680N cells were infected with 1.2x10^6 oocysts; after 4 hr, cells were washed 3x and cell medium was replaced. Samples were collected at indicated time points for

DNA samples. qPCR was used to determine the level of *C. parvum* GAPDH equivalents in the sample.

B) Oocysts counts for the same experiment in (A). Cells were fixed and stained with Pan Cp and Crypt-a-glo™. The number of oocysts were counted per field; each data point is the number of oocysts in a single 63X field.

C) Fluorescent microscopy images from the same experiment in (A) and (B). Cells were fixed and stained with Pan Cp and Crypt-a-glo™. COLO-680N monolayers are shown from day 1 and 10 post-infection. Scale bar = 20 μm.

D) Oocysts were excysted and either left unfiltered or filtered using filters with the indicated pore sizes. The oocysts/sporozoites were added to PLL-coated coverslips, fixed, and stained with Pan Cp and Crypt-a-glo™. The number of oocysts were counted per field; each data point is the number of oocysts in a single 63X field.

E) HCT-8 and COLO-680N cells were infected with oocysts filtered through a 3 or 1 μm filter. On the days indicated, Cells were fixed and stained with Pan Cp and Crypt-a-glo™. The number of oocysts were counted per field; each data point is the number of oocysts in a single 63X field.

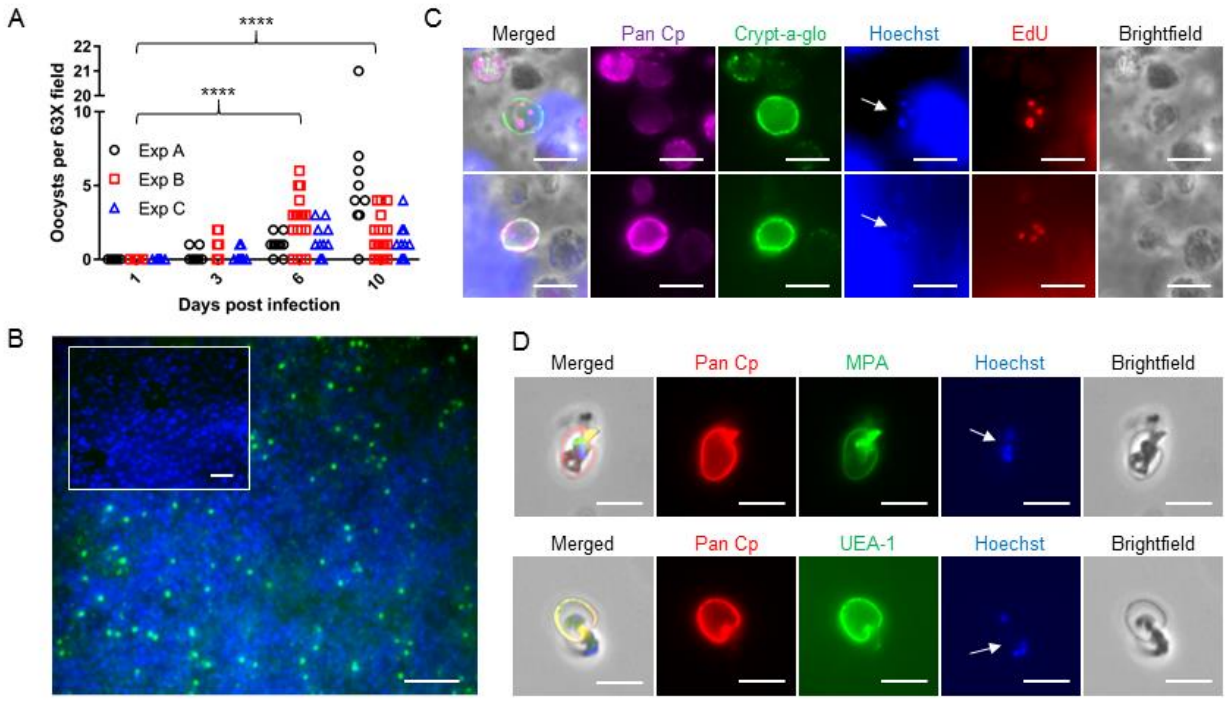

Figure 3.9. In vitro production of oocysts in ALI culture.

A) In three separate experiments, transwells were infected on day 3 post-top medium removal with filtered sporozoites. On days 1, 3, 6, and 10, transwells were fixed and stained with Crypt-a-glo™ and pan Cp to monitor oocyst development. Images were taken at 63X magnification and oocysts counted. Each data point is the number of oocysts in a single field. Statistical analysis: Two-way ANOVA corrected for multiple comparisons using the Dunnett method. The mean of each time point was compared to the mean of day 1. **** $P \leq 0.0001$.

B) Transwells were infected on day 3 post-top medium removal with filtered sporozoites. On day 2 post-infection, 10 µM EdU was added to the medium in bottom chamber and left overnight. Cells were fixed and EdU was labeled through a click chemistry reaction. *C. parvum* was labeled with pan-Cp and Crypt-a-glo™. DNA was labeled with Hoechst. Secondary antibodies used were goat anti-rabbit Alexa Fluor 647. White arrows in Hoechst images are highlighting the nuclei within the oocyst. Scale bar = 5 µm.

C) Low magnification (20X) image of transwell infected with filtered sporozoites on day 10 post-infection. Transwell is stained with Crypt-a-glo™ to detect oocysts and Hoechst to stain DNA. Inset picture is on day 1 post-infection. Scale bar = 50 µm.

D) Transwells were infected with filtered sporozoites and bleached on day 3 post-infection. Bleached material was placed on PLL-coated coverslip and stained with pan Cp, Hoechst, and either MPA or UEA-1. Secondary antibodies used were goat anti-rabbit Alexa Fluor 568. Scale bar = 5 µm.

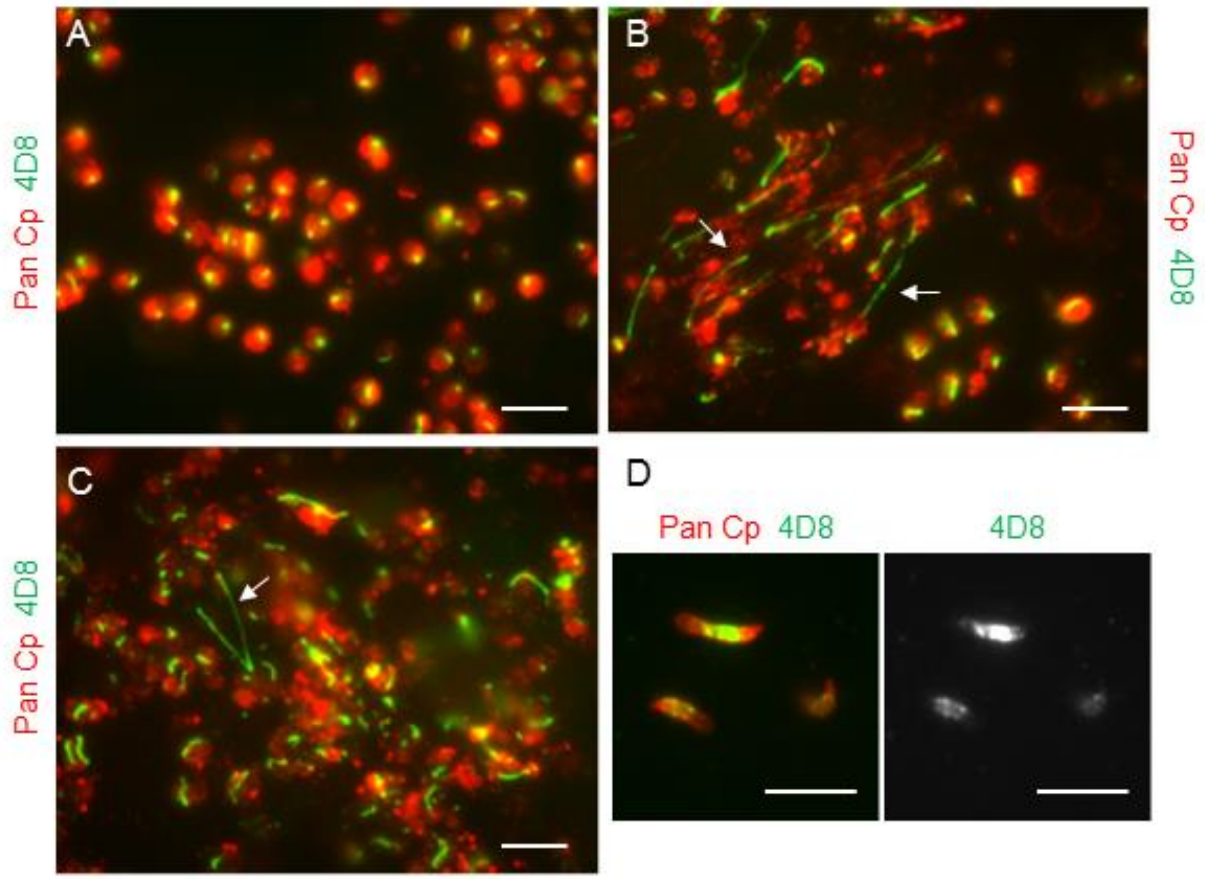

Figure 3.10. Unusual 4D8 reactivity pattern seen in infected ALI culture.

For A, B, and C) Transwells were infected with filtered sporozoites. On day 2 post infection, transwells were fixed and stained with pan Cp and 4D8. Secondary antibodies used were goat anti-rabbit Alexa Fluor 568 and goat anti-mouse Alexa Fluor 488. White arrows highlight "trails" recognized by 4D8. Scale bar = 50 µm.

D) Oocysts were excysted and plated onto PLL-coated coverslip, fixed and stained as above. Scale bar = 5 µm.

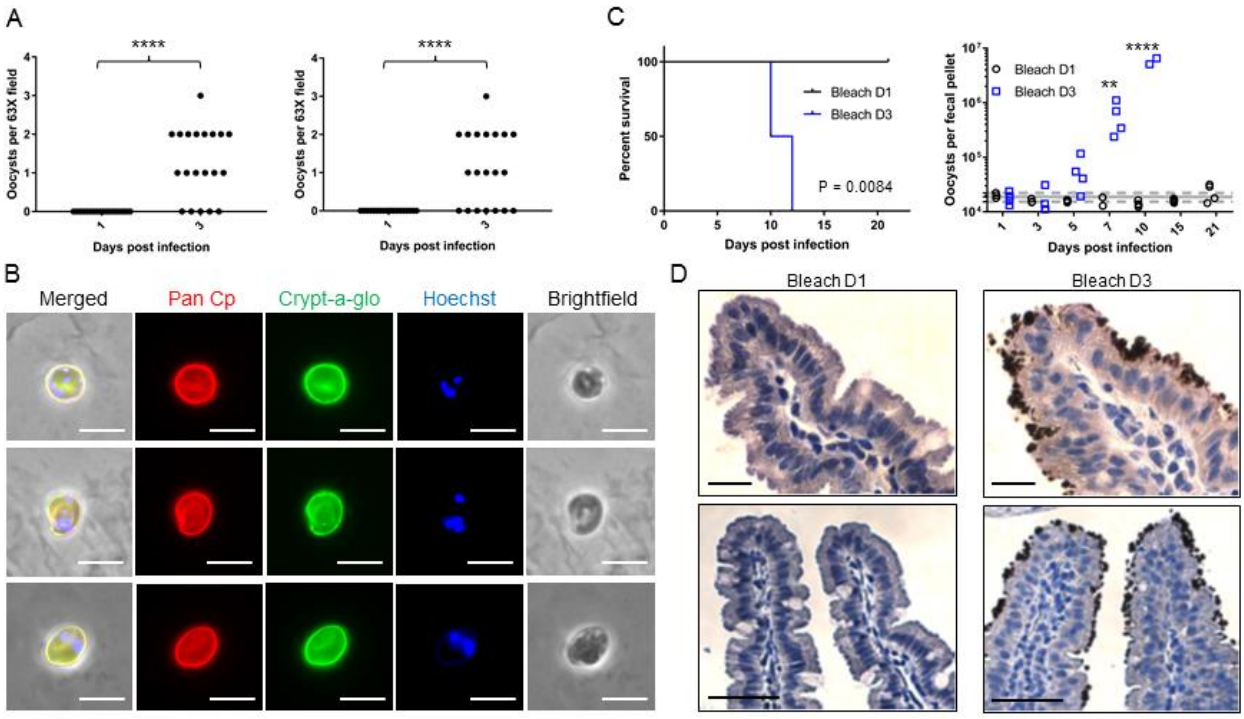

Figure 3.11. Oocysts produced *in vitro* are infectious to mice.

A) Transwells were infected with filtered sporozoites. On days 1 and 3 post-infection, transwells were either fixed and stained with pan Cp and Crypt-a-glo™, or bleached and placed on PLL-coated coverslip, then stained with pan Cp and Crypt-a-glo™. Left graph depicts oocyst counts from whole mount images of infected ALI monolayers, right graph depicts oocyst counts from bleached material. Images were taken at 63X; each data point is the number of oocysts in a single field. Data was analyzed using an unpaired T test. **** $P \leq 0.0001$.

B) Images of oocysts in bleached material of transwells on day 3 post infection. Oocysts were stained with pan Cp, Crypt-a-glo™, and Hoechst. Secondary antibodies used were goat anti-rabbit 568.

C) Transwells were infected with filtered sporozoites. On days 1 and 3 post-infection, transwells were bleached and the material was orally gavaged into mice. Each mouse received about 4

transwells' worth of bleached material. Left graph shows survival curves of the mice in the two groups. Data was analyzed using the log-rank (Mantel-Cox) test. In the right graph, fecal pellets were collected from the mice on the days indicated. DNA was isolated from the pellets and qPCR was used to determine the number of *C. parvum* gDNA equivalents present in each sample. The gray line represents the mean value of both groups for day 1, the dotted lines are the standard deviations. Data was analyzed using a 2-way ANOVA comparing the mean of each group across all time points, corrected for multiple comparisons using the two-stage step-up method of Benjamini, Kreieger, and Yektieli. ** $P \leq 0.01$, **** $P \leq 0.0001$.

D) Sections of small intestine collected from mice gavaged with the bleached material, stained with pan Cp by IHC. The mouse that received day 1 material was sacrificed on day 30 post-gavage (sections shown on left) and the mouse that received the day 3 material was sacrificed on day 9 post-gavage (sections shown on right). Scale bar in top row = 20 μm, scale bar in bottom row = 50 μm.

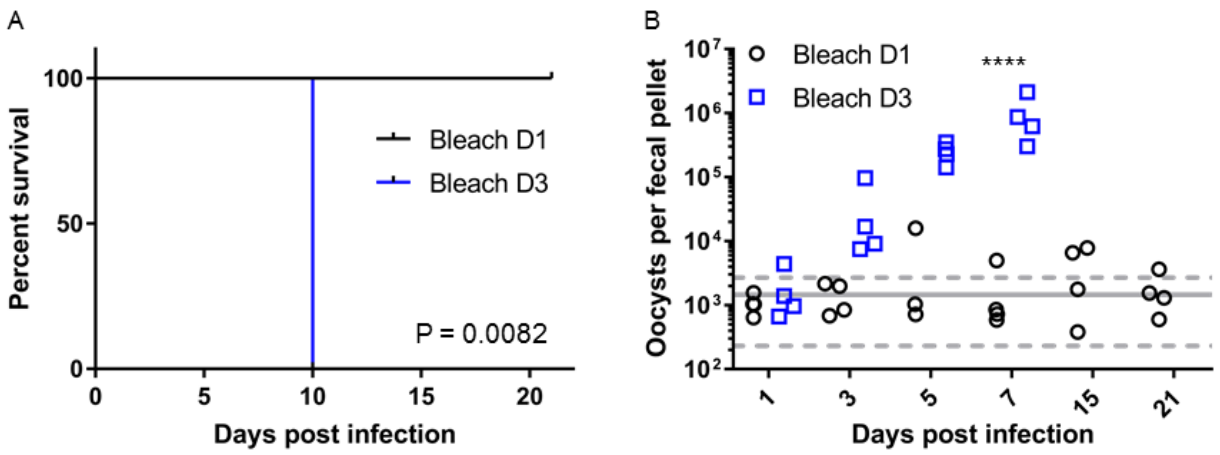

Figure 3.12. Oocysts produced *in vitro* are infectious to mice (repeat experiment).

ALI transwells were infected with filtered sporozoites. On days 1 and 3 post-infection, transwells were bleached and the material was orally gavaged into mice. Each mouse received about 4 transwells' worth of bleached material. Mice were housed individually after inoculation.

A) Survival curves of the mice in the two groups. Data was analyzed using the log-rank (Mantel-Cox) test.

B) Fecal pellets were collected from each mouse on the days specified. DNA was isolated from the pellets and qPCR was used to determine the number of *C. parvum* gDNA equivalents present in each sample. The gray line represents the mean value of both groups for day 1, the dotted lines are the standard deviations. Data was analyzed using a 2-way ANOVA comparing the mean of each group across all time points, corrected for multiple comparisons using the two-stage step-up method of Benjamini, Kreieger, and Yektieli., **** $P \leq 0.0001$.

Appendix: Attempts to serial passage *C. parvum in vitro*

When we found that the ALI system supported completed life cycle development of *C. parvum* as well as long-term growth, we expected that the system would also support serial passage of *C. parvum*. Historically, when long-term growth of a parasite is achieved in culture, the step to serial passage is minimal, which was the case with *Toxoplasma* and *Plasmodium spp.* (178, 179). However, there are exceptions; complete development of *Isospora suis*, the causative agent of piglet coccidiosis, has been achieved *in vitro* but not propagation (180). Serial passage would enable us to maintain *Cryptosporidium in vitro*, making it unnecessary to use the mouse or calf to amplify infection and make oocysts. It would also make genetic modification of *C. parvum* significantly easier, since lines could be selected for and maintained *in vitro*.

When I first began attempting to passage *C. parvum* with the ALI system, I approached it very simply and mimicked *Toxoplasma* passage in HFF cells (see row in Appendix table 1 describing syringe-lysing attempts). I scraped infected ALI cultures into warm cell culture medium using a blunt yellow tip, combined the material (about 1 ml total volume), syringe-lysed the mixture to shear the host cells and release the parasites, and then passaged to fresh transwells at roughly 1:3 or 1:4 ratio. The passaged inoculum was left on the cells for about 3-4 hours and then removed in order to maintain the ALI. I tested passaging at different time points post-infection to see if I could pinpoint what life cycle stage was capable of propagating infection: early passage (day 1-2) for asexual stages and late passage (day 3 or later) for sexual stages and oocysts. Some experiments indicated that late passage worked better and led to earlier outgrowth, but it was unclear if this was due to the presence of *in vitro*-produced oocysts or just higher numbers of parasites in the inoculum. In all experiments, it took at least 10-14 days to see any sign of growth in the transwells that received the passaged infection, and the growth was

stunted compared to what you would see in a "normal" infection. It seemed that some life cycle stage was capable of propagating infection, but it was present at a very low frequency. We know that the ALI system can amplify small doses of *C. parvum* (appendix figure 1), so even if only a few parasites can make it through the passaging process, they should be able to amplify.

The biggest issue, however, was the inconsistency in infection levels between samples that were collected at the same time point; if three samples were collected, often only one showed signs of parasite growth. I want to emphasize that this level of variability is not seen in a normal infection; while transwells from the same time point can have some variation in parasite levels, there are never transwells that are negative for infection. This inconsistency implied that whatever parasite stage, or growth promoting condition, was capable of passaging the infection was being unevenly distributed between the new monolayers. This was a major issue because it made it impractical to try serial propagation attempts, since there was no way of identifying which transwells were productively infected without looking by qPCR or microscopy, which consumes the sample.

When simple passaging methods do not seem to work or produced inconsistent infection I began testing other variables. I tested different needle gauge sizes to create a more homogenous lysate, which I thought would lead to more consistent infection in the recipient transwells. I would first syringe-lyse using a large needle gauge, like 20G, and then move to a smaller needle gauge, like 23G or 25G. This did create a more homogenous mixture, but it did not completely remove clumps of mucus and cell debris. The later the infection was passaged, the clumpier the lysate, due to the presence of increased mucus in the ALI cultures. Using different needle gauges did not solve the problem of inconsistent or unsuccessful passage.

One concern was that the parasites were being exposed to too much oxygen during the syringe-lysing process, so a few steps were taken to minimize this. I syringe-lysed the cultures in large volumes of medium (5 ml) and kept the needle below the surface and was careful to avoid making bubbles. This required centrifuging the material (2500 rpm x 3 min) after syringe lysis and resuspending in a small volume to passage the infection. I also added glutathione (GSH) to the medium at the same concentration (5 mM) used in Cytomix, a buffer used during transfection of *Toxoplasma*. Lysing the cells in a large volume and/or using GSH did not improve passaging. I also tried syringe-lysing cultures in an anaerobic hood (gas mix present: 75% N_2/20% CO_2/5% H_2) to completely remove the presence of oxygen and passing the material to fresh monolayers while still inside the hood cells (see row in Appendix table 1 describing anaerobic passage attempts). I kept the monolayers inside the hood for 60 min to allow for infection, and then moved the monolayers back to a normal incubator. This treatment did not improve passaging.

When syringe-lysing did not yield consistent positive results, I tried trypsinizing the infected cells and using the intact cells to passage infection, the logic being that the parasites could naturally egress from the cell instead of being prematurely forced out by syringe lysis cells (see row in Appendix table 1 describing trypsinizing attempts). The ALI monolayers were resistant to trypsinization, so the protocol required adding trypsin/EDTA to both the top and bottom chambers of the transwell and incubating for 20 min. This dissociated the monolayer and the cells were centrifuged at 1000 rpm for 3 min and then resuspended in a small volume to passage the infection. I tried leaving the trypsinized material on the new monolayers for short (3-4 hr) and long (overnight) periods of time to allow the parasites to egress and infect the new monolayer. I did not see any evidence of successful passage with this method. Same as syringe-

lysing, I tried trypsinizing the cells in an anaerobic hood to minimize exposure to oxygen, but this did not improve passaging.

With both syringe-lysing in a large volume and trypsinizing the cells, the infected material was centrifuged before being added to the new monolayers. I became concerned that the centrifugation step was shearing off the parasitophorous vacuoles and therefore decreasing the inoculum size, possibly explaining the poor outgrowth. So, with both conditions (syringe-lysing and trypsinization), I avoided centrifugation and directly added the material to the new transwells. This adjustment did not improve passaging outcome.

The Stappenbeck lab had preliminary evidence showing that ALI monolayers could be trypsinized and the cells split and seeded into new transwells, leading to the formation of new monolayers without using spheroids. I tried to trypsinize and split infected monolayers, combine the infected cells with uninfected cells from trypsinized spheroids, and plate the mixture into transwells cells (see row in Appendix table 1 describing splitting infected monolayers attempts). I then removed the top medium at different days post-seeding, either day 1 or day 4. I did not wait the full 7 days because we had found in other experiments that submerged transwells did not support parasite growth as well as ALI transwells. I did not find any evidence of robust outgrowth in the new transwells.

I thought that inducing parasite egress with a chemical agent like Zaprinast or A23187 could help improve passaging cells (see row in Appendix table 1 describing Zaprinast/A23187 attempts). Zaprinast is a cGMP-specific phosphodiesterase inhibitor that activates cyclic GMP-dependent protein kinase (PKG) and stimulates tachyzoite egress in *Toxoplasma* (181). A23187 is a calcium ionophore that also induces egress in *Toxoplasma* tachyzoites (181). I treated infected monolayers with both reagents separately, at concentrations used to induce egress in

Toxoplasma, for 10 min. I scraped the monolayers and passaged the infection without syringe-lysing. I did not see any outgrowth in the new transwells.

There are two caveats to interpreting data from early passaging experiments. Experiments from before June 2017 used 3 µm filters to filter out oocysts from the initial infection; later this was switched to 1 µm filters when it was found 3 µm was not sufficient to completely remove oocysts from the input inoculum. I am concerned that the partial successes of some of the earliest experiments may be due to contaminating oocysts in the input inoculum; these may have excysted after passaging and led to more outgrowth than would be expected. Also, experiments before January 2018 infected monolayers on day 0 post top media removal, but this was later changed when it was found infecting on day 3 post top media removal led to consistently better growth; therefore, all initial infections were started on day 3 ALI cultures and infections were also passaged to day 3 ALI cultures.

The lack of success with propagation using the ALI system is particularly frustrating given that we have found that Ifngr1$^{-/-}$ mice can become productively infected with syringe-lysed monolayers, even from day 1 post-infection cultures (appendix figure 2). This is possible even with monolayers that have been infected with sporozoites that have been filtered with a 1 µm filter, meaning there is no oocyst contamination. This result suggests that there is a life cycle stage besides oocysts that is capable of transmitting the infection, but for some reason, it does not occur *in vitro*. It is possible that passage through the gut "activates" the infectious stage in some way that syringe-lysing, trypsinization, etc. are not able to mimic. It is also possible that lysed cultures contain some inhibitor that prevents subsequent growth in vitro, but which is neutralized or eliminated *in vivo*.

Advice for future attempts

When designing propagation experiments, it is important to infect the initial monolayers that will be used for passaging with 1 μm filtered sporozoites. I believe infecting the initial monolayers with oocysts may lead to false positives in the set of transwells that receive the passaged infection. Set aside transwells from the initial infection to check for growth by qPCR and microscopy, to confirm robust infection and oocyst development. The set of transwells that receive the passaged infection should have a set of control transwells that are infected normally with either sporozoites or oocysts to confirm that the monolayers are able to support infection. Each time point for the passaged infection should have 3 transwells for DNA samples to check for the level of variability in infection. It is not necessary to look for evidence of infection by both microscopy and qPCR for pilot experiments; I have found qPCR to be more useful.

Appendix Table 2. Attempts at propagating *C. parvum*

Type	*Basic description*	*Variables tested*	*Notes*
Syringe-lysing	Scraping monolayers with blunt yellow pipette tip; collecting material and lysing using syringe and needle	• Passaging on days 1, 2, 3, 6, 9, and 10 • Using different needle gauges (25G, 23G, and 21G); combining multiple needle gauges • Adding 5 mM GSH to medium during lysis to protect against oxidation • Lysing in large volume (5 ml) to limit air exposure • Skipping centrifugation step (1250 g x 3 min) to avoid shearing parasitophorous vacuoles • Infecting original monolayer with high dose (1x10^6 oocysts) instead of usual low dose (2x10^5 oocysts or sporozoites)	No consistent outcomes; large variability in growth between transwells that received the passaged infection
Trypsinizing	Washing monolayers in PBS-EDTA (0.5 mM), adding trypsin to top and bottom chamber, then collecting cells after 20 min	• Passaging on days 1, 2, 3, 6, 9, and 10 • Incubating monolayers with passaged material for short pulse (2-4 hours) or overnight • Skipping centrifugation to avoid shearing parasitophorous vacuoles (200 g x 3 min)	No growth
Splitting infected monolayers	Trypsinizing infected monolayers (see text for explanation) and adding the cells to freshly trypsinized spheroids to create new monolayers	• Passaging from monolayers infected with a high and low dose of oocysts • Removing top medium day 1 or day 4 post-seeding	No growth

Zaprinast and A23187	Treating monolayers with agents to induce egress	• Treated monolayers on day 3 post-infection with either Zaprinast (100 μm) or A23187 (2 μm) for 10 min at 37°C; scraped monolayers and passaged	No growth
Anaerobic	Manipulating transwells under anaerobic conditions (75% N_2/20% CO_2/5% H_2) when passaging infection (see text for explanation)	• Syringe-lysing or trypsinizing • Day 3 and 6 post-infection • Incubated monolayers with passaged material overnight in normal 5% CO_2 incubator	No growth

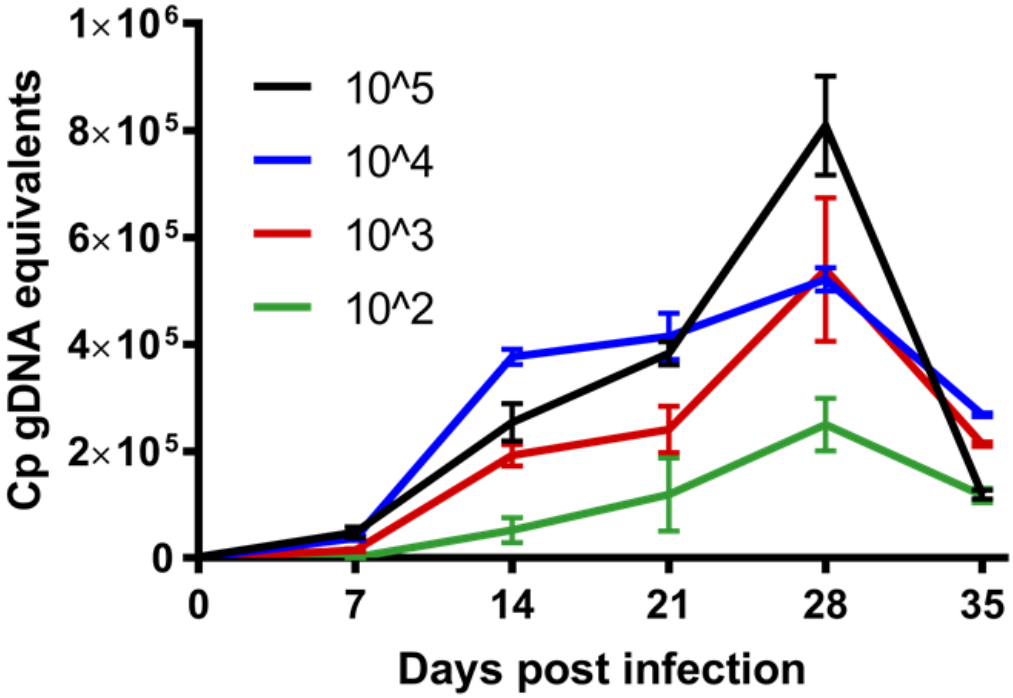

Appendix Figure 1. Oocyst dose response in ALI culture.

Transwells were infected with oocysts on day 0 of top medium removal. Samples were collected every 7 days for DNA collection. *C. parvum* genomic DNA equivalents were determined by using qPCR to measure *C. parvum* GAPDH levels.

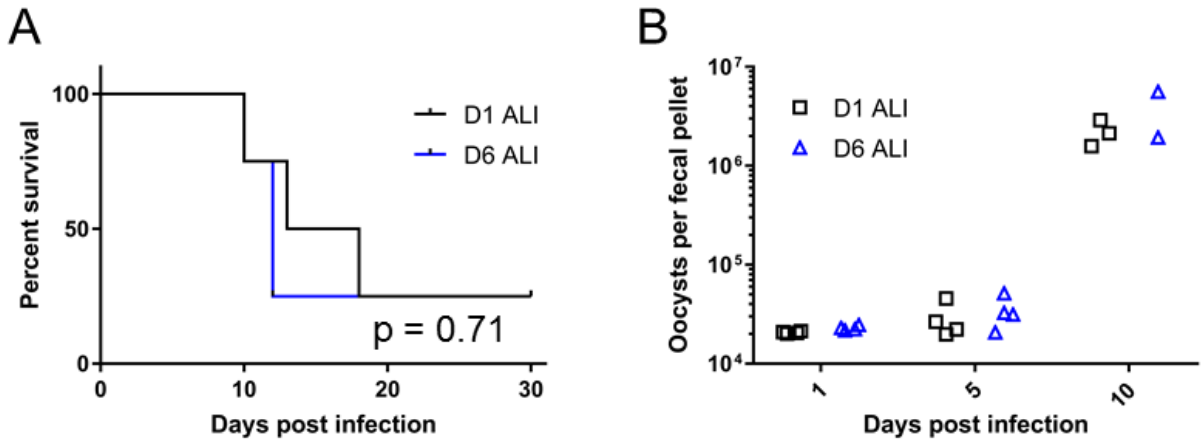

Appendix Figure 2. Inoculating Ifngr1$^{-/-}$ mice with *C. parvum*-infected ALI cultures.

ALI monolayers were infected on day 3 post-top medium removal with sporozoites filtered through 1 µm filter. On days 1 and 6 post-infection, monolayers were scraped and syringe-lysed with 20G and 23G needles. Each mouse received 1 transwells' worth of material in a 200 µl volume by oral gavage. 4 mice per group. The mice were housed individually after inoculation. Graph in (A) depicts the survival curve of each group of mice. Data was analyzed using the log-rank (Mantel-Cox) test. Graph in (B) shows the result of the qPCR performed on the DNA extracted from the fecal pellets of the mice measuring levels of genomic *C. parvum* equivalents.

Chapter 4

In vitro culture of *Cryptosporidium parvum*

in primary cells

Preface

The first complete draft of this chapter was written by GW. Comments from LDS were incorporated into the final version presented here. GW, YW and SR optimized the ALI system for *C. parvum* infection. TSS, YW and WW provided key biological reagents and advice. TSS and LDS provided advice and supervision.

This chapter is an invited review for Methods and Molecular Biology, to be submitted:

Wilke, G., Wang, Y., Ravindran, S., Stappenbeck, T.S., Witola, W., Sibley, L.D. (2018) *In vitro* culture of *Cryptosporidium parvum* using primary/stem cells.

Summary

C. parvum has a complex life cycle consisting of asexual and sexual phases that culminate in oocyst formation in vivo. The most widely used cell culture platforms to study *C. parvum* only support a few days of growth and do not allow the parasite to proceed past the sexual stages to complete oocyst formation. Additionally, these cell culture platforms are mostly adenocarcinoma cell lines, which do not adequately model the parasite's natural environment in the small intestine. We describe here a method to create primary intestinal epithelial cell monolayers that support long-term *C. parvum* growth. Monolayers were derived from intestinal stem cells grown as spheroids and plated onto transwells, allowing for separate apical and basolateral compartments. In the apical chamber, the cell growth medium was removed to create an "air-liquid interface" that enhanced host cell differentiation and *C. parvum* growth. The use of primary intestinal cells to grow *C. parvum* in vitro will be a valuable tool for studying host-parasite interactions using a convenient in vitro model that resembles the intestinal environment.

1 Introduction

A significant barrier to *Cryptosporidium* research is the lack of a cell culture system that enables long-term growth *in vitro*. Historically, human adenocarcinoma cells have been used to study asexual and early sexual growth of the parasite (142). These cell lines support growth of the parasite over 2-3 days but after the parasite enters the sexual part of its life cycle, numbers rapidly diminish because oocyst formation is blocked (78, 79, 142). This limitation greatly affects the type of studies researchers can pursue when investigating *Cryptosporidium* biology.

Recently, there have been several reports of cell culture platforms capable of supporting complete life cycle development of *C. parvum*, a species of *Cryptosporidium* frequently associated with disease in humans and animals. (2-4). One platform utilizes a hollow fiber system to mimic the intestine by allowing for separate control of the apical and basolateral compartments (95); this system enables the creation of an environment with redox and nutrient conditions optimal for parasite growth. However, it requires the use of expensive equipment and the hollow fiber cannot be "opened" during the experiment, making microscopy studies difficult. Also, the expense of the hollow fiber system means that experiments are not easily scalable, and perturbations to the system are often done serially, instead of in parallel, a major limitation for any kind of drug study. Another novel platform is a 3D intestinal model that uses silk protein as a scaffold for cell growth (96); this model also has a lumen, creating two separate compartments. This platform involves the use of specialized equipment to create the 3D scaffolds, making it more challenging for other researchers to adopt. While both platforms have limitations, they are capable of producing oocysts that are infectious to cells (95, 96) and mice (95), which enables continuous culture *in vitro*.

The two new platforms use adenocarcinoma cells (HCT-8 and Caco-2 cells), which are likely very different from the cell types *C. parvum* infects *in vivo*, in terms of differentiation status, metabolism, and proliferation rate. To accurately reproduce *in vivo* host-parasite interactions in cell culture, it is necessary to utilize primary cells. Advancements in stem cell biology have made it possible to propagate intestinal stem cells as spheroids in medium containing specific growth factors (125, 126). The required cell culture medium has become relatively easy to make due to the creation of a supportive cell line, L-WRN, that secretes Wnt, R-spondin, and noggin, creating conditioned medium that is used to support spheroid growth (125). Cells derived from spheroids can be used to create primary intestinal epithelial cell monolayers grown on transwell membranes that recapitulate aspects of the gut, including development of specific cell lineages such as goblet and Paneth cells (131, 138). Murine ileal monolayers derived from this method support robust *C. parvum* growth, which enabled the creation of novel antibodies to intracellular parasite stages (167). These monolayers, however, typically only last 2-5 days, which make them unsuitable for studying long-term *C. parvum* growth.

In the last few years, a protocol for creating primary intestinal monolayers that exhibit dramatic differentiation and long-term viability has been published (132). This method relies on the inclusion of a feeder cell layer to support stem cell growth and the introduction of an air-liquid interface (ALI) at the surface of the cells. ALI has been used to enhance differentiation of airway tract epithelial cells for many years (133-135) and has also recently been applied to intestinal epithelial cell culture, resulting in increased expression of markers associated with cell differentiation and also significant changes in cell metabolism (136, 137).

Epithelial monolayers grown with an ALI and feeder cell layer can survive for weeks (132), making them attractive candidates for a cell culture platform for *C. parvum*. We have found that primary intestinal monolayers grown on transwells in L-WRN-conditioned medium with an ALI support long-term *C. parvum* growth. Parasite growth can last for weeks in this system without affecting host cell viability. We believe that this cell culture system will support further research into the life cycle of *C. parvum* and enable more thorough investigation of potential growth inhibitors.

2 Materials

2.1 Creating irradiated 3T3 (i3T3) cell stocks for feeder cell layer

1. Biosafety cabinet and 37°C, 5% CO_2 incubator
2. Mouse fibroblast cells (NIH/3T3, ATCC, cat. no. CRL-1658)
3. 37°C water bath
4. 15 and 50 ml polypropylene conical tubes
5. 3T3 growth medium: For 500 ml, combine 445 ml of Dulbecco's Modified Eagle's Medium (DMEM) modified to contain 4 mM L-glutamine, 4500 mg/L glucose, 1 mM sodium pyruvate, and 1500 mg/L sodium bicarbonate (ATCC, cat. no. 30-2002) with 50 ml heat-inactivated fetal bovine serum (FBS; Sigma, cat. no. F6178) and 5 ml 100X penicillin/streptomycin (Sigma, cat. no. P4333).
6. Centrifuge capable of holding 15 and 50 ml conical tubes that can spin at 200 x g
7. Tissue culture supplies such as 25, 75, and 150 cm^2 cell culture flasks (T-25, T-75, T-150) and disposable plastic pipettes
8. Dulbecco's Phosphate-Buffered Saline (DPBS)-EDTA: For 500 ml, add 500 µl 0.5 M EDTA pH 8.0 solution (Invitrogen, cat. no. 15575020) to 500 ml tissue culture grade DPBS.
9. Trypsin-EDTA: For 100 ml, add 10 ml 10X trypsin solution (Sigma, cat. no. T4549) to 90 ml DPBS-EDTA. Can be aliquoted and stored at -20°C for months; aliquots can be thawed and stored at 4°C for 7-10 days.
10. Machine capable of irradiating 15 ml conical at 3000 rads (such as the Xstrahl Small Animal Radiation Research Platform or SARRP)

11. Hemocytometer and cover glass
12. 3T3 freezing medium: For 50 ml, combine 10 ml FBS, 2.5 ml DMSO, and 37.5 ml 3T3 growth medium.
13. Cryovials, 1.5 ml volume
14. -80°C freezer
15. LN_2 tank

2.2 Plating i3T3 cells on transwells

1. Biosafety cabinet
2. Matrigel (Corning, cat. no. 354234)
3. Cold DPBS
4. Transwell with 0.4 µm pore polyester membrane insert (Corning Costar, cat. no. 3470)
5. Tissue culture supplies such as 15 ml conicals, 1.7 ml Eppendorf tubes
6. Vacuum flask and sterile disposable glass Pasteur pipettes
7. 37°C, 5% CO_2 incubator

2.3 Passaging spheroids

1. Spheroid line established according to Miyoshi & Stappenbeck 2013; for our purposes, we used a line isolated from the ileum of 8-10 week old C57BL/6J mouse. Lines can be frozen 1-2 passages after the original derivation and thawed as needed; use single line for 20-25 passages.
2. 37°C water bath

3. Tissue culture supplies such as 12 well plates, disposable pipettes, 15 and 50 ml conical centrifuge tubes, 1.7 ml Eppendorf tubes
4. Washing medium: Add 50 ml FBS, 5 ml 100X penicillin/streptomycin, 5 ml100X L-glutamine to DMEM/F12 with HEPES (Sigma, cat. no. D6421-500ML).
5. Matrigel (Corning, cat. no. 354234)
6. Biosafety cabinet
7. Cell scrapers (Biotium, cat. no. 22003)
8. Centrifuge capable of holding 15 conical tubes that can spin at 200 x g
9. Centrifuge capable of holding 1.7 ml Eppendorf tubes that can spin at 200 x g
10. DPBS-EDTA and trypsin-EDTA
11. Conditioned medium prepared according to Miyoshi & Stappenbeck 2013; requires L-WRN cell line (ATCC CRL-3276).
12. Primary medium: Add 6.25 ml 100X L-glutamine (Sigma, cat. no. G7513), 6.25 ml 100X penicillin/streptomycin (Sigma, cat. no. P4333), and 125 ml heat-inactivated FBS (Sigma, cat. no. F6178) to 500 ml Advanced DMEM/F12 (Thermo Fisher, cat. no. 12634)
13. ROCK inhibitor (Tocris, Y-27632)
14. 37°C, 5% CO_2 incubator.

2.4 Creating primary cell monolayers *for C. parvum* infection

1. Biosafety cabinet
2. Cell scrapers (Biotium, cat. no. 22003)

3. Tissue culture supplies such as 12 well plates, disposable pipettes, 15 and 50 ml conical centrifuge tubes
4. Centrifuge capable of holding 15 conical tubes that can spin at 200 x g
5. DPBS-EDTA and trypsin-EDTA
6. 37°C water bath
7. Washing medium: Add 50 ml FBS, 5 ml 100X penicillin/streptomycin, 5 ml100X L-glutamine to DMEM/F12 with HEPES (Sigma, cat. no. D6421-500ML).
8. Conditioned medium prepared according to Miyoshi & Stappenbeck 2013; requires L-WRN cell line (ATCC CRL-3276).
9. Primary medium: Add 6.25 ml 100X L-glutamine (Sigma, cat. no. G7513), 6.25 ml 100X penicillin/streptomycin (Sigma, cat. no. P4333), and 125 ml heat-inactivated FBS (Sigma, cat. no. F6178) to 500 ml Advanced DMEM/F12 (Thermo Fisher, cat. no. 12634)
10. ROCK inhibitor (Tocris, Y-27632)
11. ROCK inhibitor (Tocris, Y-27632)
12. Sterile cell strainers, 40 µm (Fisher, cat. no. 22363547)
13. 37°C, 5% CO_2 incubator.

2.5 Preparing and maintaining *C. parvum* oocysts for infection

1. Biosafety cabinet
2. Purified oocysts, stored in 50 mM Tris-10 mM EDTA, pH 7.2.
3. Cold DPBS
4. 15 ml conical tubes

5. Commercial laundry bleach containing 8.25% sodium hypochlorite
6. Centrifuge capable of holding 15 conical tubes that can spin at 800 and 1250 x g
7. Centrifuge buckets with sealed biohazard caps
8. Cold DPBS + 1% BSA
9. Excystation buffer: To make 5 ml, dissolve 0.75 g sodium taurocholate (Sigma, cat. no. 86339) into 5 ml DPBS (1.5% w/v sodium taurocholate solution). May need vortexing to dissolve completely. Filter steril9ize with 0.2 µm filter. Can be stored at 4°C for several weeks.
10. 37°C water bath
11. Glass slides and square coverslips (22x22 mm)
12. Swin-Lok filter holders (source), 25 mm
13. Whatman Nuclepore hydrophilic membranes, 25 mm circle, 1.0 µm pore size (VWR International, cat. no. 28158-373)
14. 3 or 5 ml plastic syringe
15. Cell growth medium (e.g. conditioned medium for ALI)

2.6 Measuring host and parasite replication in primary cell monolayers by qPCR

1. Qiagen QIAamp DNA Mini Kit (cat. no. 51394 or 51306)
2. Blunt pipette tips (20-200 µl pipette tips with ends snipped off)
3. 1.7 ml Eppendorf tubes
4. 56°C water bath
5. 70°C heat block
6. Ethanol, 200 proof

7. Centrifuge capable of spinning Eppendorf tubes and spin columns at 7000 x g
8. Sterile H_2O
9. 2X SYBR Green mix or similar qPCR reaction mix (e.g. TB Green Advantage qPCR premix, Takara Bio)
10. 96-well reaction plate compatible with qPCR machine (e.g. MicroAmp Optical 96-well Reaction Plate with Barcode, Applied Biosystems)
11. Adhesive film for sealing reaction plate (e.g. MicroAmp Optical Adhesive Film, Applied Biosystems)
12. Centrifuge capable of spinning 96-well plates
13. qPCR machine with 96-well block (such as the QuantStudio 3 Real-Time PCR system, Thermo Fisher Scientific)

2.7 Monitoring life cycle progression in primary cell monolayers by microscopy

1. PBS
2. Fixative such as 4% formaldehyde (Polysciences, cat. no. 04018)
3. Permeabilization agent such as Triton X-100 or saponin
4. Normal goat serum
5. Fetal bovine serum
6. Hoechst (Thermo Fisher, cat. no. 33258; 1 mg/ml stock solution) or another DNA stain
7. Scalpel and forceps
8. Mounting reagent such as ProLong Gold (Thermo Fisher, cat. no. P36930)
9. Glass slides and square coverslips (22x22 mm)

3 Methods

3.1 Creating irradiated 3T3 (i3T3) cell stocks for feeder cell layer

This protocol is based on the standard protocols for maintaining 3T3 cells in culture and preparing 3T3 cells for feeder cell layers. All cell manipulation is performed inside a biosafety cabinet under sterile conditions.

1. Thaw a frozen vial of 3T3 cells (**see note 4.1**) in 37°C water bath. Remove vial immediately when cells have thawed.
2. Add thawed cell mixture to 15 ml conical containing 10 ml 3T3 growth medium.
3. Spin at 200 x g for 3 min. Remove supernatant.
4. Resuspend pellet in 5 ml growth medium and pipette 8-10 times to evenly distribute cells.
5. Transfer to T-25 flask and culture in 37°C, 5% CO2 incubator.
6. When cells are ~90% confluent, remove the medium from the flask and wash with 10 ml DPBS-EDTA.
7. Add trypsin-EDTA to flask in a volume sufficient to cover cell monolayer (1 ml for T-25, 3 ml for T-75, 6 ml for T-150). Swirl flask to ensure complete cell coverage.
8. Keep flask at room temperature for 2-3 minutes. Swirl flask to see if cells have detached.
9. Once cells have detached, add sufficient volume of growth medium to cover flask and resuspend the cells (4 ml for T-25, 6 ml for T-75, 7 ml for T-150). The medium will stop the action of the trypsin.
10. Pipette the medium over the surface of the flask 3 times to ensure all cells are in suspension. Pipette up and down 8-10 times to create a single cell suspension.
11. Transfer cell mixture to 15 ml conical and spin at 200 x g for 3 min.

12. Remove supernatant and resuspend pellet in desired amount of medium.
13. Pipette mixture up and down 5-10 times to ensure even distribution of cells and transfer desired amount of cell to new flasks. Swirl flasks to ensure cells are covering flask surface.
14. The passage ratio determines the length of time it takes the flask to reach 90-100% confluency. Passage ratio of 1:2.5 will reach confluency in 2 days, 1:5 in 3 days, and 1:10 in 4 days.
15. Expand the cells into the number of flasks desired for the irradiation process.
16. When final flasks become confluent, trypsinize cells as described in steps 1-6. The irradiation protocol can be scaled up or down depending on the number of irradiated cells required. For example, 3 T-T150s, once trypsinized, can be pooled into one 50 ml conical and spun down at 200 x g for 3 min.
17. Remove supernatant and resuspend pellet in 10 ml growth medium and transfer cell mixture to 15 ml conical.
18. Irradiate cells at 3000 rads. We use the Xstrahl SARRP for this purpose.
19. Pipette cells to ensure even distribution and take 10 µl to determine cell density using hemocytometer. Cells should not be clumpy and should appear uniformly round.
20. Spin down cells at 200 x g for 3 min.
21. Resuspend pellet in sufficient volume of freezing medium to achieve 2x10^6 cells/0.5 ml.
22. Aliquot cells for freezing, 0.5 ml per cryovial. Three T-150s typically yield 20-25 vials at the above cell density.
23. Move cryovials to -80°C freezer for short-term storage (days to weeks) and then to LN2 tank for long-term storage (months).

3.2 Plating i3T3 cells on transwells

This step occurs the day before the stem cell spheroids are split and plated onto the transwells. All cell manipulation is performed inside a biosafety cabinet under sterile conditions.

1. Make 10% Matrigel solution: dilute Matrigel (**see note 4.2**) in cold DPBS (keep DPBS and Matrigel on ice), pipette to ensure even distribution. Prepare sufficient volume for 100 µl of solution per transwell.
2. Add 100 ul 10% Matrigel solution to each transwell. Move plate with transwells to 37°C incubator for 20-30 minutes to allow the Matrigel to polymerize while finishing the following steps.
3. Thaw vial(s) of frozen i3T3 cells in 37°C water bath. Once thawed, immediately add to 15 ml conical containing 10 ml 3T3 growth medium.
4. Spin down cells at 200 x g for 3 min.
5. Remove supernatant and resuspend cells in 1-3 ml of growth medium.
6. Count cells using hemocytometer. Each transwell will be plated with 8x10^4 cells in 100 µl volume; resuspend cells accordingly.
7. After transwells have been in 37°C incubator for at least 20 minutes, remove and aspirate Matrigel using vacuum flask and glass pipette. Alternatively, Matrigel can be removed with pipet tip.
8. Add i3T3 cell suspension to each transwell.
9. Add 400 µl growth medium to bottom chamber of each transwell.
10. Place transwells in 37°C, 5% CO_2 incubator.

3.3 Passaging spheroids

This is a very brief summary of the protocol described in Miyoshi & Stappenbeck 2013. Growing the spheroids (and primary cell monolayers described in 3.4) requires the use of medium conditioned by the L-WRN cell line ("conditioned medium"). The production of this medium is also described in Miyoshi & Stappenbeck 2013; it requires the L-WRN cell line (ATCC CRL-3276). The paper also describes how to scale production of conditioned medium to suit the needs of the researcher. The final step of preparing conditioned medium is to add the conditioned medium to an equal volume of primary medium (recipe included in materials section), therefore all conditioned medium used in these protocols is "50% conditioned medium".

1. Thaw vial of spheroids isolated and frozen according to Miyoshi & Stappenbeck 2013. Place vial in 37°C water bath until contents are thawed (1-2 min).
2. Transfer cells to 15 ml conical containing 5 ml pre-warmed washing medium.
3. Centrifuge at 200 g x 5 min.
4. Aspirate supernatant, being careful not to disturb pellet.
5. Add 1 ml washing medium and resuspend cells by gentle pipetting. Transfer to 1.5 ml Eppendorf tube.
6. Centrifuge at 200 g for 5 min.
7. Remove supernatant with a pipette, being careful not to disturb pellet.
8. Place tube on ice and chill for 5 min.

9. Add Matrigel to cells for desired volume. For example, if plating a 12-well plate, the volume of Matrigel/cell suspension for each well is 30 µl. Pipette cells gently, avoiding bubbles. Hold tube by rim while pipetting to avoid warming Matrigel.
10. Place tissue culture plate (e.g. a 12-well plate) on ice. This can be done inside or outside biosafety cabinet.
11. Remove lid from plate and place on sterile surface.
12. Pipette appropriate volume of Matrigel/cell suspension into the middle of each well. Carefully spread out Matrigel using pipette tip; do not let Matrigel touch sides of well.
13. Cover plate with lid, remove from ice, flip upside down (this is done to prevent the cells from touching plate bottom), and place into 37°C incubator for 10 min. Matrigel will solidify.
14. Remove plate from incubator, flip right side-up, and add appropriate volume of 50% conditioned medium with 10 µM ROCK inhibitor (e.g. 800 µl/well for 12-well plate).
15. Place cells in 37°C, 5% CO2 incubator.
16. Two days after plating, aspirate medium and add fresh 50% conditioned medium.
17. Three days after plating, scrape Matrigel/cell suspension into medium using a cell scraper or pipette tip. Combine wells into 15 ml conical (6 wells of a 12 well plate can be combined into 1 conical).
18. Spin cells at 200 g x 3 min.
19. Aspirate supernatant and resuspend cells in 5 ml DPBS-EDTA.
20. Spin cells at 200 g x 5 min (longer spin time is necessary to ensure adequate exposure to DPBS-EDTA).

21. Aspirate supernatant and add 300 µl trypsin-EDTA to cells. Pipette 2-3 times to ensure even mix.
22. Add cells to 37°C water bath, incubate for 1.5 min.
23. Remove cells from water bath, pipette gently 10-12 times. Add 5 ml washing medium.
24. Spin cells at 200 x g for 3 min.
25. Aspirate supernatant and resuspend cells in 1 ml 50% conditioned medium with 10 µM ROCK inhibitor. Move cell suspension to 1.7 ml Eppendorf tube.
26. Spin cells at 200 x g for 3 min.
27. Remove supernatant with pipette tip. Place tube on ice. Let chill for 5 min.
28. Add desired volume of Matrigel to cell pellet (volume is dependent on the number of wells being plated). Spheroid lines have different optimal passage ratios; for the murine ileal lines used to grow C. parvum, a 1:6 passage ratio is often used. Passage ratios will need to be adjusted in response to spheroid density; murine ileal spheroids should not be maintained at a very high density or else they will not grow well. Pipette Matrigel gently to mix, avoid bubbles.
29. Plate spheroids as described in steps 10-15.
30. Passage spheroids every 3 days.

3.4 Creating primary cell monolayers for *C. parvum* infection

This protocol is based on the use of murine stem cells passaged as spheroids as described in Miyoshi & Stappenbeck 2013, which also describes the protocol for making the conditioned medium used to grow both the spheroids and primary cells. All cell manipulation is performed inside a biosafety cabinet under sterile conditions.

1. Scrape spheroids and Matrigel into medium using pipette tip or cell scraper. Combine wells with 5 ml plastic pipette and move cell suspension into 15 ml conical tube. Six wells of a 12-well plate can be combined in one 15 ml tube.
2. Spin spheroids down at 200 x g for 3 min.
3. Remove medium and resuspend spheroids in 5 ml DPBS-EDTA. At this time, warm aliquot of trypsin-EDTA in 37°C water bath.
4. Spin spheroids down at 200 x g for 5 min (longer spin time is necessary to ensure adequate exposure to DPBS-EDTA).
5. Remove DPBS-EDTA and add 300 µl warm trypsin-EDTA to pellet. Pipette up and down to ensure cells are evenly exposed to trypsin.
6. Move cells to 37°C water bath, incubate for 1.5 min.
7. Remove cells from bath and pipette 20-30 times to break up spheroids.
8. Add 5 ml washing medium to cells.
9. Place sterile cell strainer (40 µm) on top of 50 ml conical tube. Pre-wet strainer with 2 ml washing medium. Pipette cell mixture on top of strainer. Two 15 ml conicals' worth of cells (equivalent to one 12-well plate of spheroids) can be combined onto one cell strainer.
10. Tap strainer against conical to force liquid through; move filtrate from 50 ml conical to 15 ml conical.
11. Spin at 200 x g for 3 min.
12. Remove washing medium and resuspend cells in 1-3 ml of 50% conditioned medium with 10 µM ROCK inhibitor (Y-27632, **see note 4.3**). Count cells using hemocytometer.

Cells will be very clumpy. Each transwell will be plated with 5x10^4 cells in 200 µl medium, resuspend cells accordingly (**see note 4.4**).

13. Remove transwells plated with i3T3 cells from 37°C incubator; confirm i3T3 monolayer is uniform under microscope.
14. Remove 3T3 growth medium from top chamber of compartment using pipette tip (do not use vacuum flask because aspiration will disturb the monolayer).
15. Add stem cells to transwells.
16. Remove 3T3 growth medium from bottom chamber of transwell compartment and add 400 µl conditioned medium with 10 µM ROCK inhibitor.
17. Move transwells to 37°C, 5% CO_2 incubator.
18. Change medium in top and bottom chambers of transwells every 2 days. Add 200 and 400 µl 50% conditioned medium with 10 µM ROCK inhibitor to the top and bottom chambers, respectively. Remove medium from top chamber with pipette tip only; aspiration can disturb cell layer. Cells can tolerate a 2-day gap between feedings; medium can be changed on a Monday, Wednesday, Friday schedule with no ill effects.
19. After 7 days, remove medium from top chamber with pipette tip and do not replace. This is “day 0 of top media removal” and the creation of the ALI.
20. Continue to change medium in bottom chamber 3 times weekly (**see note 4.5**).
21. On day 3 post top media removal, remove liquid/mucus from top chamber of transwells (**see note 4.6**). Resuspend desired infectious dose of *C. parvum* oocysts or sporozoites in 30 µl 50% conditioned medium per transwell. Add oocysts or sporozoites to transwell.
22. After incubation period (1-2 hours for sporozoites, 3-4 hours for oocysts), remove liquid and wash with DPBS if required for assay.

3.5 Preparing and maintaining *C. parvum* oocysts for infection

We have used the AUCP-1 isolate of *C. parvum* for growth in the ALI system (**see note 4.**7) and other lines would need to be tested for efficiency. It is a requirement of our biosafety protocol to use plastic caps on the centrifuge buckets when spinning the oocysts. Only open the caps inside a biosafety cabinet. Autoclave the buckets and caps after the protocol in case of accidental contamination. All pipette tips and other material contaminated with oocysts should be disposed of in a container that can be sealed before removing from the biosafety cabinet and placing in biohazard waste. An absorbent mat pad can be placed in biosafety cabinet during this procedure in case of spills.

1. Store purified oocysts at 4°C in 50 mM Tris-10 mM EDTA, pH 7.2.
2. Before infection, dilute $1x10^8$ oocysts into 1 ml cold DPBS in a 15 ml conical. Place on ice.
3. Add 1 ml of 40% bleach (diluted in cold DPBS) to oocysts. Pipette multiple times to ensure even mix.
4. Bleach oocysts on ice for 10 min.
5. Spin at 800 x g for 3 min. Remove bleach, resuspend pellet in cold DPBS + 1% BSA. Move oocyst mixture to new 15 ml conical.
6. Spin at 800 x g for 3 min. Remove supernatant and resuspend pellet in cold DPBS + 1% BSA. Repeat centrifugation and washing step 3 times to remove all traces of bleach.

7. After final centrifugation step, resuspend oocysts in cold DPBS + 1% BSA at a concentration of $1x10^8$/ml. Bleached oocysts can be stored at 4°C for up to 2 weeks. After 2 weeks, the excystation rate will decline.
8. Oocysts can be diluted into cell culture medium at desired concentration for infection.
9. If sporozoites are needed for infection, add required amount of oocysts to the same volume of excystation buffer in a 15 ml conical. For example, if 500 µl of oocysts ($0.5x10^8$ oocysts total) is required, add the oocysts to 500 µl excystation buffer. Final concentration of sodium taurocholate in solution will be 0.75% w/v.
10. Incubate oocysts in 37°C water bath for 45-60 min. Check excystation rate by pipetting 10 µl onto glass slide, cover sporozoites with glass coverslip, and look under microscope. Sporozoites are best seen at 40X magnification. Excystation rate should be high (80-100%) by 60 min. Lower excystation rates indicate that the viability of the oocysts is declining and the subsequent growth *in vitro* will not be optimal.
11. After incubation period is over, remove plunger from 3 or 5 ml plastic syringe and place upright in biosafety cabinet. Attach syringe to plastic filter holder containing filter membrane with 1 µm pore size. Place filter with syringe on top of 15 ml conical.
12. Pipet 1 ml of cell growth medium into syringe. Pipet excysted oocysts into syringe. Insert plunger into syringe and push contents through filter. Remove filter with syringe and place aside. Filter can be carefully disassembled and dropped in an autoclave-safe container filled with H_2O and autoclaved. Autoclave cycle must not include any drying time, because this can warp the filters. Membrane can be discarded after autoclaving.
13. Spin filtered sporozoites at 1250 x g for 3 min.

14. Remove supernatant and resuspend sporozoites in desired volume of cell growth medium. For infecting ALI monolayers, resuspend sporozoites in 50% conditioned medium (without ROCK inhibitor), 30 µl per transwell.
15. To confirm oocysts have been completely removed from inoculum, check filtered sporozoites under microscope by pipetting onto glass slide and covering with glass coverslip. Infected monolayers can also be fixed on the same day of infection and stained with an antibody that recognizes *C. parvum* oocysts, such as Crypt-a-glo™ (Waterborne, Inc.)

3.6 Measuring host and parasite replication in primary cell monolayers by qPCR

This method relies on measuring parasite replication by measuring *C. parvum* genomic DNA equivalents. Host viability can be assessed by measuring host genomic DNA equivalents from the same sample. The following is a modified protocol from the Qiagen QIAamp DNA mini kit. Buffers ATL, AL, AW1, AW2, and AE are provided in the kit.

1. Add 100 µl of Buffer ATL to transwell. Thoroughly scrape cells into buffer with blunt pipette tip; be careful not to puncture transwell membrane. Lysed cells will be sticky and clumpy.
2. Move entire contents of transwell (will likely be more than 100 µl due to presence of mucus/liquid in top chamber) to 1.7 ml Eppendorf tube. Add 20 µl proteinase K. Vortex to mix.
3. Incubate in 56°C water bath for 3-24 hr.
4. Briefly centrifuge tube to remove drops from inside of lid.

5. Add 200 µl Buffer AL to sample, vortex briefly to mix. A white precipitate is likely to form. Briefly centrifuge tube to remove drops from inside the lid.
6. Incubate in 70°C heat block for 10 min.
7. Add 200 µl ethanol to sample, vortex briefly to mix. Briefly centrifuge tube to remove drops from inside the lid.
8. Move sample from Eppendorf tube to spin column. When pipetting sample, be careful not to wet the rim of the spin column. Spin at 7000 x g for 1 min.
9. Place spin column in new collection tube, discard tube containing filtrate.
10. Add 500 µl Buffer AW1 to spin column (be sure not to wet the rim). Centrifuge at 7000 x g for 1 min.
11. Place spin column in new collection tube, discard tube containing filtrate.
12. Add Buffer AW2 to spin column (be sure not to wet the rim). Centrifuge at maximum speed for 3 min.
13. Place spin column in clean 1.7 ml Eppendorf tube and discard the tube containing filtrate. Add 100 µl Buffer AE to the spin column, incubate at room temperature for 1 min, then centrifuge at 7,000 x g for 1 min.
14. Dilute DNA sample 10-fold with sterile H_2O.
15. To make primer mix for qPCR reaction mix: make 200 µM master stocks of forward and reverse primers in sterile H_2O. Combine equal volume of forward and reverse master stocks to make 100 µM master mix. Dilute 100 µM master mix in sterile H_2O to make 5 µM working mix.

16. To make qPCR reaction mix: 9.0 µl 2X SYBR Green mix, 1.8 µl 5 µM primer mix, 5.2 µl H_2O (16 µl total volume). Scale up volume for number of wells needed. Pipet mix into required number of wells of 96-well qPCR reaction plate.
17. Add 2 µl of diluted DNA sample to well. Seal plate with optical film. Centrifuge briefly to ensure DNA and mix are combined.
18. Primers to measure C. parvum GAPDH: forward – GAAGATGCGCTGGGAACAAC, reverse – CGGATGGCCATACCTGTGAG.
19. Primers to measure mouse GAPDH: forward – GCCATGAGTGGACCCTTCTT, reverse – GAAAACACGGGGGCAATGAG.
20. qPCR thermocycler protocol:

    Step 1: Priming, 95°C for 2 min

    Step 2: Denaturing, 95°C for 10 sec

    Step 3: Annealing, 60°C for 20 sec

    Step 4: Extension: 72°C for 30 sec (read fluorescence)

    Step 5: Go to Step 2, 40X

    Step 6: Melt curve, 95°C for 15 sec, 60°C to 95°C for 15 sec

    Step 7: Hold at 4°C.
21. Place reaction plate in qPCR machine and run thermocycler protocol.
22. In order to correlate C_t values with actual genomic DNA numbers, it is necessary to make a standard for *C. parvum* and mouse cells. For *C. parvum*, DNA from a known number of oocysts can be extracted using the Qiagen QIAamp DNA Mini Kit and diluted to make a standard. For example, DNA from 1x10^7 oocysts can be extracted. After extraction, the number of gDNA equivalents will be 4x10^7 per 100 µl (since each oocyst contains 4

sporozoites and the DNA is eluted in a 100 µl volume) or 4x10^5/µl. Create a dilution series (1:2 to 1:16, for a total of 5 values including the undiluted sample to make up the curve). For mouse cells, a known number of cells can be lysed after the cells are quantified in step 12 of Method 2.2 and a dilution series set up in the same way as for *C. parvum*.

23. Because the DNA sample was diluted 10X before running the qPCR reaction, the number of gDNA equivalents determined to be present in 2 µl of sample needs to be multiplied by 10 to be accurate. To determine the number of gDNA equivalents present in the entire sample/transwell, multiple the adjusted number by 50 (since the sample was 100 µl before diluting).
24. An example of qPCR data of *C. parvum* growth and host cell viability over 21 days in the ALI system is shown in **figure 4.1**.

3.7 Monitoring life cycle progression in primary cell monolayers by microscopy

1. Move transwells to 24-well plate. Add 500 µl PBS to bottom chamber of transwell.
2. Fix transwells in desired fixative. For example, 4% formaldehyde for 10 min.
3. Wash transwells 2X with PBS. Use pipette to remove liquid from transwell because aspiration may disturb cell layer. If there is a significant mucus layer present (likely if the transwells are at day 7 or later of top media removal), the mucus layer can be removed through pipetting.
4. After fixing, transwells can be stored at 4°C for up to 10 days before staining (helpful in experiments that span over multiple days).

5. Permeabilize and block cells with desired agents. For example, 0.1% Triton X-100 for 3-5 min or 0.05% saponin for 10 min. If using Triton X-100, dilute in PBS containing 1% BSA. This buffer can be used throughout the staining protocol as a blocking buffer and as a vehicle for primary and secondary antibodies. If using saponin, block with 0.05% saponin in PBS containing 5% normal goat serum (NGS) and 5% fetal bovine serum. For antibody dilution and wash steps, drop the saponin concentration down to 0.01% in PBS containing 1% NGS.
6. After blocking, dilute primary antibody in buffer and stain for 60 min at room temperature or overnight at 4°C.
7. Wash 3X with buffer.
8. Dilute secondary antibody (for example, goat anti-mouse IgG conjugated to Alexa Fluor dyes, Invitrogen) in buffer and stain for 60 min at room temperature. Protect from light.
9. Wash 3X with buffer
10. Stain with 1 µg/ml Hoechst (1:1000 dilution of stock solution) for 10-30 min. Protect from light.
11. Wash 1X with PBS.
12. Dot 30-50 µl of ProLong Gold or other antifade mountant onto glass slide. Cut membrane from transwell insert with scalpel. Using forceps, place membrane onto mountant, cell side up.
13. Place square coverslip over membrane and push firmly down to remove air pockets. If there is an air pocket that will not go away, check membrane for plastic “curlicues” that can be created during the cutting process – these will stop the coverslip from lying flush with the membrane. Two membranes can fit under one coverslip, but this increases the

chance the coverslip will not lie flush with the membranes and air pockets can develop overnight as the mountant dries. It is important to thoroughly press down on the coverslip to remove all bubbles. Excess mountant will be pushed out and can be wiped off.

14. Protect slides from light and let dry overnight at room temperature.
15. An example of fluorescent staining of *C. parvum* grown in ALI monolayers is shown in **figure 4.2**.

4 Notes

4.1 3T3 stocks should be kept at low passage numbers (<10). Check appearance of 3T3 cells; unhealthy cells will grow slowly and have vacuolated cytoplasm.

4.2 Matrigel arrives from manufacturer in glass bottles containing 10 ml and should be stored at -20°C. To prepare Matrigel aliquots, thaw Matrigel overnight on ice in a Styrofoam container in a 4°C fridge. Remove cap and pipette Matrigel up and down 3 times using 10 ml pipette (only draw up 9 ml to avoid creation of bubbles). Aliquot Matrigel in 1 ml aliquots in 1.7 ml Eppendorf tubes and store at -20°C. Move aliquots to 4°C to thaw. Do not keep aliquots in "warm spots" in fridge such as the door because they may solidify. Aliquots will keep at 4°C for several weeks, but it is best to use quickly. Frozen aliquots can be thawed rapidly (30-60 min) by placing in an ice slurry or placing on top of ice. Do not thaw aliquots in 37°C water bath or room temperature because the Matrigel will solidify. Solidified Matrigel can be refrozen at -20°C and will thaw into a liquid, though it is not clear if this negatively affects the product. When handling thawed aliquots of Matrigel, do not grip tube with hand, because this will cause the mixture to solidify. Keep the aliquots on ice as much as possible. Always dilute Matrigel into cold DPBS; if the DPBS is warm, the Matrigel will solidify upon contact and will not create a homogenous solution.

4.3 Y-27632 arrives from manufacturer as a powder that can be stored at room temperature. Add sterile H_2O to powder to make 10 mM stock solution. Aliquot in 50-150 µl amounts and store at -20°C. Aliquots can be thawed and refrozen. Do not store aliquots at 4°C.

4.4 The amount of spheroids required for different numbers of transwells can very slightly from person to person. 15-20 wells (12-well plate format) of healthy spheroids should give enough cells to plate 48 transwells at the $5x10^4$ seeding density. If it takes significantly more wells, the spheroids are likely too sparse. The $5x10^4$ seeding density was determined to be optimal for *C. parvum* growth (**see figure 4.3**); higher seeding densities lead to decreased cell growth. If *C. parvum* is not growing well, try a dilution series of different seeding densities.

4.5 It is important to observe the color of the medium when feeding the cells, since it is an indicator of viability. Four to six days after plating the stem cells, the medium should become bright yellow in between feedings. After the ALI is created (7 days after plating the stem cells), the medium will continue to turn yellow between feedings for 3-5 days, but the color change will gradually become less dramatic. Eventually the medium will remain pink in between feedings. If the medium is remaining pink before the creation of the ALI, it is likely the cells are unhealthy and the monolayer is too sparse. Additionally, there will be some liquid and mucus that forms in the top chamber after the start of the ALI; if there is copious liquid in the top chamber in addition to pink medium, these are signs the monolayer is dead.

4.6 The day of infection strongly affects the outcome of infection. Infecting too early after the creation of the ALI (day 0 to day 2) leads to poor growth and cell death. Infecting too late (day 7 and later) leads to poor growth, possibly due to the presence of the mucus layer, which may act as a physical barrier to the oocysts and sporozoites (**see figure 4.4**).

4.7 It is preferable that the oocysts are purified from cow feces using Sheather's sugar flotation and discontinuous sucrose density gradient centrifugation; oocysts purified using cesium chloride gradients are less viable and exhibit lower excystation and infection rates in the ALI system.

Acknowledgements

Supported by a Grand Challenges Grant from the Bill and Melinda Gates Foundation (OPP1098828, OPP1139330). G. Wilke was partially supported by an Institutional Training Grant to Washington University (AI007172).

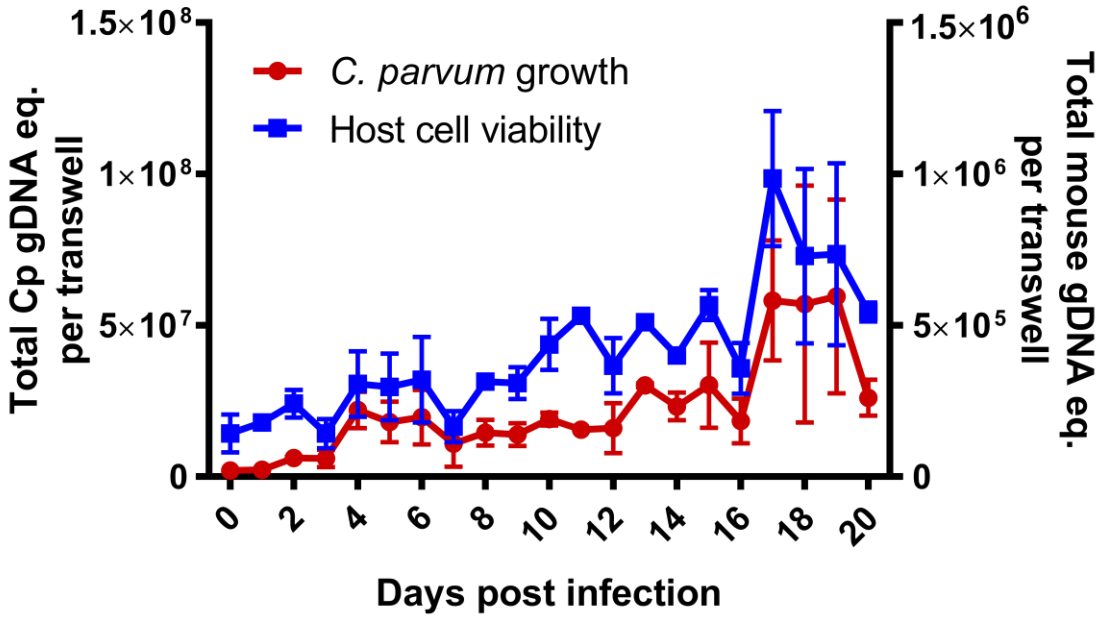

Figure 4.1. ALI monolayers support long-term *C. parvum* growth and host cell viability. ALI monolayers were infected 3 days post top medium removal with 2x10^5 oocysts. Monolayers were incubated with oocysts for 4 hr and then washed 3 times. DNA samples were collected daily. Graph depicts qPCR measuring *C. parvum* and mouse GAPDH in DNA samples; data is presented as genomic DNA equivalents (gDNA eq.). Each data point represents the mean and standard deviation of two transwells.

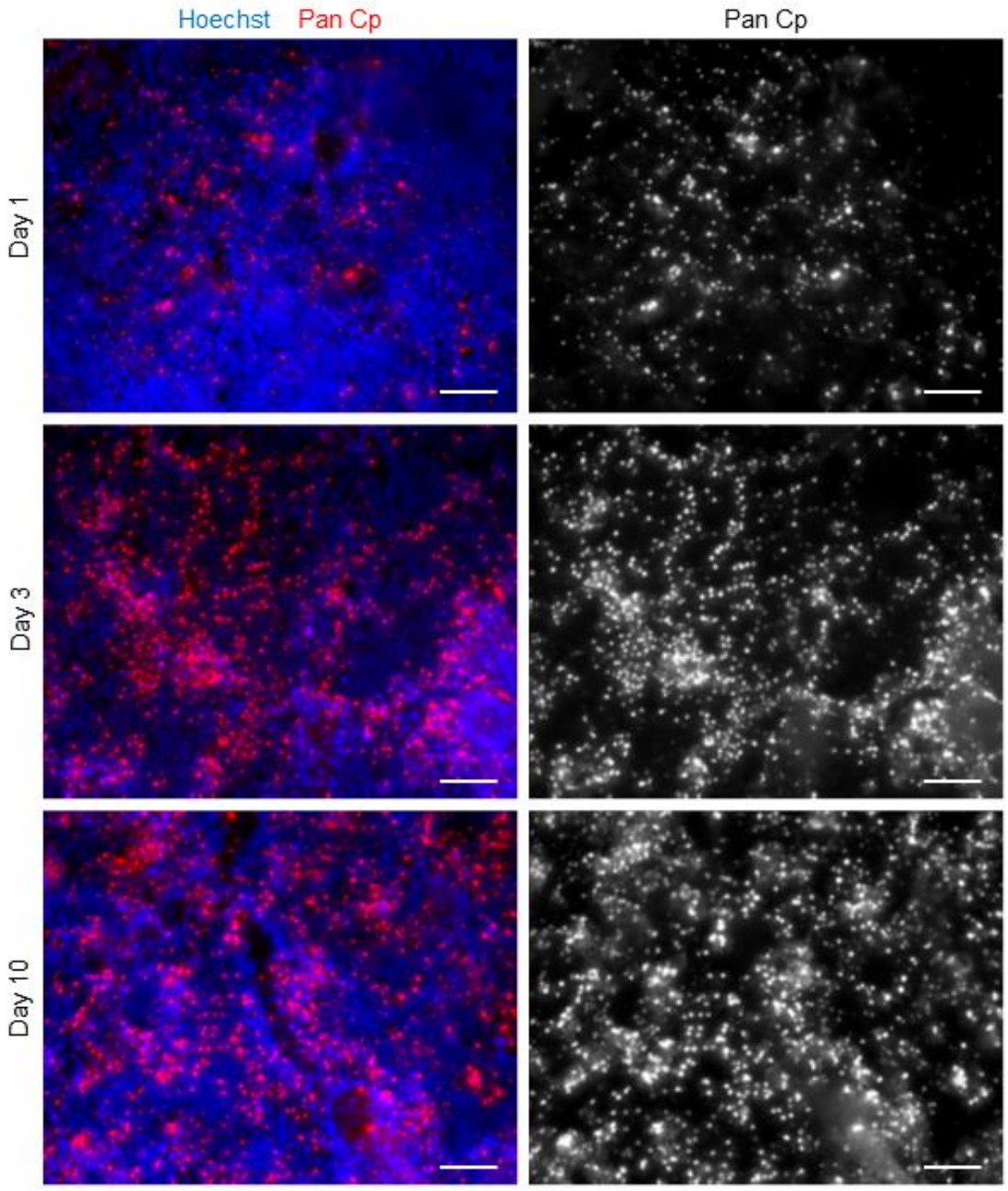

Figure 4.2. Immunofluorescent staining of infected ALI monolayers.

ALI monolayers were infected on day 3 post top medium removal with 2x10^5 oocysts. Monolayers were incubated with oocysts for 4 hr and then washed 3 times. On different days post infection, monolayers were fixed and stained with pan-Cp (rabbit polyclonal raised against *C. parvum* oocysts and sporozoites) and Hoechst. Secondary antibodies used were goat anti-rabbit Alexa Fluor 555. Scale bar = 50 µm.

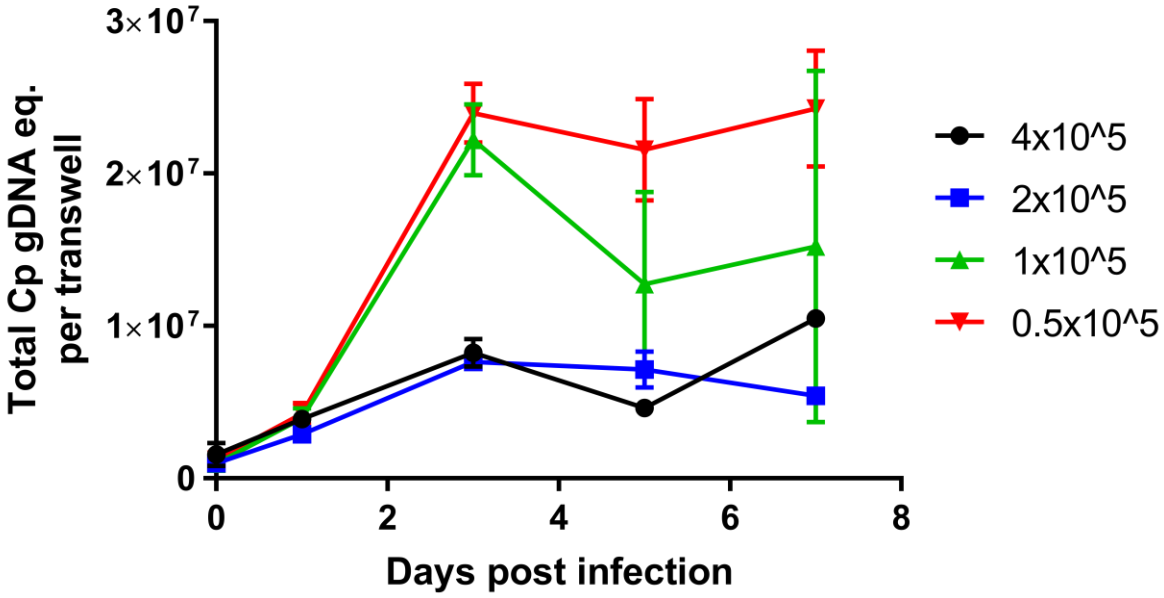

Figure 4.3. Lower cell seeding density improves *C. parvum* growth.

Stem cells were seeded at different densities. Seven days post-seeding, top media was removed to create the ALI. Three days post top medium removal, monolayers were infected with 2x10^5 oocysts. Monolayers were incubated with oocysts for 4 hr and then washed 3 times. DNA samples were collected daily. Graph depicts qPCR measuring *C. parvum* and mouse GAPDH in DNA samples; data is presented as genomic DNA equivalents (gDNA eq.). Each data point represents the mean and standard deviation of two transwells.

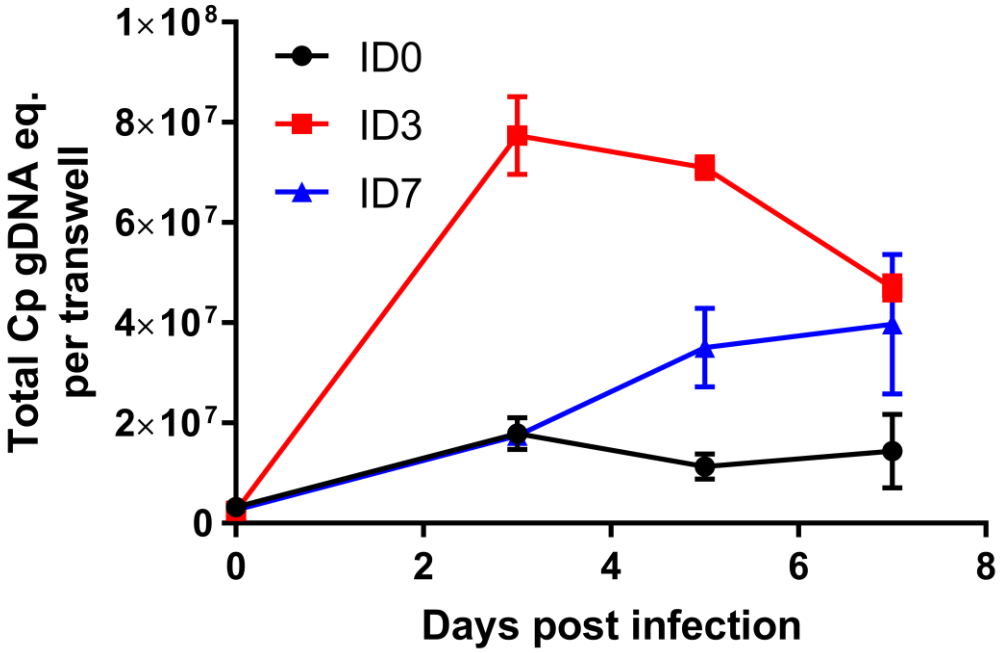

Figure 4.4. Infecting on day 3 post top medium removal improves *C. parvum* growth.

ALI monolayers were infected on day 0, day 3, or day 7 (ID0, ID3, ID7) of top medium removal with 2x10^5 oocysts. Monolayers were incubated with oocysts for 4 hr and then washed 3 times. DNA samples were collected on day 0, 3, 5 and 7 post-infection. Graph depicts qPCR measuring *C. parvum* and mouse GAPDH in DNA samples; data is presented as genomic DNA equivalents (gDNA eq.). Each data point represents the mean and standard deviation of two transwells.

Chapter 5

Conclusion and future directions

The first draft of this chapter was written by GW. Comments from LDS were incorporated into the final chapter here.

Conclusions

The significance of *Cryptosporidium* as a global health problem was underestimated for many years; it was thought to primarily cause sporadic waterborne outbreaks of self-limiting diarrhea as well as long-term disease only in immunocompromised patients. However, recent studies have exposed *Cryptosporidium* as a major gastrointestinal pathogen in children in Africa and southeast Asia, along with familiar culprits such as rotavirus and *Shigella spp* (19, 20). Additionally, subclinical *Cryptosporidium* infections have been found to be associated with growth faltering and declining cognitive function in children in the underdeveloped regions (23, 24, 182, 183). The prevalence of *Cryptosporidium* in these areas is extremely concerning because the only drug available to treat cryptosporidiosis, nitazoxanide, is not effective in malnourished children (30). Therapeutic interventions have already been implemented or are currently in development for the other major gastrointestinal pathogens identified by these studies, but research on *Cryptosporidium* has been slow-moving due to the intractability of the parasite. However, the new understanding of *Cryptosporidium*'s significant contribution to pediatric disease has led to more focused investigation into breaking down the barriers hindering research in this field.

Currently, there are no accessible culture systems for *Cryptosporidium* that support propagation and/or complete life cycle development *in vitro*. For years, this made the development of any kind of genetics system for *Cryptosporidium* almost impossible, however, this issue was recently circumvented by using immunodeficient mice to grow transgenic parasites (66). This system was used to create luciferase-expressing line that enabled a drug screen in *C. parvum*, which identified pyrazolopyridines as effective inhibitors of parasite growth and potential drug candidates for cryptosporidiosis (33). This advance is a great example of how

a previous major gap in the *Cryptosporidium* research field – lack of a genetics system – has been overcome, quickly enabling investigation into new therapies.

While genetic manipulation of *Cryptosporidium* is now possible, it is still a difficult system to adopt because it requires a surgical procedure to inoculate the parasites into the intestine and the parasites need to be passaged through a mouse to generate infectious oocysts. Because of this requirement, essential genes are almost impossible to study; any perturbation to life cycle progression cannot be visualized as the mouse intestine is a "black box". Transgenic parasites still cannot be selected for and maintained entirely *in vitro* due to the ongoing lack of a culture system. The main purpose of this thesis was to develop an *in vitro* culture system for *C. parvum* that would be a tool for the *Cryptosporidium* research community and facilitate investigation into the parasite life cycle and hopefully enable continuous propagation. While developing the culture system, we were also able to create library of monoclonal antibodies that recognize different life cycle stages of *C. parvum* – another valuable tool for *Cryptosporidium* research, since the previously available antibodies were limited in scope. The culture system and antibodies fill two reagent gaps in the field and will enable new lines of investigation into *C. parvum* biology.

Creation of a hybridoma library against intracellular stages of C. parvum

The first iteration of a primary cell culture system we used to grow *C. parvum* relied on monolayers derived from murine intestinal stem cell spheroids (126). These monolayers were grown on transwells and contained the differentiated lineages of the intestinal epithelium (131). The system had been previously been used to study aspects of intestinal cell function (131) so it was an accepted model of the intestinal environment. We found that these monolayers supported

robust asexual growth of *C. parvum* over a 3-day period, but did not support complete life development, or even sexual stage development. This may have been because the monolayers only lasted a very short time; with or without infection, the host cells began to die by day 2 and the monolayer was severely compromised by day 3. The monolayer could not replenish itself because the primary cells had lost the ability to proliferate after being removed from the spheroid culture system. It is likely the asexual stages of the parasite could not continue developing because there were simply no healthy cells left to infect. We attempted to propagate the asexual stages of the parasite using this system but were unsuccessful.

While the primary monolayers, or "1st generation transwells", were not a viable system for studying *C. parvum* development, they presented a unique opportunity. We realized we could use this system to immunize mice with infected cell lysate in order to generate a panel of novel antibodies to intracellular stages of *C. parvum*. Previously, there had been no reports of a mouse epithelial cell line that supported robust *Cryptosporidium* growth, so generating antibodies using this method was not possible. The adenocarcinoma cell lines routinely used to grow *C. parvum* are all human in origin (HCT-8, Caco-2, HT-29) and could not be used for the same purpose due to the unavoidable production of host-specific antibodies. Therefore, all available antibodies against *Cryptosporidium* have been made against extracellular stages (oocysts, sporozoites) or recombinant proteins. These antibodies can be useful in microscopy studies but the epitopes they recognize do not have stage-specific expression, so identification of different life cycle stages requires knowledge of other markers, such as nuclei number and timing of appearance.

We immunized mice with infected cell lysate and developed a hybridoma library against *C. parvum*. We identified several antibodies with unique reactivity patterns in different life cycle stages, enabling unambiguous identification of those stages. For example, two antibodies (1F9

and 1B5) had a “doughnut-shaped” recognition pattern in trophozoites and appeared to localize to the base of the parasite, which contains the feeder organelle. It is possible these mAbs recognize transporters that are involved in nutrient uptake from the host cell cytoplasm or proteins that direct host cytoskeletal rearrangement in the area around the parasite.

mAb 4D8 recognized an epitope with a striking line- or V-shaped pattern in macrogamonts. We identified a “fiber” running through macrogamonts by electron microscopy which resembles the object recognized by 4D8; this structure has not previously been described in other EM studies of *C. parvum*. Unfortunately, attempts to show direct recognition of the fiber by 4D8 by immuno-EM were unsuccessful for technical reasons. In the future, 4D8 could be used to identify the components of the fiber via immunoprecipitation studies, which could lead to new insight into macrogamont development.

Several antibodies (e.g. 1A5) had a polarized recognition pattern in mature meronts, enabling the differentiation between mature type II meronts, which contain 4 merozoites/nuclei, and immature type I meronts, which contain 4 nuclei but no fully-formed merozoites. Previously, it was virtually impossible to distinguish type II meronts from early type I meronts in fluorescent microscopy studies (they do however have ultrastructural differences that are visible by electron microscopy); these antibodies can be used to study the timing and frequency of appearance of type II meronts in culture. Many of these antibodies that had a polarized recognition pattern in mature meronts also had a polarized pattern in sporozoites suggesting, that they recognize proteins located in the apical secretory organelles and could be discharged during gliding motility or host cell invasion.

Currently, these mAbs have great utility in facilitating life cycle description of *C. parvum* in different culture systems. There are very few “maps” of the *Cryptosporidium* life cycle using

fluorescent images, most are based on electron microscopy (36). Often papers quantify the different stages of *C. parvum* present in a cell culture system but fail to provide any visual evidence (86). This lack of clarity regarding the parasite life cycle can be frustrating as a new investigator to the field; therefore, we hope that these mAbs will serve as a basic "antibody toolkit" to simply life cycle stage identification of *C. parvum*. In future studies, the targets of the mAbs could be identified to learn more about the structures they recognize; for example, 1B5 and the feeder organelle, 4D8 and the macrogamont fiber, and 1A5 and the apical secretory organelles. The antibodies could also be screen in an invasion inhibition assay to identify proteins involved in parasite adhesion, motility and invasion.

Complete life cycle development of C. parvum in vitro

When the "first generation transwells" did not support propagation or complete life cycle development of *C. parvum*, we looked for ways to improve primary cell viability and differentiation status to create a long-lasting monolayer that recapitulated aspects of the intestinal environment. We incorporated aspects of a recently published protocol (132) that grew long-lasting primary monolayers with our current methods for propagating stem cell spheroids and creating primary monolayers. The main changes to our first-generation protocol involved using a feeder cell layer to support the primary cells, maintaining the monolayers in medium containing stem cell growth factors, and creating an "air-liquid interface" (ALI) at the surface of the monolayer. The ALI triggered a dramatic differentiation cascade in the monolayers leading to the development of enterocytes and secretory cells such as goblet cells. These "second generation" or ALI transwells lasted for many weeks due to a portion of the cells remaining proliferative, allowing the monolayer to be continually replenished as terminally differentiated cells sloughed

off. This continuous cell division, something the first generation transwells lacked, was likely due to the inclusion of the stem cell growth medium.

We found that the ALI monolayers supported weeks of continuous *C. parvum* growth. This growth was dependent on the ALI, since submerged transwells did not support the same quantity of growth. Optimal growth required infection of monolayers that were in the process of differentiating, i.e. several days after the creation of the ALI. Infecting the monolayers on the same day the top medium was removed, when the monolayers were undifferentiated, led to poor growth and host cell viability. When infected at the optimal time, host cells continued to proliferate and even increased in number during infection, implying that the monolayers maintained integrity in the presence of continuous parasite replication. Sections of infected transwells showed the cells retained their dramatic cell height, a marker of differentiation (168), during infection, mimicking what is seen *in vivo*.

The long-term *C. parvum* growth in ALI cultures suggested the parasite was undergoing complete life cycle development, leading to the production of oocysts and reinfection of the monolayer by sporozoites. We identified all life cycle stages in the monolayers, and most importantly, we found evidence of oocyst production *in vitro*. We infected ALI cultures with sporozoites that had been filtered to remove unexcysted oocysts and oocyst shells and looked for oocyst development by microscopy. We found that oocysts appeared as early as day 2 post-infection and continued to appear on subsequent days, without a clear pattern of "peaks" and "troughs". The numbers of oocysts did not increase dramatically as time went on, suggesting that the oocysts were not simply accumulating on the surface of the monolayer; it is likely that the oocysts were excysting almost immediately upon release from the host cell, leading to reinfection.

To determine if the *in vitro*-produced oocysts were infectious, we bleached infected monolayers on day 1 and day 3 post infection and inoculated Ifngr1$^{-/-}$ mice with the material by oral gavage. Day 1 cultures only contain asexual parasite forms, which are not bleach-resistant, while day 3 cultures contain oocysts, which are bleach-resistant. We found that only the mice that received bleached material from day 3 cultures developed a productive infection, leading to oocyst shedding and eventually death. This result supports the visual evidence of oocyst production in ALI culture and demonstrates the infectivity of the *in vitro*-produced oocysts.

The long-term growth in ALI culture as well as infectious oocyst production suggested these monolayers would also be able to support propagation of *C. parvum*. Unfortunately, all attempts to passage *C. parvum* from one ALI culture to another were unsuccessful. It seems that whatever life cycle stage is capable of propagating the infection is present in low numbers or is damaged during the propagation process, which involves some form of dissociating the monolayer, whether by syringe-lysing or trypsinizing.

Despite the (present) inability to passage the infection using the ALI system, the fact that this cell culture platform supports robust, long-term growth and complete life cycle development *in vitro* makes it a significantly better model for studying parasite biology than currently available systems. Adenocarcinoma cell lines support only a few days of growth and no oocyst development (142) and cell culture systems claiming oocyst production *in vitro* rely on expensive or inaccessible equipment (95, 96). Due to the required equipment, these systems are not easily scalable and make simple microscopy or gene expression studies difficult. These other cell culture systems also use adenocarcinoma cell lines, which do not accurately model the epithelial cell lining of the intestine. ALI monolayers are derived from stem cells that differentiate into all of the lineages naturally found in the gut, making it an ideal system to study

host-parasite interactions. The ALI system relies on commercially available cell culture supplies and well-established protocols for stem cell propagation and is easily scalable for studies requiring conditions to be examined in parallel. For these reasons, the ALI system is an excellent platform for modeling how *C. parvum* develops *in vivo* and will aid future investigation into pathogenesis mechanisms and drug target identification.

Future Directions

Future efforts should be focused on expanding the utility of the ALI system for investigating *Cryptosporidium* biology *in vitro*, such as enabling serial passage, selection of transfected lines, cryopreservation, testing drug efficacy, and growth of *C. hominis.*

Propagating C. parvum in the ALI system

Past attempts to propagate *C. parvum* in ALI monolayers have been unsuccessful. A summary of the attempted methods is provided in the appendix to Chapter 3. Essentially, all the "obvious" methods have been tried and found insufficient, necessitating some unorthodox thinking about how to passage the infection from one monolayer to another. The failure to propagate infection by simply syringe-lysing the monolayer to release the intracellular parasites, like what is done for *T. gondii*, is strange because we have found that syringe-lysed *C. parvum*-infected ALI cultures can productively infect Ifngr1$^{-/-}$ mice. Even syringe-lysed day 1 cultures, which only contain asexual forms of the parasite and no oocysts, are infectious to mice and cause productive oocyst shedding and even death. However, these same cultures are not infectious to new ALI monolayers. It is possible that passage through the stomach and proximal small intestine conditions the parasites in some way that prepares them for reinfection, but it is still surprising that the asexual forms can survive the harsh conditions of the stomach. In fact, the research group that used the CRISPR/Cas9 system to genetically modify *C. parvum* found that it was necessary to use a surgical procedure to directly inoculate the small intestine with transfected sporozoites (66) because oral gavage produced inconsistent results. It is possible that in the syringe-lysed cultures, the mucus and host cell debris protect the asexual stages from the acidic environment, allowing the parasites to reach the small intestine. This still does not explain how those stages are able to reestablish infection *in vivo* but not *in vitro*. Also, the idea that the

cultures need to be "activated" by some signal in the intestine in order to re-initiate their life cycle does not explain how infections can last for weeks in ALI culture without any outside intervention.

In light of the ability of syringe-lysed cultures to infect Ifngr1$^{-/-}$ mice, future attempts to passage *C. parvum* could test treating the lysed cultures with acid or bile salts to try to mimic passage through the gut, to see if these exposures "activate" the parasites for reinfection. Bile acids have been demonstrated to positively affect protein secretion and gliding motility of sporozoites, separate from their ability to trigger oocyst excystation (184). It is possible that bile acids also affect the behavior of merozoites or other life cycle stages that could passage the infection.

The activating signal might be more elusive, such as a metabolite or the absence/presence of a nutrient. As of now, no metabolite or nutrient has been identified as having a positive effect on *C. parvum* growth in the intestine. However, high fecal indole levels have been negatively associated with susceptibility to *C. parvum* infection in humans (185) and depletion of intestinal flora with antibiotics enhances susceptibility of mice to infection (66, 186), so there is precedent for specific metabolites and the microbiota having an effect on *C. parvum* infection, albeit a negative one. *C. parvum* infection causes changes to the intestinal microbiota (187) and the metabolite profile of the gut in mice (188) and humans (189); it is possible that some of these changes reflect active reshaping of the gut environment by *C. parvum* and may provide clues to what nutrients have a positive impact on *C. parvum* infection. These nutrients could be added to syringe-lysed cultures to see if they increase the efficiency of propagation.

We had assumed that any kind of pretreatment of the syringe-lysed cultures would not be required for propagation because the parasite can grow uninterrupted for weeks in the ALI

culture. However, it is clear something about the propagation process disrupts the parasite's normal growth and a signal is needed to reboot the cycle. Passage through the mouse stomach and intestine provides that signal; we just need to identify it.

The success of infecting of Ifngr1$^{-/-}$ mice with bleached ALI cultures suggests we should try bleaching the monolayers before passage. Bleaching would restrict the parasite stages present to oocysts, since intracellular parasites cannot survive bleaching. Bleaching the monolayers may appear not worth testing – the oocysts are present in both bleached and unbleached cultures; if unbleached cultures do not reliably passage the infection, why would bleaching increase the infectiousness of the oocysts present? However, it is possible that syringe-lysing the cultures releases an inhibitory factor that kills the parasite or blocks binding sites on host cells; passage through the stomach may destroy this inhibitory factor, explaining why the cultures can infect mice but not monolayers. Bleach could achieve the same effect while restricting the inoculum to oocysts only. If bleached cultures can infect fresh monolayers, it would remove ambiguity about which parasite stage is actually passaging the infection. It is true that syringe-lysed day 1 cultures can productively infect mice, but we do not have a way of identifying which stage is transmitting the infection in that model. Limiting the infection to oocysts only may make the results easier to interpret.

One major obstacle to propagation has been the variability in infection levels in the transwells that received the passage infection. This issue has made attempts to serially propagate the infection impractical. Because there is a fair number of "negative" transwells at each time point tested, it is not feasible to pool together transwells and try passaging the infection again – the inoculum is likely to be extremely low and the inconsistency in infection will persist in the second round. If the propagated infection was consistent, it could be possible to serially passage

the parasite and eventually create a lab-adapted strain. If we had a way to track growth *in vitro* without fixing the monolayer for microscopy or lysing the monolayer for DNA collection, we could identify the positive transwells and pool them for the next passage. One way to do this would be to use live cell imaging to visualize GFP-positive parasites in the transwells. With enough passages, the line could become adapted to *in vitro* culture conditions and the inconsistency in infection between transwells could disappear. It is quite common for parasites to require some level of adaptation before thriving in *in vitro* culture conditions. For example, there is significant variability in the time it takes different field-derived *P. falciparum* strains to adapt to culture (190). When freshly isolated *Leishmania spp* are initially introduced to *in vitro* culture, they require the addition of biopterin in the culture medium to significantly increase growth; over serial passages, the requirement for biopterin goes away as the parasites adapt (191). It is possible that other strains of *C. parvum* would be more amenable to serial passaging or the addition of a nutrient is required for the first few serial passages to ensure success.

Successful propagation of *C. parvum* using the ALI system will require thinking outside the box of typical methods used to passage parasites *in vitro*. For example, the first system that supported continuous culture of *P. falciparum* required low oxygen (179), which is not a logical requirement for *Plasmodium* growth *in vitro* since asexual stages of *Plasmodium* grow in red blood cells. It is possible that continuous culture of *Cryptosporidium* will require something equally unexpected.

Transfection of C. parvum in the ALI system

For decades, genetic modification of *C. parvum* was not possible due to several barriers: inability to select for and propagate transfected lines *in vitro*, lack of non-homologous

recombination in *Cryptosporidium spp*, and few known drugs with associated resistance genes that could be used for selection. Despite these roadblocks, a recent breakthrough has demonstrated that it is possible to both transiently and stably transfect *C. parvum* (66, 192). To optimize transient transfection, the authors used nanoluciferase (Nluc) as a reporter, which is more sensitive than firefly luciferase or fluorescent proteins. They also optimized the electroporation protocol and determined the *C. parvum* enolase promoter to be the strongest at driving reporter expression. Additionally, they tested codon optimization because the *C. parvum* genome is AT rich (43) and found that this enhanced reporter expression as well. For selection, they used a neomycin resistance marker (Neo), which confers resistance to paramomycin (193), an aminoglycoside antibiotic that effectively targets *C. parvum* in tissue culture (66) and mice (67). They found that transient expression of a fused Nluc-Neo cassette led to increased resistance to paramomycin, which was determined by measuring the luciferase activity of the transfected parasites.

After optimizing transient transfection, the authors developed a method for creating stably transfected parasites using a modified CRISPR-Cas9 system. Sporozoites were transfected two plasmids: a CRISPR/Cas9 plasmid containing the *S. pyogenes cas9* gene and the *C. parvum* U6 RNA promoter to drive guide RNA expression targeting the gene of interest, and a plasmid containing a repair cassette with the Nluc-Neo fusion. Depending on the design of the repair cassette, integration of the cassette can replace/delete the gene of interest or modify it by adding an epitope tag, for example. The transfected sporozoites were inoculated directly onto the mouse intestinal epithelium via a surgical procedure. The latter step was necessary because the sporozoites could not survive passage through the stomach. Treating the mice with paramomycin led to selection of stable transfectants within the mouse; oocysts shed in the fecal pellets were

positive for the Nluc-Neo fusion protein and exhibited paramomycin resistance in subsequent studies.

In the original publication describing the method for stable transfection, the authors targeted the thymidine kinase (TK) locus for insertion of the Nluc-Neo cassette (66). Analysis of the *C. parvum* genome has revealed that the parasite is dependent on salvage from the host for both purines and pyrimidines (43, 194); TK is a salvage enzyme that provides an alternate route to dTMP that bypasses DHFR-TS (dihydrofolate reductase-thymidylate synthase) (194). TK is unique to *C. parvum* among apicomplexan parasites and it confers *Cryptosporidium*'s resistance to antifolates (e.g. trimethoprim), which target DHFR-TS and are used to treat other apicomplexan infections. The authors chose TK as the site of insertion to test the hypothesis that TK was nonessential; they found that loss of TK did not impact parasite viability under normal conditions, but it did increase *C. parvum*'s susceptibility to trimethoprim (66).

The protocol for stable transfection of *C. parvum* is well-tested and we could incorporate the ALI system into the method to streamline the process. Maintaining transgenic *C. parvum* lines entirely *in vitro* using the ALI system will not be possible until propagation is solved. However, the ALI platform can still be useful for selecting and enriching for stably-transfected parasites *in vitro* before inoculating mice to generate oocysts. Since we know syringe-lysed ALI cultures can productively infect mice, we could avoid the surgical procedure required to inoculate sporozoites directly into the intestine. The ALI system could also be used to cryopreserve transgenic lines, as discussed later, in order to avoid continually passaging the line through mice to maintain infectivity. In a lab where dozens of lines have been created, this process can become incredibly burdensome.

We could also use stably transfected lines to demonstrate sexual recombination *in vitro*, which would bolster the evidence of oocyst development. This experiment would require crossing two strains *in vitro*. Our lab has already modified the plasmid containing the Nluc-Neo fusion gene and repair cassette to introduce GFP and mCherry genes (separate plasmids) into the TK locus with expression driven by the *C. parvum* actin promoter. We are in the process of identifying another non-essential gene to serve as a target locus. One candidate is uracil phosphoribosyltransferase (UPRT), which is also involved pyrimidine salvage pathway. UPRT may not be essential because *C. parvum* has another enzyme, uridine kinase-uracil phosphoribosyltransferase (UK-UPRT) that is part of the same pathway and performs the same function as UPRT. If UPRT is non-essential, it can be targeted for insertion of the mCherry or GFP gene. We are in the process of making stable lines by inoculating mice with ALI cultures infected with transfected parasites. The mice are treated with paramomycin to select for stable transfectants. The level of shedding of stable transfectants can be measured by a luciferase activity assay of the fecal pellets. We will then purify stably transfected oocysts from the fecal pellets of the mice. If we have two stable lines – for example, one line with GFP in the TK locus and one line with mCherry in the UPRT locus – we can infect ALI culture with both lines simultaneously and look for visual evidence of recombination, i.e. a yellow parasite. This could be done by microscopy or potentially flow cytometry, if the levels of recombination are high enough. Demonstrating sexual recombination *in vitro* has not been accomplished in other cell culture systems claiming complete life cycle development (95-97). This outcome would truly be a novel finding and unambiguous evidence of meiosis and oocyst formation occurring *in vitro*. Additionally, if the levels of recombination are high enough, it would be proof of principle that

the system could be used to cross different lines/strains. This would be helpful for future studies identifying virulence determinants or host restriction factors in different strains.

Stable lines of two different colors can also be used to observe parasite processes in real time with live cell imaging. For example, fertilization of the macrogamont by the microgamont is a poorly understood process. It is thought that the block in life cycle development in most cell culture systems used to study *C. parvum* is the fertilization event; micro- and macrogamonts develop but there is no zygote production. This could be true or alternatively, fertilization could occur but the downstream processes of oocyst wall development, etc. are blocked. Observing micro- and macrogamonts in the ALI system and a control system like HCT-8 cells could shed light on the nature of the life cycle block.

We can also use the stable transfection protocol to tag different genes to visualize stage-specific gene expression. There has been one major study examining *C. parvum* gene expression during *in vitro* infection (89); this data was analyzed and genes were organized into clusters based on the timing of their expression (195). This data set has been used by our lab to identify potential stage-specific genes, such as oocyst wall proteins for macrogamonts. We are most interested in identifying a sporozoite-specific gene in order to visualize sporozoite development within the ALI system. Successful tagging of sporozoite gene would contribute to the evidence of complete life cycle development occurring in this cell platform. We could also tag oocyst wall proteins to visualize their organization process as the macrogamont develops and becomes fertilized. We observed wall-forming bodies (WFBs), which contain oocyst wall proteins, forming a circular pattern in macrogamonts in ALI culture, something we have not observed in other cell culture systems. We termed these macrogamonts “late-stage” because it appeared the WFBs were organizing, either in response to fertilization or in preparation for it. If the WFBs

organize after fertilization, these late-stage macrogamonts are actually zygotes, which have been impossible to identify in cell culture or even *in vivo* studies.

Stable transfection can also be used to create a conditional knockdown system in *C. parvum* to investigate genes that may be essential to life cycle progression. Our lab has recently developed an auxin-inducible degron (AID) system in *T. gondii* (196) and it has also been used in *Plasmodium* (197). This system has been adapted from plants, which use auxins (type of plant hormone) to target proteins for proteasomal degradation. It requires a plant auxin receptor called transport inhibitor response (TIR1) and a protein tagged with an AID. Treatment with auxin activates a specific ubiquitin ligase complex that directs AID-tagged proteins to ubiquitin-dependent proteasomal degradation. This system allows depletion of a protein to be restricted to a precise length of time during an experiment, allowing essential genes to be studied. CRISPR/Cas9 genome editing can be used to introduce AID tags to genes of interest (196).

We could adapt the AID system to *C. parvum* and use it to study genes that are required for life cycle development. For example, the continuous growth we see in ALI culture could either be due to complete life cycle development of the parasite and reinfection of the monolayer by new oocysts, or ongoing rounds of asexual division (merogony). In the latter scenario, oocyst development clearly still occurs but does not significantly contribute to the high parasite burden seen in the monolayers. It has been hypothesized that the parasite can undergo asexual division continuously in the gut as an explanation for the long-lasting infections seen in immunocompromised patients, but there is no concrete evidence of this. We could tag a micro- or macrogamont-specific gene with an AID and treat the infected cultures with auxin to induce temporary depletion of the protein. Candidate genes would include transcription factors; there is precedent in other apicomplexan parasites for stage-specific transcription factors, for example in

T. gondii bradyzoites (198) and *Plasmodium* gametocytes (199, 200). There are also genes associated with meiosis that could be targeted. Ablation of a transcription factor or other protein required for micro- or macrogamont development in ALI culture and observation of its effect on growth would provide significant insight into whether *C. parvum* can cycle asexually indefinitely.

Temporary gene knockdown in *C. parvum* has been achieved by methods that do not require stable transfection. Morpholinos have been used to knockdown *C. parvum* lactate dehydrogenase and sporozoite 60K protein during infection both *in vivo* and *in vitro* (201, 202), leading to a drop in parasite numbers, demonstrating that both genes are essential. This technique is another approach that could be taken to interfere with sexual development in ALI culture if the AID system cannot be adapted to *C. parvum*.

Cryopreservation

Currently, there are no established protocols for cryopreserving *C. parvum*. Because there is no long-term culture system, there is no method for freezing infected cells, like what is possible with *T. gondii* tachyzoites. There has been a lot of interest in cryopreserving oocysts in order to avoid continually passaging lines through calves, mice, or pigs in order to maintain infectivity. Also, for the purpose of drug screens and human challenge studies, cryopreservation would enable the distribution of the same *C. parvum* or *C. hominis* line to all researchers, allowing results to be directly compared without worrying about strain variability. A recent preliminary report describes a method for cryopreservation of *C. parvum* oocysts that involves permeabilization of the oocyst wall using bleach to allow uptake of cryoprotective agents and loading oocysts into microcapillary tubes before submerging in liquid nitrogen (203). This

protocol has some limitations (only been tested on two strains, <100 µl volume), but does show that cryopreservation of oocysts is possible. Another recent publication reported cryopreservation of *C. parvum*, but with infected cells instead of oocysts (97). In this model, infected cells were frozen; after thawing, the cells began producing oocysts within three days. This method is based on a cancer cell line that is reported to support complete life cycle development *in vitro*, but we have been unable to replicate this initial result in our lab.

We plan to try cryopreserving infected ALI cultures, but it is likely that thawed cultures will not be able to infect new monolayers for the same unknown reasons that propagation has not yet worked in the ALI system. However, we could inoculate the thawed cultures into mice by oral gavage and collect oocysts from the pellets. If this is successful, it would enable the preservation of transgenic lines without needing to reintroduce them into mice to make new infectious oocysts every 3-6 months (66). For labs that have adopted the stable transfection system for *C. parvum*, this process has become incredibly burdensome as the number of lines that need to be maintained steadily multiplies. Successful cryopreservation would allow valuable resources and time to be directed elsewhere.

Transcriptomics

In order to identify host pathways that help create a supportive environment for *C. parvum* growth, we have performed RNA-seq studies comparing gene expression of uninfected monolayers on day 0 of top medium removal and day 3 post-top medium removal. We chose these time points because we had found that infecting on day 3 post-top medium removal led to robust parasite growth as well as increased host cell viability while infecting on day 0 led to poor parasite growth and monolayer disruption. After the top medium is removed to create the ALI,

the cells begin to differentiate, leading to the development of terminal cell types such as goblet and endocrine cells. This differentiation cascade is seen in initial analyses of the RNA-seq data, which show upregulation of notch signaling, a known regulator of intestinal stem cell proliferation and differentiation (204) as well upregulation of genes associated with DNA replication and G1 to S cell cycle transition, which mirrors the increased host cell proliferation we saw in the monolayers after the ALI was established. While these results are not surprising, it is important to establish what pathways are up- and downregulated in the monolayers after the introduction of the ALI in order to begin to understand why this system supports complete development of *C. parvum*.

If we can identify certain metabolic pathways that are differentially regulated in the ALI vs. non-ALI monolayers, that could provide clues to the ideal nutrient conditions for *C. parvum* within the host. For example, genes associated with glycolysis are downregulated in ALI monolayers on day 3 post-top medium removal compared to day 0, which is a reflection of the restriction of the stem cell population and development of terminally differentiated cells that occurs after ALI is introduced. Many types of stem cells are heavily dependent on anaerobic glycolysis (205) and high levels of glycolysis occur at the base of the crypt, where the intestinal stem cells are located (206, 207). *C. parvum* did not grow well in "submerged" transwells compared to ALI transwells, suggesting that stem cells, which are the predominant population in submerged transwells, do not support parasite growth. This result could partly be due to the stem cells' reliance on glycolysis, the byproducts of which would create a very different pool of nutrients for *C. parvum* to scavenge compared to oxidative phosphorylation. Similarly, cancer cell lines such as HCT-8 and Caco-2, which are used to study short-term *C. parvum* growth, heavily rely on glycolysis (208). Long-term growth of *C. parvum* could require a pool of host

cells primarily relying on oxidative phosphorylation, which is likely present in the ALI monolayers. There has been a report of increased oxidative phosphorylation occurring in porcine epithelial cells when they are grown under ALI conditions (137). This outcome could be confirmed in our system using a Seahorse assay, which can measure oxygen consumption rate and extracellular acidification rate; this assay has previously been used to study metabolism of colonic spheroids (207). Directly manipulating oxidative phosphorylation rates in the ALI monolayer to prove a connection with *C. parvum* growth will be difficult, however, since most inhibitors of oxidative phosphorylation are toxic to the cell.

Specific host genes that are up- or downregulated during *C. parvum* infection could be investigated by establishing ALI monolayers from knockout cell lines. For example, a recent report described the upregulation of type I interferon signaling in intestinal organoids infected with *C. parvum* (209); if we see the same signal in our RNA-seq data, we could pursue this phenotype by studying infection in monolayers that are deficient for different components of the interferon signaling pathway.

Host gene expression analysis will definitely play a key role in understanding the success of the ALI system in supporting robust *C. parvum* growth, but it would also be interesting to look at parasite gene expression in different culture systems to identify gene signatures associated with continuous growth. Currently, there is very limited gene expression data available for *C. parvum*; there is one study that looked at growth in HCT-8 cells and examined gene expression by RT-qPCR (89). It would be valuable to examine parasite gene expression in ALI cultures to identify genes that are turned on during complete life cycle development. If we could compare this to parasite gene expression in HCT-8 cells, we could identify the block in life cycle development in cancer cell lines. The potential issue with this experiment is the low growth

of *C. parvum* in HCT-8 cells compared to the ALI monolayers; it is possible that the parasite gene signature will be overwhelmed by host gene expression. However, if we able to create stable lines with stage-specific reporters, we could flow-sort infected cells and perform single cell RNA-seq to identify gene expression associated with each life stage. If we did this in both HCT-8 and primary cells, we could compare gene expression throughout the life cycle directly between the two cell types and identify pathways that are positively associated with complete life development. Fluorescent microscopy studies that we have performed in infected ALI monolayers already hint at differential gene expression in *C. parvum* in this system; for example, the reactivity of microgamonts to antibodies that recognize oocyst wall proteins (OW50 and Crypt-a-glo^{TM}), something that does not occur in HCT-8 cells. Identification of unique parasite signaling pathways in ALI culture will provide the basis for much future investigation into the *C. parvum* life cycle.

Culturing C. hominis in vitro

The majority of human cryptosporidiosis cases are caused by *C. hominis*, not *C. parvum* (2-4). *C. parvum* is used most often for *in vitro* studies because it can be produced in large quantities by calves; *C. hominis* oocysts have limited availability and are only routinely produced by one lab (Tzipori, Tufts University). *C. hominis* is most frequently cultured in neonatal piglets (71) but can infect calves (71, 72) and immunosuppressed gerbils (74). The neonatal piglet model is most often used to study drug efficacy against *C. hominis* (70, 77). The only cell culture systems available for *C. hominis* are human cancer cell lines that only support a few days of growth, which obviously limits *in vitro* studies. Just like for *C. parvum*, there is interest in developing an *in vitro* culture system that can support *C. hominis* development and propagation.

This system would facilitate drug studies and enable evaluation of drug efficacy *in vitro* before moving drugs into the neonatal piglet model.

We have already attempted to grow *C. hominis* in the murine ALI monolayers but were unsuccessful, which is unsurprising because *C. hominis* does not grow in mice. However, we plan to establish ALI cultures with human ileal cells to see if these would support *C. hominis* growth. It also may be worthwhile to try porcine or bovine ileal cells to see if there are any differences in growth. For all these cell types, it will be necessary to confirm that the monolayers support *C. parvum* growth first as a positive control. It may also be necessary to re-test a lot of the variables that were fine-tuned to enhance *C. parvum* growth in the murine monolayers, such as host cell seeding density, timing of infection post top medium removal, and infectious dose.

If *C. parvum* and *C. hominis* can both grow in human ALI monolayers, it would be possible to perform crossing experiments to create recombinant strains. There is evidence of recombinant strains occurring in nature (210) so it could be possible to force this to happen *in vitro*. These kinds of studies could lead to the identification of genes that control host specificity.

Concluding remarks

Due to its ability to support long-term growth and complete life cycle development, the ALI system will be a great platform for future investigation into *C. parvum* biology. Essentially, this culture system is a key that unlocks many parasite processes that were previously unable to be studied *in vitro*. This system will greatly aid research into basic scientific questions about *C. parvum*, which will further our understanding of this previously intractable pathogen and importantly, support innovative drug development and identification of new therapeutic targets.

REFERENCES

1. Šlapeta J. 2013. Cryptosporidiosis and Cryptosporidium species in animals and humans: a thirty colour rainbow? International Journal for Parasitology 43:957-970.
2. Sow SO, Muhsen K, Nasrin D, Blackwelder WC, Wu Y, Farag TH, Panchalingam S, Sur D, Zaidi AK, Faruque AS, Saha D, Adegbola RA, Alonso PL, Breiman RF, Bassat Q, Tamboura B, Sanogo D, Onwuchekwa U, Manna B, Ramamurthy T, Kanungo S, Ahmed S, Qureshi S, Quadri F, Hossain A, Das SK, Antonio M, Hossain MJ, Mandomando I, Nhampossa T, Acácio S, Omore R, Oundo JO, Ochieng JB, Mintz ED, O'Reilly CE, Berkeley LY, Livio S, Tennant SM, Sommerfelt H, Nataro JP, Ziv-Baran T, Robins-Browne RM, Mishcherkin V, Zhang J, Liu J, Houpt ER, Kotloff KL, Levine MM. 2016. The Burden of Cryptosporidium Diarrheal Disease among Children < 24 Months of Age in Moderate/High Mortality Regions of Sub-Saharan Africa and South Asia, Utilizing Data from the Global Enteric Multicenter Study (GEMS). PLoS Negl Trop Dis 10:e0004729.
3. Chalmers RM, Smith R, Elwin K, Clifton-Hadley FA, Giles M. 2011. Epidemiology of anthroponotic and zoonotic human cryptosporidiosis in England and Wales, 2004-2006. Epidemiol Infect 139:700-12.
4. Cacciò SM, Chalmers RM. 2016. Human cryptosporidiosis in Europe. Clin Microbiol Infect 22:471-80.
5. Current WL, Garcia LS. 1991. Cryptosporidiosis. Clin Microbiol Rev 4:325-358.
6. Tyzzer EE. 1907. A sporozoan found in the peptic glands of the common mouse. Proc Soc Exp Biol Med 5:12-3.

7. Tyzzer EE. 1910. An extracellular coccidium, Cryptosporidium muris (gen. et sp. nov.), of the gastric glands of the common mouse. J Med Res 23:487-509.

8. Tyzzer EE. 1912. Cryptosporidium parvum (sp. nov.), a coccidium found in the small intestine of the common mouse. Arch Protistenkd 26:394-412.

9. Nime FA, Burek JD, Page DL, Holscher MA, Yardley JH. 1976. Acute enterocolitis in a human being infected with the protozoan Cryptosporidium. Gastroenterology 70:592-598.

10. Ma P. 1984. Cryptosporidium and the enteropathy of immune deficiency. Gastroenterol Nutri 3:488-90.

11. Pitlik SD, Fainstein V, Garza D, Guarda L, Bolivar R, Rios A, Hopfer RL, Mansell PA. 1983. Human cryptosporidiosis: spectrum of disease. Report of six cases and review of the literature. Arch Intern Med 143:2269-75.

12. Guarda LA, Stein SA, Cleary KA, Ordóñez NG. 1983. Human cryptosporidiosis in the acquired immune deficiency syndrome. Arch Pathol Lab Med 107:562-6.

13. Forgacs P, Tarshis A, Ma P, Federman M, Mele L, Silverman ML, Shea JA. 1983. Intestinal and bronchial cryptosporidiosis in an immunodeficient homosexual man. Ann Intern Med 99:793-4.

14. Navin TR, Juranek DD. 1984. Cryptosporidiosis: clinical, epidemiologic, and parasitologic review. Rev Infect Dis 6:313-27.

15. Richardson AJ, Frankenberg RA, Buck AC, Selkon JB, Colbourne JS, Parsons JW, Mayon-White RT. 1991. An outbreak of waterborne cryptosporidiosis in Swindon and Oxfordshire. Epidemiol Infect 107:485-495.

16. MacKenzie WR, Hoxie NJ, Proctor ME, Gradus MS, Blair KA, Peterson DE, Kazmierczak JJ, Addiss DG, Fox KR, Rose JB. 1994. A massive outbreak in Milwaukee of Cryptosporidium infection transmitted through the public water supply. N Engl J Med 331:161-7.

17. Betancourt WQ, Rose JB. 2004. Drinking water treatment processes for removal of Cryptosporidium and Giardia. Vet Parasitol 126:219-34.

18. Hlavsa MC, Roellig DM, Seabolt MH, Kahler AM, Murphy JL, McKitt TK, Geeter EF, Dawsey R, Davidson SL, Kim TN, Tucker TH, Iverson SA, Garrett B, Fowle N, Collins J, Epperson G, Zusy S, Weiss JR, Komatsu K, Rodriguez E, Patterson JG, Sunenshine R, Taylor B, Cibulskas K, Denny L, Omura K, Tsorin B, Fullerton KE, Xiao L. 2017. Using Molecular Characterization to Support Investigations of Aquatic Facility-Associated Outbreaks of Cryptosporidiosis - Alabama, Arizona, and Ohio, 2016. MMWR Morb Mortal Wkly Rep 66:493-497.

19. Kotloff KL, Nataro JP, Blackwelder WC, Nasrin D, Farag TH, Panchalingam S, Wu Y, Sow SO, Sur D, Breiman RF, Faruque AS, Zaidi AK, Saha D, Alonso PL, Tamboura B, Sanogo D, Onwuchekwa U, Manna B, Ramamurth T, Kanungo S, Ochieng JB, Omore R, Oundo JO, Hossain A, Das SK, Ahmed S, Qureshi S, Quadri F, Adegbola RA, Antonio M, Hossain MJ, Akinsola A, Mandomando I, Nhampossa T, Acácio S, Biswas K, O'Reilly CE, Mintz ED, Berkeley LY, Muhsen K, Sommerfelt H, Robins-Browne RM, Levine MM. 2013. Burden and aetiology of diarrhoeal disease in infants and young children in developing countries (the Global Enteric Multicenter Study, GEMS): a prospective, case-control study. Lancet 382:209-22.

20. MAL ED Network Investigators. 2014. The MAL-ED study: a multinational and multidisciplinary approach to understand the relationship between enteric pathogens, malnutrition, gut physiology, physical growth, cognitive development, and immune responses in infants and children up to 2 years of age in resource-poor environments. Clin Infect Dis 59:S193-296.

21. Platts-Mills JA, Babji S, Bodhidatta L, Gratz J, Haque R, Havt A, McCormick BJ, McGrath M, Olortegui MP, Samie A, Shakoor S, Mondal D, Lima IF, Hariraju D, Rayamajhi BB, Qureshi S, Kabir F, Yori PP, Mufamadi B, Amour C, Carreon JD, Richard SA, Lang D, Bessong P, Mduma E, Ahmed T, Lima AA, Mason CJ, Zaidi AK, Bhutta ZA, Kosek M, Guerrant RL, Gottlieb M, Miller MA, Kang G, Houpt ER, Investigators. M-EN. 2015. Pathogen-specific burdens of community diarrhoea in developing countries: a multisite birth cohort study (MAL-ED). Lancet Glob Health 3:e564-75.

22. Mølbak K, Andersen M, Aaby P, Højlyng N, Jakobsen M, Sodemann M, da Silva AP. 1997. Cryptosporidium infection in infancy as a cause of malnutrition: a community study from Guinea-Bissau, west Africa. Am J Clin Nutr 65:149-52.

23. Checkley W, Epstein LD, Gilman RH, Black RE, Cabrera L, Sterling CR. 1998. Effects of Cryptosporidium parvum infection in Peruvian children: growth faltering and subsequent catch-up growth. Am J Epidemiol 148:497-506.

24. Steiner KL, Ahmed S, Gilchrist CA, Burkey C, Cook H, Ma JZ, Korpe PS, Ahmed E, Alam M, Kabir M, Tofail F, Ahmed T, Haque R, Petri WAJ, Faruque ASG. 2018. Species of Cryptosporidia Causing Subclinical Infection Associated with Growth

Faltering in Rural and Urban Bangladesh - a Birth Cohort Study. Clin Infect Dis Epub ahead of print.

25. Mølbak K, Højlyng N, Gottschau A, Sá JC, Ingholt L, da Silva AP, Aaby P. 1993. Cryptosporidiosis in infancy and childhood mortality in Guinea Bissau, west Africa. BMJ 307:417-20.

26. Liu L, Johnson HL, Cousens S, Perin J, Scott S, Lawn JE, Rudan I, Campbell H, Cibulskis R, Li M, Mathers C, Black RE, UNICEF CHERGoWa. 2012. Global, regional, and national causes of child mortality: an updated systematic analysis for 2010 with time trends since 2000. Lancet 379:2151-61.

27. Guerrant RL, Schorling JB, McAuliffe JF, de Souza MA. 1992. Diarrhea as a cause and an effect of malnutrition: diarrhea prevents catch-up growth and malnutrition increases diarrhea frequency and duration. Am J Trop Med Hyg 47:28-35.

28. Striepen B. 2013. Parasitic infections: Time to tackle cryptosporidiosis. Nature 503:189-91.

29. Rossignol JF, Ayoub A, Ayers MS. 2001. Treatment of diarrhea caused by Cryptosporidium parvum: a prospective randomized, double-blind, placebo-controlled study of Nitazoxanide. J Infect Dis 184:103-106.

30. Amadi B, Mwiya M, Musuku J, Watuka A, Sianongo S, Ayoub A, Kelly P. 2002. Effect of nitazoxanide on morbidity and mortality in Zambian children with cryptosporidiosis: a randomised controlled trial. Lancet 360:1375-80.

31. Abubakar I, Aliyu SH, Arumugam C, Usman NK, Hunter PR. 2007. Treatment of cryptosporidiosis in immunocompromised individuals: systematic review and meta-analysis. British Journal of Clinical Pharmacology 63:387-393.

32. Hulverson MA, Vinayak S, Choi R, Schaefer DA, Castellanos-Gonzalez A, Vidadala RSR, Brooks CF, Herbert GT, Betzer DP, Whitman GR, Sparks HN, Arnold SLM, Rivas KL, Barrett LK, White ACJ, Maly DJ, Riggs MW, Striepen B, Van Voorhis WC, Ojo KK. 2017. Bumped-Kinase Inhibitors for Cryptosporidiosis Therapy. J Infect Dis 215:1275-1284.

33. Manjunatha UH, Vinayak S, Zambriski JA, Chao AT, Sy T, Noble CG, Bonamy GMC, Kondreddi RR, Zou B, Gedeck P, Brooks CF, Herbert GT, Sateriale A, Tandel J, Noh S, Lakshminarayana SB, Lim SH, Goodman LB, Bodenreider C, Feng G, Zhang L, Blasco F, Wagner J, Leong FJ, Striepen B, Diagana TT. 2017. A Cryptosporidium PI(4)K inhibitor is a drug candidate for cryptosporidiosis. Nature 546:376-380.

34. Love MS, Beasley FC, Jumani RS, Wright TM, Chatterjee AK, Huston CD, Schultz PG, McNamara CW. 2017. A high-throughput phenotypic screen identifies clofazimine as a potential treatment for cryptosporidiosis. PLoS Negl Trop Dis 11:e0005373.

35. Fayer R, Leek RG. 1984. The effects of reducing conditions, medium, pH, temperature, and time on in vitro excystation of Cryptosporidium. J Protozool 31:567-9.

36. Current WL, Reese NC. 1986. A comparison of endogenous development of three isolates of Cryptosporidium in suckling mice. J Protozool 33:98-108.

37. Current WL, Long PL. 1983. Development of human and calf Cryptosporidium in chicken embryos. J Infect Dis 148:1108-13.

38. Wetzel DM, Schmidt J, Kuhlenschmidt M, Dubey JP, Sibley LD. 2005. Gliding motility leads to active cellular invasion by *Cryptosporidium parvum* sporozoites. Infect Immun 73:5379-5387.

39. Valigurová A, Jirků M, Koudela B, Gelnar M, Modrý D, Slapeta J. 2008. Cryptosporidia: epicellular parasites embraced by the host cell membrane. Int J Parasitol 38:913-922.

40. Lumb R, Smith K, O'Donoghue PJ, Lanser JA. 1988. Ultrastructure of the attachment of Cryptosporidium sporozoites to tissue culture cells. Parasitol Res 74:531-6.

41. Marcial MA, Madara JL. 1986. Cryptosporidium: cellular localization, structural analysis of absorptive cell-parasite membrane-membrane interactions in guinea pigs, and suggestion of protozoan transport by M cells. Gastroenterology 90:583-94.

42. Tzipori S, Griffiths JK. 1998. Natural history and biology of Cryptosporidium parvum. Adv Parasitol 40:5-36.

43. Abrahamsen MS, Templeton TJ, Enomoto S, Abrahante JE, Zhu G, Lancto CA, Deng M, Liu C, Widmer G, Tzipori S, Buck GA, Xu P, Bankier AT, Dear PH, Konfortov BA, Spriggs HF, Lakshminarayan I, Anantharaman V, Aravind L, Kapur V. 2004. Complete genome sequence of the apicomplexan, *Cryptosporidium parvum*. Sciencexpress 304:441-445.

44. Perkins ME, Riojas YA, Wu TW, Le Blancq SM. 1999. CpABC, a Cryptosporidium parvum ATP-binding cassette protein at the host-parasite boundary in intracellular stages. Proc Natl Acad Sci (USA) 96:5734-9.

45. Barta JR, Thompson RC. 2006. What is Cryptosporidium? Reappraising its biology and phylogenetic affinities. Trends Parasitol 22:463-8.

46. Carreno RA, Martin DS, Barta JR. 1999. *Cryptosporidium* is more closely related to the gregarines than to coccidia as shown by phylogenetic analysis of apicomplexan parasites inferred using small-subunit ribosomal RNA gene sequences. Parasitol Res 85:899-904.

47. Thompson RC, Olson ME, Zhu G, Enomoto S, Abrahamsen MS, Hijjawi NS. 2005. Cryptosporidium and cryptosporidiosis. Adv Parasitol 59:77-158.

48. Morgan-Ryan UM, Fall A, Ward LA, Hijjawi N, Sulmaiman I, Fayer R, Thompson RC, Olson M, Lal AA, Xiao L. 2002. *Cryptosporidium hominis* n. sp. (Apicomplexa: Cryptosporidiidae) from *Homo sapiens*. J Euk Microbiol 49:433-440.

49. Enriquez FJ, Sterling CR. 1991. Cryptosporidium infections in inbred strains of mice. J Protozool 38:100S-102S.

50. Ren X, Zhao J, Zhang L, Ning C, Jian F, Wang R, Lv C, Wang Q, Arrowood MJ, Xiao L. 2012. Cryptosporidium tyzzeri n. sp. (Apicomplexa: Cryptosporidiidae) in domestic mice (Mus musculus). Exp Parasitol 130:274-81.

51. Sherwood D, Angus KW, Snodgrass DR, Tzipori S. 1982. Experimental cryptosporidiosis in laboratory mice. Infect Immun 38:471-5.

52. Novak SM, Sterling CR. 1991. Susceptibility dynamics in neonatal BALB/c mice infected with Cryptosporidium parvum. J Protozool 38:103S-104S.

53. Upton SJ, Gillock HH. 1996. Infection dynamics of Cryptosporidium parvum in ICR outbred suckling mice. Folia Parasitol (Praha) 43:101-6.

54. Costa LB, JohnBull EA, Reeves JT, Sevilleja JE, Freire RS, Hoffman PS, Lima AA, Oriá RB, Roche JK, Guerrant RL, Warren CA. 2011. Cryptosporidium-malnutrition interactions: mucosal disruption, cytokines, and TLR signaling in a weaned murine model. J Parasitol 97:1113-20.

55. Liu J, Bolick DT, Kolling GL, Fu Z, Guerrant RL. 2016. Protein Malnutrition Impairs Intestinal Epithelial Cell Turnover, a Potential Mechanism of Increased Cryptosporidiosis in a Murine Model. Infect Immun 84:3542-3549.

56. Katona P, Katona-Apte J. 2008. The interaction between nutrition and infection. Clin Infect Dis 46:1582-8.

57. Guerrant RL, Lima AA, Davidson F. 2000. Micronutrients and infection: interactions and implications with enteric and other infections and future priorities. J Infect Dis 182:S134-8.

58. Heine J, Moon HW, Woodmansee DB. 1984. Persistent Cryptosporidium infection in congenitally athymic (nude) mice. Infect Immun 43:856-9.

59. Kuhls TL, Greenfield RA, Mosier DA, Crawford DL, Joyce WA. 1992. Cryptosporidiosis in adult and neonatal mice with severe combined immunodeficiency. J Comp Pathol 106:399-410.

60. Aguirre SA, Mason PH, Perryman LE. 1994. Susceptibility of major histocompatibility complex (MHC) class I- and MHC class II-deficient mice to Cryptosporidium parvum infection. Infect Immun 62:697-9.

61. Downey AS, Chong CR, Graczyk TK, Sullivan DJ. 2008. Efficacy of pyrvinium pamoate against Cryptosporidium parvum infection in vitro and in a neonatal mouse model. Antimicrob Agents Chemother 52:3106-12.

62. Tilley M, Upton SJ, Freed PS. 1990. A comparative study on the biology of Cryptosporidium serpentis and Cryptosporidium parvum (Apicomplexa: Cryptosporidiidae). J Zoo Wildl Med 21:463-7.

63. Mead JR, Arrowood MJ, Sidwell RW, Healey MC. 1991. Chronic Cryptosporidium parvum infections in congenitally immunodeficient SCID and nude mice. J Infect Dis 163:1297-304.

64. Mead JR, Ilksoy N, You X, Belenkaya Y, Arrowood MJ, Fallon MT, Schinazi RF. 1994. Infection dynamics and clinical features of cryptosporidiosis in SCID mice. Infect Immun 62:1691-5.

65. Griffiths JK, Theodos C, Paris M, Tzipori S. 1998. The gamma interferon gene knockout mouse: a highly sensitive model for evaluation of therapeutic agents against Cryptosporidium parvum. J Clin Microbiol 36:2503-8.

66. Vinayak S, Pawlowic MC, Sateriale A, Brooks CF, Studstill CJ, Bar-Peled Y, Cipriano MJ, Striepen B. 2015. Genetic modification of the diarrhoeal pathogen Cryptosporidium parvum. Nature 523:477-480.

67. Theodos CM, Griffiths JK, D'Onfro J, Fairfield A, Tzipori S. 1998. Efficacy of nitazoxanide against Cryptosporidium parvum in cell culture and in animal models. Antimicrob Agents Chemother 42:1959-65.

68. Zambriski JA, Nydam DV, Bowman DD, Bellosa ML, Burton AJ, Linden TC, Liotta JL, Ollivett TL, Tondello-Martins L, Mohammed HO. 2013. Description of fecal shedding of Cryptosporidium parvum oocysts in experimentally challenged dairy calves. Parasitol Res 112:1247-54.

69. Zambriski JA, Nydam DV, Wilcox ZJ, Bowman DD, Mohammed HO, Liotta JL. 2013. Cryptosporidium parvum: determination of ID50 and the dose-response relationship in experimentally challenged dairy calves. Vet Parasitol 197:104-12.

70. Lee S, Ginese M, Beamer G, Danz HR, Girouard DJ, Chapman-Bonofiglio SP, Lee M, Hulverson MA, Choi R, Whitman GR, Ojo KK, Arnold SLM, Van Voorhis WC, Tzipori S. 2018. Therapeutic Efficacy of Bumped Kinase Inhibitor 1369 in the Acute Pig Model of Cryptosporidium hominis. Antimicrob Agents Chemother AAC.00147-18.

71. Akiyoshi DE, Feng X, Buckholt MA, Widmer G, Tzipori S. 2002. Genetic analysis of a Cryptosporidium parvum human genotype 1 isolate passaged through different host species. Infect Immun 70:5670-5.

72. Razakandrainibe R, Diawara EHI, Costa D, Le Goff L, Lemeteil D, Ballet JJ, Gargala G, Favennec L. 2018. Common occurrence of Cryptosporidium hominis in asymptomatic and symptomatic calves in France. PLoS Negl Trop Dis 12:e0006355.

73. Baishanbo A, Gargala G, Delaunay A, François A, Ballet JJ, Favennec L. 2005. Infectivity of Cryptosporidium hominis and Cryptosporidium parvum genotype 2 isolates in immunosuppressed Mongolian gerbils. Infect Immun 73:5252-5.

74. Baishanbo A, Gargala G, Duclos C, François A, Rossignol JF, Ballet JJ, Favennec L. 2006. Efficacy of nitazoxanide and paromomycin in biliary tract cryptosporidiosis in an immunosuppressed gerbil model. J Antimicrob Chemother 57:353-5.

75. Gargala G, François A, Favennec L, Rossignol JF. 2013. Activity of halogeno-thiazolides against Cryptosporidium parvum in experimentally infected immunosuppressed gerbils (Meriones unguiculatus). Antimicrob Agents Chemother 57:2821-3.

76. Chappell CL, Okhuysen PC, Langer-Curry R, Widmer G, Akiyoshi DE, Tanriverdi S, Tzipori S. 2006. Cryptosporidium hominis: experimental challenge of healthy adults. Am J Trop Med Hyg 75:851-7.

77. Lee S, Harwood M, Girouard D, Meyers MJ, Campbell MA, Beamer G, Tzipori S. 2017. The therapeutic efficacy of azithromycin and nitazoxanide in the acute pig model of Cryptosporidium hominis. PLoS One 12:e0185906.

78. Flanigan TP, Aji T, Marshall R, Soave R, Aikawa M, Kaetzel C. 1991. Asexual development of Cryptosporidium parvum within a differentiated human enterocyte cell line. Infect Immun 49:234-9.

79. Gut J, Petersen C, Nelson R, Leech J. 1991. Cryptosporidium parvum: in vitro cultivation in Madin-Darby canine kidney cells. J Protozool 38:72S-73S.

80. Arrowood MJ, Xie LT, Hurd MR. 1994. In vitro assays of maduramicin activity against Cryptosporidium parvum. J Eukaryot Microbiol 41:23S.

81. Arrowood MJ, Mead JR, Xie L, You X. 1996. In vitro anticryptosporidial activity of dinitroaniline herbicides. FEMS Microbiol Lett 136:245-9.

82. You X, Schinazi RF, Arrowood MJ, Lejkowski M, Juodawlkis AS, Mead JR. 1998. In-vitro activities of paromomycin and lasalocid evaluated in combination against Cryptosporidium parvum. J Antimicrob Chemother 41:293-6.

83. Upton SJ, Tilley M, Brillhart DB. 1994. Comparative development of Cryptosporidium parvum (Apicomplexa) in 11 continuous host cell lines. FEMS Microbiol Lett 118:233-6.

84. Upton SJ, Tilley M, Brillhart DB. 1995. Effects of select medium supplements on in vitro development of Cryptosporidium parvum in HCT-8 cells. J Clin Microbiol 33:371-5.

85. Upton SJ, Tilley M, Nesterenko MV, Brillhart DB. 1994. A simple and reliable method of producing in vitro infections of Cryptosporidium parvum (Apicomplexa). FEMS Microbiol Lett 118:45-9.

86. Cordón GP, Marin C, Romero D, Rosales C, Sánchez Moreno M, Rosales MJ. 2007. More productive in vitro culture of Cryptosporidium parvum for better study of the intra- and extracellular phases. Mem Inst Oswaldo Cruz 102:567-571.

87. Morada M, Pendyala L, Wu G, Merali S, Yarlett N. 2013. Cryptosporidium parvum induces an endoplasmic stress response in the intestinal adenocarcinoma HCT-8 cell line. J Biol Chem 288:30356-64.

88. Inomata A, Murakoshi F, Ishiwa A, Takano R, Takemae H, Sugi T, Cagayat Recuenco F, Horimoto T, Kato K. 2015. Heparin interacts with elongation factor 1α of Cryptosporidium parvum and inhibits invasion. Sci Rep 5:11599.

89. Mauzy MJ, Enomoto S, Lancto CA, Abrahamsen MS, Rutherford MS. 2012. The Cryptosporidium parvum transcriptome during in vitro development. PLoS One 7.

90. Griffiths JK, Moore R, Dooley S, Keusch GT, Tzipori S. 1994. Cryptosporidium parvum infection of Caco-2 cell monolayers induces an apical monolayer defect, selectively increases transmonolayer permeability, and causes epithelial cell death. Infect Immun 62:4506-14.

91. Maillot C, Gargala G, Delaunay A, Ducrotte P, Brasseur P, Ballet JJ, Favennec L. 2000. Cryptosporidium parvum infection stimulates the secretion of TGF-beta, IL-8 and RANTES by Caco-2 cell line. Parastiol Res 86:947-9.

92. Hijjawi NS, Meloni BP, Ng'anzo M, Ryan UM, Olson ME, Cox PT, Monis PT, Thompson RC. 2004. Complete development of Cryptosporidium parvum in host cell-free culture. Int J Parasitol 34:769-77.

93. Girouard D, Gallant J, Akiyoshi DE, Nunnari J, Tzipori S. 2006. Failure to propagate Cryptosporidium spp. in cell-free culture. J Parasitol 92:399-400.

94. Woods KM, Upton SJ. 2007. In vitro development of Cryptosporidium parvum in serum-free media. Lett Appl Microbiol 44:520-3.

95. Morada M, Lee S, Gunther-Cummins L, Weiss LM, Widmer G, Tzipori S, Yarlett N. 2016. Continuous culture of Cryptosporidium parvum using hollow fiber technology. Int J Parasitol 46:21-9.

96. DeCicco RePass MA, Chen Y, Lin Y, Zhou W, Kaplan DL, Ward HD. 2017. Novel Bioengineered Three-Dimensional Human Intestinal Model for Long-Term Infection of Cryptosporidium parvum. Infect Immun 85:e00731-16.

97. Miller CN, Jossé L, Brown I, Blakeman B, Povey J, Yiangou L, Price M, Cinatl J, Xue WF, Michaelis M, Tsaousis AD. 2018. A cell culture platform for Cryptosporidium that enables long-term cultivation and new tools for the systematic investigation of its biology. Int J Parasitol 48:197-201.

98. Bushkin GG, Motari E, Carpentieri A, Dubey JP, Costello CE, Robbins PW, Samuelson J. 2013. Evidence for a structural role for acid-fast lipids in oocyst walls of Cryptosporidium, Toxoplasma, and Eimeria. MBio 4:e00387-13.

99. Mazumdar J, Striepen B. 2007. Make it or take it: fatty acid metabolism of apicomplexan parasites. Eukaryot Cell 6:1727-35.

100. Chen Y, Lin Y, Davis KM, Wang Q, Rnjak-Kovacina J, Li C, Isberg RR, Kumamoto CA, Mecsas J, Kaplan DL. 2015. Robust bioengineered 3D functional human intestinal epithelium. Sci Rep 5:13708.

101. Current WL, Reese NC, Ernst JV, Bailey WS, Heyman MB, Weinstein WM. 1983. Human cryptosporidiosis in immunocompetent and immunodeficient persons. Studies of an outbreak and experimental transmission. N Engl J Med 308:1252-7.

102. Centers for Disease Control. 1982. Cryptosporidiosis: assessment of chemotherapy of males with acquired immune deficiency syndrome (AIDS). MMWR Morb Mortal Wkly Rep 31:589-92.

103. Current WL, Haynes TB. 1984. Complete development of Cryptosporidium in cell culture. Science 224:604-605.

104. Yang S, Healey MC, Du C, Zhang J. 1996. Complete development of Cryptosporidium parvum in bovine fallopian tube epithelial cells. Infect Immun 64:349-54.

105. Hijjawi NS, Meloni BP, Morgan UM, Thompson RC. 2001. Complete development and long-term maintenance of Cryptosporidium parvum human and cattle genotypes in cell culture. Int J Parasitol 31:1048-55.

106. Gaur S, Kuhlenschmidt TB, M.S. K, Andrade JE. 2018. Effect of oregano essential oil and carvacrol on Cryptosporidium parvum infectivity in HCT-8 cells. Parasitol Int 67:170-5.

107. Kuhlenschmidt TB, Rutaganira FU, Long S, Tang K, Shokat KM, Kuhlenschmidt MS, Sibley LD. 2015. Inhibition of Calcium-Dependent Protein Kinase 1 (CDPK1) In Vitro by Pyrazolopyrimidine Derivatives Does Not Correlate with Sensitivity of Cryptosporidium parvum Growth in Cell Culture. Antimicrob Agents Chemother 60:570-9.

108. Cevallos AM, Bhat N, Verdon R, Hamer DH, Stein B, Tzipori S, Pereira ME, Keusch GT, Ward HD. 2000. Mediation of Cryptosporidium parvum infection in vitro by mucin-like glycoproteins defined by a neutralizing monoclonal antibody. Infect Immun 68:5167-5175.

109. Cevallos AM, Zhang X, Waldor MK, Jaison S, Zhou X, Tzipori S, Neutra MR, Ward HD. 2000. Molecular cloning and expression of a gene encoding Cryptosporidium parvum glycoproteins gp40 and gp15. Infect Immun 68:4108-16.

110. Gut J, Nelson RG. 1994. Cryptosporidium parvum sporozoites deposit trails of 11A5 antigen during gliding locomotion and shed 11A5 antigen during invasion of MDCK cells in vitro. J Eukaryot Microbiol 41:42S-43S.

111. Strong WB, Gut J, Nelson RG. 2000. Cloning and sequence analysis of a highly polymorphic Cryptosporidium parvum gene encoding a 60-kilodalton glycoprotein and characterization of its 15- and 45-kilodalton zoite surface antigen products. Infect Immun 68:4117-34.

112. Bhat N, Joe A, PereiraPerrin M, Ward HD. 2007. Cryptosporidium p30, a galactose/N-acetylgalactosamine-specific lectin, mediates infection in vitro. J Biol Chem 282:34877-87.

113. Gregorieff A, Clevers H. 2005. Wnt signaling in the intestinal epithelium: from endoderm to cancer. Genes Dev 19:877-90.

114. Barker N, van Es JH, Kuipers J, Kujala P, van den Born M, Cozijnsen M, Haegebarth A, Korving J, Begthel H, Peters PJ, Clevers H. 2007. Identification of stem cells in small intestine and colon by marker gene Lgr5. Nature 449:1003-7.

115. Hsu SY, Liang SG, Hsueh AJ. 1998. Characterization of two LGR genes homologous to gonadotropin and thyrotropin receptors with extracellular leucine-rich repeats and a G protein-coupled, seven-transmembrane region. Mol Endocrinol 12:1830-45.

116. Snyder JC, Rochelle LK, Barak LS, Caron MG. 2013. The stem cell-expressed receptor Lgr5 possesses canonical and functionally active molecular determinants critical to β-arrestin-2 recruitment. PLoS One 8:e84476.

117. Van der Flier LG, Sabates-Bellver J, Oving I H, A., De Palo M, Anti M, Van Gijn ME, Suijkerbuijk S, Van de Wetering M, Marra G, Clevers H. 2007. The Intestinal Wnt/TCF Signature. Gastroenterology 132:628-32.

118. Potten CS, Booth C, Pritchard DM. 1997. The intestinal stem cell: the mucosal governor. Int J Exp Pathol 78:219-43.

119. Pinto D, Gregorieff A, Begthel H, Clevers H. 2003. Canonical Wnt signals are essential for homeostasis of the intestinal epithelium. Genes Dev 17:1709-13.

120. Haramis AP, Begthel H, van den Born M, van Es JH, Jonkheer S, Offerhaus GJ, Clevers H. 2004. De novo crypt formation and juvenile polyposis on BMP inhibition in mouse intestine. Science 303:1684-6.

121. Hofmann C, Obermeier F, Artinger M, Hausmann M, Falk W, Schoelmerich J, Rogler G, J. G. 2007. Cell-cell contacts prevent anoikis in primary human colonic epithelial cells. Gastroenterology 132:587-600.

122. Sato T, Vries RG, Snippert HJ, van de Wetering M, Barker N, Stange DE, van Es JH, Abo A, Kujala P, Peters PJ, Clevers H. 2009. Single Lgr5 stem cells build crypt-villus structures in vitro without a mesenchymal niche. Nature 459:262-5.

123. Sato T, Stange DE, Ferrante M, Vries RG, Van Es JH, Van den Brink S, Van Houdt WJ, Pronk A, Van Gorp J, Siersema PD, Clevers H. 2011. Long-term expansion of epithelial organoids from human colon, adenoma, adenocarcinoma, and Barrett's epithelium. Gastroenterology 141:1762-72.

124. Jung P, Sato T, Merlos-Suárez A, Barriga FM, Iglesias M, Rossell D, Auer H, Gallardo M, Blasco MA, Sancho E, Clevers H, Batlle E. 2011. Isolation and in vitro expansion of human colonic stem cells. Nat Med 17:1225-7.

125. Miyoshi H, Ajima R, Luo C, Yamaguchi TP, Stappenbeck TS. 2012. Wnt5a potentiates TGF-beta signaling to promote colonic crypt regeneration after tissue injury. . Science 338:108-13.

126. Miyoshi H, Stappenbeck TS. 2013. In vitro expansion and genetic modification of gastrointestinal stem cells in spheroid culture. Nat Protoc 8:2471-82.

127. Kim KA, Kakitani M, Zhao J, Oshima T, Tang T, Binnerts M, Liu Y, Boyle B, Park E, Emtage P, Funk WD, Tomizuka K. 2005. Mitogenic influence of human R-spondin1 on the intestinal epithelium. Science 309:1256-9.

128. Kang E, Yousefi M, Gruenheid S. 2016. R-Spondins Are Expressed by the Intestinal Stroma and are Differentially Regulated during Citrobacter rodentium- and DSS-Induced Colitis in Mice. PLoS One 11:e0152859.

129. Haegebarth A, Clevers H. 2009. Wnt signaling, lgr5, and stem cells in the intestine and skin. Am J Pathol 174:715-21.

130. Willert K, Brown JD, Danenberg E, Duncan AW, Weissman IL, Reya T, Yates Jr, Nusse R. 2003. Wnt proteins are lipid-modified and can act as stem cell growth factors. Nature 423:448-52.

131. Moon C, VanDussen KL, Miyoshi H, Stappenbeck TS. 2014. Development of a primary mouse intestinal epithelial cell monolayer culture system to evaluate factors that modulate IgA transcytosis. Mucosal Immunol 7:818-28.

132. Wang X, Yamamoto Y, Wilson LH, Zhang T, Howitt BE, Farrow MA, Kern F, Ning G, Hong Y, Khor CC, Chevalier B, Bertrand D, Wu L, Nagarajan N, Sylvester FA, Hyams JS, Devers T, Bronson R, Lacy DB, Ho KY, Crum CP, McKeon F, Xian W. 2015. Cloning and variation of ground state intestinal stem cells. Nature 522:173-8.

133. Whitcutt MJ, Adler KB, Wu R. 1988. A biphasic chamber system for maintaining polarity of differentiation of cultured respiratory tract epithelial cells. In Vitro Cell Dev Biol 24:420-8.

134. Pezzulo AA, Starner TD, Scheetz TE, Traver GL, Tilley AE, Harvey BG, Crystal RG, McCray PB, Zabner J. 2011. The air-liquid interface and use of primary cell cultures are important to recapitulate the transcriptional profile of in vivo airway epithelia. Am J Physiol Lung Cell Mol Physiol 300:L25-31.

135. O'Boyle N, Sutherland E, Berry CC, Davies RL. 2017. Temporal dynamics of ovine airway epithelial cell differentiation at an air-liquid interface. PLoS One 12:e0181583.

136. Nossol C, Diesing AK, Walk N, Faber-Zuschratter H, Hartig R, Post A, Kluess J, Rothkötter HJ, Kahlert S. 2011. Air-liquid interface cultures enhance the oxygen supply and trigger the structural and functional differentiation of intestinal porcine epithelial cells (IPEC). Histochem Cell Biol 136:103-15.

137. Klasvogt S, Zuschratter W, Schmidt A, Kröber A, Vorwerk S, Wolter R, Isermann B, Wimmers K, Rothkötter HJ, Nossol C. 2017. Air-liquid interface enhances oxidative phosphorylation in intestinal epithelial cell line IPEC-J2. Cell Death Discov Feb 27:17001.

138. VanDussen KL, Marinshaw JM, Shaikh N, Miyoshi H, Moon CS, Tarr PI, Ciorba MA, Stappenbeck TS. 2014. Development of an enhanced human gastrointestinal epithelial culture system to facilitate patient-based assays. Gut 64:911-20.

139. O'Connor RM, Shaffie R, Kang G, Ward HD. 2011. Cryptosporidiosis in patients with HIV/AIDS. AIDS 25:549-560.

140. Gorla SK, McNair NN, Yang G, Gao S, Hu M, Jala VR, Haribabu B, Striepen B, Cuny GD, Mead JR, Hedstrom L. 2014. Validation of IMP dehydrogenase inhibitors in a mouse model of cryptosporidiosis. Antimicrob Agents Chemother 58:1603-14.

141. Blagburn BL, Drain KL, Land TM, Kinard RG, Moore PH, Lindsay DS, Patrick DA, Boykin DW, Tidwell RR. 1998. Comparative efficacy evaluation of dicationic carbazole compounds, nitazoxanide, and paromomycin against Cryptosporidium parvum infections in a neonatal mouse model. Antimicrob Agents Chemother 42:2877-82.

142. Arrowood MJ. 2002. In vitro cultivation of cryptosporidium species. Clin Microbiol Rev 15:390-400.

143. Bouzid M, Hunter PR, Chalmers RM, Tyler KM. 2013. Cryptosporidium pathogenicity and virulence. Clinical Microbiology Reviews 26:115-34.

144. Weir C, Vesey G, Slade M, Ferrari B, Veal DA, Williams K. 2000. An Immunoglobulin G1 Monoclonal Antibody Highly Specific to the Wall of Cryptosporidium Oocysts. Clin Diagn Lab Immunol 7:745-750.

145. von Oettingen J, Nath-Chowdhury M, Ward BJ, Rodloff AC, Arrowood MJ, Ndao M. 2008. High-yield amplification of Cryptosporidium parvum in interferon gamma receptor knockout mice. Parasitology 135:1151-6.

146. O'Connor RM, Wanyiri JW, Cevallos AM, Priest JW, Ward HD. 2007. Cryptosporidium parvum glycoprotein gp40 localizes to the sporozoite surface by association with gp15. Mol Biochem Parasitol 156:80-3.

147. Osaki SC, Costa AO, Troiano LD, Kruger ER, Pereira JT, Fernandes NL, Silva MB, Soccol V. 2011. Production of anti-Cryptosporidium polyclonal antibodies and standardization of direct immunofluorescence for detecting oocysts in water. Rev Soc Bras Med Trop 44:587-90.

148. McDonald V, Stables R, Warhurst DC, Barer MR, Blewett DA, Chapman HD, Connolly GM, Chiodini PL, McAdam KP. 1990. In vitro cultivation of Cryptosporidium parvum and screening for anticryptosporidial drugs. Antimicrob Agents Chemother 34:1498-500.

149. Martinez F, Mascaro C, Rosales MJ, Diaz J, Cifuentes J, Osuna A. 1992. In vitro multiplication of Cryptosporidium parvum in mouse peritoneal macrophages. Vet Parasitol 42:27-31.

150. Greenberg PD, Koch J, Cello JP. 1996. Diagnosis of Cryptosporidium parvum in patients with severe diarrhea and AIDS. Dig Dis Sci 41:2286-90.

151. Smith HV, Campbell BM, Paton CA, Nichols RAB. 2002. Significance of Enhanced Morphological Detection of Cryptosporidium sp. Oocysts in Water Concentrates Determined by Using 4′,6′-Diamidino-2-Phenylindole and Immunofluorescence Microscopy. Appl Environ Microbiol 68:5198-5201.

152. Petry F. 2004. Structural analysis of Cryptosporidium parvum. Microsc Microanal 10:586-601.

153. Sterling CR, Arrowood MJ. 1986. Detection of Cryptosporidium sp. infections using a direct immunofluorescent assay. Pediatr Infect Dis 5:S139-42.

154. Chen XM, Huang BQ, Splinter PL, Orth JD, Billadeau DD, McNiven MA, LaRusso NF. 2004. Cdc42 and the actin-related protein/neural Wiskott-Aldrich syndrome protein network mediate cellular invasion by Cryptosporidium parvum. Infect Immun 72:3011-21.

155. Elliott DA, Clark DP. 2000. Cryptosporidium parvum induces host cell actin accumulation at the host-parasite interface. Infect Immun 68:2315-22.

156. Elliott DA, Coleman DJ, Lane MA, May RC, Machesky LM, Clark DP. 2001. Cryptosporidium parvum infection requires host cell actin polymerization. Infect Immun 69:5940-2.

157. Current WL, Reese NC. 1986. A comparison of endogenous development of three isolates of Cryptosporidium in suckling mice. J Protozool 33:98-108.

158. Xu P, Widmer G, Wang Y, Ozaki LS, Alves JM, Serrano MG, Puiu D, Manque P, Akiyoshi D, Mackey AJ, Pearson WR, Dear PH, Bankier AT, Peterson DL, Abrahamsen MS, Kapur V, Tzipori S, Buck GA. 2004. The genome of Cryptosporidium hominis. Nature 431:1107-12.

159. Tzipori S, Griffiths JK. 1998. Natural history and biology of Cryptosporidium parvum. Adv Parasitol 40:5-36.

160. Tetley L, Brown SM, McDonald V, Coombs GH. 1998. Ultrastructural analysis of the sporozoite of Cryptosporidium parvum. Microbiology 144:3249-55.

161. Bargieri D, Lagal V, Andenmatten N, Tardieux I, Meissner M, Ménard R. 2014. Host cell invasion by apicomplexan parasites: the junction conundrum. Plos Pathog 10(9):e1004273.

162. Chen XM, O'Hara SP, Huang BQ, Nelson JB, Lin JJC, Zhu G, Ward HD, LaRusso NF. 2004. Apical organelle discharge by *Cryptosporidium parvum* is temperature, cytoskeleton, and intracellular calcium dependent and required for host cell invasion. Infect Immun 72:6806-6816.

163. Lefkowitch JA, Krumholz S, Fengchen K, Griffin P, Despommier D, Brasitus TA. 1984. Cryptosporidiosis of the human small intestine: A light and electron microscopic study. Human Pathology 15:746-752.

164. Morrissette NS, Sibley LD. 2002. Cytoskeleton of apicomplexan parasites. Microbiol Mol Biol Rev 66:21-38; table of contents.

165. Padmanabhan J. 2015. Immunostaining analysis of tissue cultured cells and tissue sections using phospho-Histone H3 (Serine 10) antibody. Methods Mol Biol 1288:231-44.

166. Kearney JF, Radbruch A, Liesegang B, Rajewsky K. 1979. A new mouse myeloma cell line that has lost immunoglobulin expression but permits the construction of antibody-secreting hybrid cell lines. J Immunol 123:1548-50.

167. Wilke G, Ravindran S, Funkhouser-Jones L, Barks J, Wang Q, VanDussen KL, Stappenbeck TS, Kuhlenschmidt TB, Kuhlenschmidt MS, Sibley LD. 2018. Monoclonal Antibodies to Intracellular Stages of Cryptosporidium parvum Define Life Cycle Progression In Vitro. mSphere 3:e00124-18.

168. Liu JY, Seno H, Miletic AV, Mills JC, Swat W, Stappenbeck TS. 2009. Vav proteins are necessary for correct differentiation of mouse cecal and colonic enterocytes. J Cell Sci 122:324-34.

169. Rosales MJ, Arnedo T, Mascaró C. 1998. Ultrastructural details of Cryptosporidium parvum development in calf intestine. Mem Inst Oswaldo Cruz 93:847-50.

170. Chatterjee A, Banerjee S, Steffen M, O'Connor RM, Ward HD, Robbins PW, Samuelson J. 2010. Evidence for mucin-like glycoproteins that tether sporozoites of Cryptosporidium parvum to the inner surface of the oocyst wall. Eukaryot Cell 9:84-96.

171. Fayer R. 1995. Effect of sodium hypochlorite exposure on infectivity of Cryptosporidium parvum oocysts for neonatal BALB/c mice. Appl Environ Microbiol 61:844-6.

172. Sasahara T, Maruyama H, Aoki M, Kikuno R, Sekiguchi T, Takahashi A, Satoh Y, Kitasato H, Takayama Y, Inoue M. 2003. Apoptosis of intestinal crypt epithelium after Cryptosporidium parvum infection. J Infect Chemother 9:278-81.

173. McCole DF, Eckmann L, Laurent F, Kagnoff MF. 2000. Intestinal epithelial cell apoptosis following Cryptosporidium parvum infection. Infect Immun 68:1710-1713.

174. Liu J, Deng M, Lancto CA, Abrahamsen MS, Rutherford MS, Enomoto S. 2009. Biphasic modulation of apoptotic pathways in Cryptosporidium parvum-infected human intestinal epithelial cells. Infect Immun 77:837-849.

175. Thulin JD, Kuhlenschmidt M, Rolsma MD, Current WL, Gelberg HB. 1994. An intestinal zenograph model for *Cryptosporidium parvum* infection. Infect Immun 62:329 - 331.

176. Moore R, Tzipori S, Griffiths JK, Johnson K, De Montigny L, Lomakina I. 1995. Temporal changes in permeability and structure of piglet ileum after site-specific infection by Cryptosporidium parvum. Gastroenterology 108:1030-9.

177. Pereira SJ, Ramirez NE, Xiao L, Ward LA. 2002. Pathogenesis of human and bovine Cryptosporidium parvum in gnotobiotic pigs. J Infect Dis 186:715-8.

178. Hughes HP, Hudson L, Fleck DG. 1986. In vitro culture of Toxoplasma gondii in primary and established cell lines. Int J Parasitol 16:317-22.

179. Trager W, Jensen JB. 1976. Human malaria parasites in continuous culture. Science 193:673-675.

180. Worliczek HL, Ruttkowski B, Schwarz L, Witter K, Tschulenk W, Joachim A. 2013. Isospora suis in an epithelial cell culture system - an in vitro model for sexual development in coccidia. PLoS One 8:e69797.

181. Lourido S, Tang K, Sibley LD. 2012. Distinct signalling pathways control Toxoplasma egress and host-cell invasion. EMBO J 31:4524-4534.

182. Korpe PS, Haque R, Gilchrist C, Valencia C, Niu F, Lu M, Ma JZ, Petri SE, Reichman D, Kabir M, Duggal P, Petri WAJ. 2016. Natural History of Cryptosporidiosis in a Longitudinal Study of Slum-Dwelling Bangladeshi Children: Association with Severe Malnutrition. PLoS Negl Trop Dis 10:e0004564.

183. Guerrant DI, Moore SR, Lima AA, Patrick PD, Schorling JB, Guerrant RL. 1999. Association of early childhood diarrhea and cryptosporidiosis with impaired physical fitness and cognitive function four-seven years later in a poor urban community in northeast Brazil. Am J Trop Med Hyg 61:707-13.

184. Feng H, Nie W, Sheoran A, Zhang Q, Tzipori S. 2006. Bile acids enhance invasiveness of Cryptosporidium spp. into cultured cells. Infect Immun 74:3342-6.

185. Chappell CL, Darkoh C, Shimmin L, Farhana N, Kim DK, Okhuysen PC, Hixson J. 2016. Fecal Indole as a Biomarker of Susceptibility to Cryptosporidium Infection. Infect Immun 84:2299-306.

186. Harp JA, Chen W, Harmsen A, G. 1992. Resistance of severe combined immunodeficient mice to infection with Cryptosporidium parvum: the importance of intestinal microflora. Infect Immun 60:3509-12.

187. Ras R, Huynh K, Desoky E, Badawy A, Widmer G. 2015. Perturbation of the intestinal microbiota of mice infected with Cryptosporidium parvum. Int J Parasitol 45:567-73.

188. Ng Hublin JS, Ryan U, Trengove R, Maker G. 2013. Metabolomic Profiling of Faecal Extracts from Cryptosporidium parvum Infection in Experimental Mouse Models. PLoS One 8:e77803.

189. Ng JS, Ryan U, Trengove RD, Maker GL. 2012. Development of an untargeted metabolomics method for the analysis of human faecal samples using Cryptosporidium-infected samples. Mol Biochem Parasitol 185:145-50.

190. White J, Mascarenhas A, Pereira L, Dash R, Walke JT, Gawas P, Sharma A, Manoharan SK, Guler JL, Maki JN, Kumar A, Mahanta J, Valecha N, Dubhashi N, Vaz M, Gomes E, Chery L, Rathod PK. 2016. In vitro adaptation of Plasmodium falciparum reveal variations in cultivability. Malar J 15:33.

191. Roy G, Kündig C, Olivier M, Papadopoulou B, Ouellette M. 2001. Adaptation of Leishmania cells to in vitro culture results in a more efficient reduction and transport of biopterin. Exp Parasitol 97:161-8.

192. Pawlowic MC, Vinayak S, Sateriale A, Brooks CF, Striepen B. 2017. Generating and Maintaining Transgenic Cryptosporidium parvum Parasites. Curr Protoc Microbiol 46:20B2.1-20B.2.32.

193. Gueiros-Filho FJ, Beverley SM. 1994. On the introduction of genetically modified Leishmania outside the laboratory. Exp Parasitol 78:425-8.

194. Striepen B, Pruijssers AJ, Huang J, Li C, Gubbels MJ, Umejiego NN, Hedstrom L, Kissinger JC. 2004. Gene transfer in the evolution of parasite nucleotide biosynthesis. Proc Natl Acad Sci (USA) 101:3154-3159.

195. Oberstaller J, Joseph SJ, Kissinger JC. 2013. Genome-wide upstream motif analysis of Cryptosporidium parvum genes clustered by expression profile. BMC Genomics 14.

196. Brown KM, Long S, Sibley LD. 2018. Conditional Knockdown of Proteins Using Auxin-inducible Degron (AID) Fusions in Toxoplasma gondii. Bio Protoc 8:e2728.

197. Kreidenweiss A, Hopkins AV, Mordmüller B. 2013. 2A and the auxin-based degron system facilitate control of protein levels in Plasmodium falciparum. PLoS One 8:e78661.

198. Huang S, Holmes MJ, Radke JB, Hong DP, Liu TK, White MW, Sullivan WJJ. 2017. Toxoplasma gondii AP2IX-4 Regulates Gene Expression during Bradyzoite Development. mSphere 2: e00054-17.

199. Sinha A, Hughes KR, Modrzynska KK, Otto TD, Pfander C, Dickens NJ, Religa AA, Bushell E, Graham AL, Cameron R, Kafsack BFC, Williams AE, Llinas M, Berriman M, Billker O, Waters AP. 2014. A cascade of DNA-binding proteins for sexual commitment and development in Plasmodium. Nature 507:253-257.

200. Kafsack BF, Rovira-Graells N, Clark TG, Bancells C, Crowley VM, Campino SG, Williams AE, Drought LG, Kwiatkowski DP, Baker DA, Cortés A, Llinás M. 2014. A transcriptional switch underlies commitment to sexual development in malaria parasites. Nature 507:248-52.

201. Witola WH, Zhang X, Kim CY. 2017. Targeted gene knockdown validates the essential role of lactate dehydrogenase in Cryptosporidium parvum. Int J Parasitol 47:867-874.

202. Zhang X, Kim CY, Worthen T, Witola WH. 2018. Morpholino-mediated in vivo silencing of Cryptosporidium parvum lactate dehydrogenase decreases oocyst shedding and infectivity. Int J Parasitol 48:649-656.

203. Jaskiewicz J, Sandlin R, Swei A, Widmer G, Toner M, Tzipori S. 2018. Cryopreservation of infectious Cryptosporidium parvum oocysts. bioRxiv.

204. VanDussen KL, Carulli AJ, Keeley TM, Patel SR, Puthoff BJ, Magness ST, Tran IT, Maillard I, Siebel C, Kolterud Å, Grosse AS, Gumucio DL, Ernst SA, Tsai YH, Dempsey PJ, Samuelson LC. 2012. Notch signaling modulates proliferation and differentiation of intestinal crypt base columnar stem cells. Development 139:488-97.

205. Ito K, Suda T. 2014. Metabolic requirements for the maintenance of self-renewing stem cells. Nat Rev Mol Cell Biol 15:243-56.

206. Stringari C, Edwards RA, Pate KT, Waterman ML, Donovan PJ, Gratton E. 2012. Metabolic trajectory of cellular differentiation in small intestine by Phasor Fluorescence Lifetime Microscopy of NADH. Sci Rep 2:568.

207. Kaiko GE, Ryu SH, Koues OI, Collins PL, Solnica-Krezel L, Pearce EJ, Pearce EL, Oltz EM, Stappenbeck TS. 2016. The Colonic Crypt Protects Stem Cells from Microbiota-Derived Metabolites. Cell 165:1708-1720.

208. Xu W, Zhang Z, Zou K, Cheng Y, Yang M, Chen H, Wang H, Zhao J, Chen P, He L, Chen X, Geng L, Gong S. 2017. MiR-1 suppresses tumor cell proliferation in colorectal cancer by inhibition of Smad3-mediated tumor glycolysis. Cell Death Dis 8:e2761.

209. Heo I, Dutta D, Schaefer DA, Iakobachvili N, Artegiani B, Sachs N, Boonekamp KE, Bowden G, Hendrickx APA, Willems RJL, Peters PJ, Riggs MW, O'Connor R, Clevers

H. 2018. Modelling Cryptosporidium infection in human small intestinal and lung organoids. Nat Microbiol 3:814-823.

210. Widmer G. 2004. Population genetics of Cryptosporidium parvum. Trends Parasitol 20:3-6.